UNIVERSITÀ DEGLI STUDI DI PADOVA

UNIVERSITÁ DEGLI STUDI DI PADOVA

Dipartimento di Ingegneria Industriale

Corso di Laurea Magistrale in Ingegneria Aerospaziale

"ANALYSIS OF THE EFFECT OF SEQUENTIAL INJECTION MOLDING ON WELD LINES PROPERTIES"

Relatore: Prof. GIOVANNI LUCCHETTA

Correlatori: Ing. ANDREA SCANTAMBURLO

Laureanda: IRENE DE ZUANI 1134262

ANNO ACCADEMICO 2018-2019

“No one wants to learn by mistakes,
but we cannot learn enough from successes
to go beyond the state of the art.”
— Henry Petroski

ABSTRACT

Nowadays, polymeric materials are increasingly used to replace many other conventional materials such as metal, wood and glass in manufacturing products in modern industries thanks to their affordable price and higher strength-to-weight ratio. With the development of modern industries, the functional requirements for plastic parts tend to get more comprehensive and strict. It is demanded that the plastic parts should meet the basic requirements of appearance quality and mechanical properties.
Injection molding is one of the most important methods in the plastic sector, able to manufacture products having complex structure with precise dimensions in high efficiency with its fully automated processing cycle. Anyway, this process may cause defects in the plastic product, called weld lines, that can occur when two flow fronts meet due to either multi-gated molds or inserts. The weld line influences the aesthetic and structural quality of the products, decreasing the local mechanical properties and leaving marks on the surface of injection molded products.
Researches have been conducted to investigate how to strengthen the mechanical properties of weld lines and improve their appearance, considering different process parameters and design conditions.
In this study, a double nozzle injection molding machine has been used, to create two concurrent opposite flows, in order to produce a weld line. This effect could be obtained even in a single nozzle machine, with an appropriate runner design, but it was chosen to use two nozzles to have an independent flow control. Thus, it was set a filling phase where both nozzles are active, while during packing phase, only one is active to exploit in-flow phenomena in enhancing weld line properties.
Results show how this design is effective in repositioning weld line surface, stretching it thanks to the pressure gradient generated. The fact that weld line surface is stretched and moved means that also fibers have been reoriented during process leading to better mechanical properties of samples, since the fiber orientation tensor is higher than in no-in-flow case. Moreover, VARIOTHERM technique has been applied letting mold temperature to be kept as high as 152°C. The combination of higher mold temperature and in-flow phenomenon generated specimens with nearly absent frozen skin layer at the end of fill, and the subsequent flow is believed to be capable of weld line surface marks elimination.

INDEX

CHAPTER 1

Introduction

In order to replace common used materials in manufacturing products, such as metals, wood and glass, in the last century in which spacecrafts and new materials have been produced in order to cope with the needs of today's industries, and thanks to the innovations and improvements in science and technology, materials which are more economical and technically more applicable compared to before mentioned materials have been investigated.
As a result of this development in science and technology, composite materials produced by combining different materials which have different qualities by special methods have gained importance. One of the most important materials in the last century are polymers.
This class of materials presents suitable properties in a wide range of applications, with benefits in cost and weight reduction, lower process temperatures, resistant to corrosion, good electrical and heat insulation. These characteristics make them suitable for productions of complex structure with precise dimensions in high efficiency with its fully automated processing cycle, compared to traditional techniques.
Injection molding, which is used in the production of thermoplastic parts, is one of the most important methods, to produce polymer components.

1.1 Injection molding

Injection molding is a manufacturing process to produce parts from polymers melt, from the smallest components to entire automotive structures, such as body panels.
The process consists in feeding material into a heated barrel, and mixing and pushing it forward to the nozzle with a helical screw so that the polymer can be brought to mold and thanks to a specific pattern, it can reach the mold cavity to be formed into desired shape. This process is vastly used because it is very advantageous in terms of high production volumes, reduced cycle times and high automation.
The figure below shows the principal components of an injection molding machine.

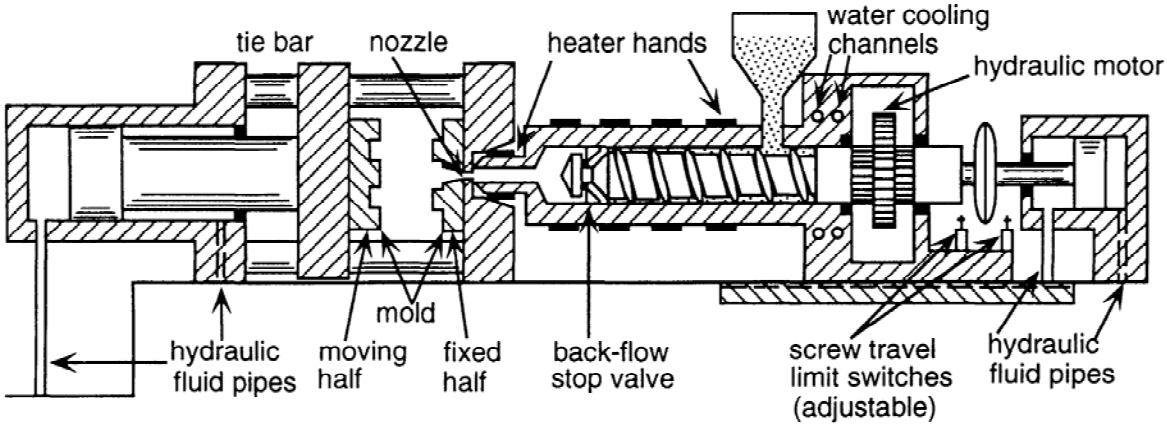

Figure 1. Schematic representation of injection molding machine.

The hopper is the reservoir of material that will be used for a number of cycles and the pellets of material are fed to heated barrel by gravity, to be melted and processed.
The plasticizing screw is designed to perform different functions. As shown in Figure 2, three zones can be distinguished, namely feed, compression and metering zone.

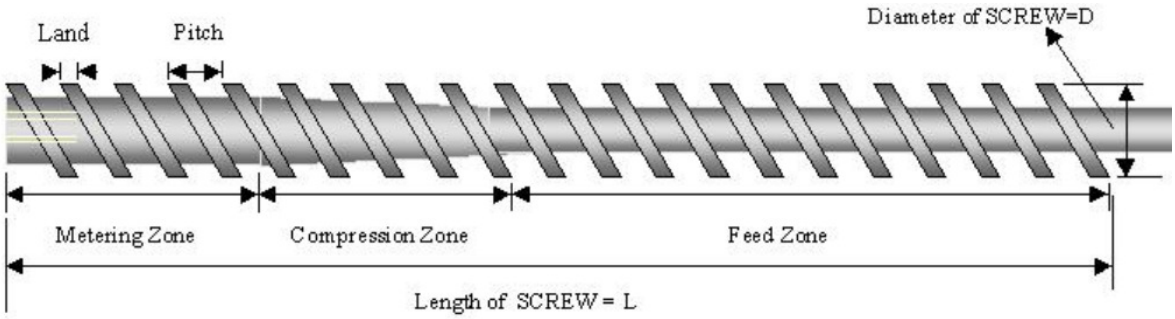

Figure 2. Plasticizing screw design.

Feed zone is the first screw section the solid material encounter, and it is designed to move forward the granules and pre-heat them. Compression zone is where the melting process starts, thanks to the heated cylinder and mechanical shear from the screw rotational movement. In this zone, screw diameter raises, reducing the space the melt can occupy, so pressure increases and air can be eliminated. The metering zone is the final zone where diameter is now constant again, and is designed to push the material towards the injection nozzle.
In a reciprocating screw injection molding machine, the screw itself moves backward to leave a space where melt can be accumulated, to then be compressed and pushed through the nozzle when the screw moves forward. The screw still forward until the molten material hardened in the mold and the gate is closed, and is then retracted to start another cycle.
Moreover, to ensure the melt does not flow backward, a check valve or non-return valve is attached to the end of screw.

Injection molding process can be divided into several stages:

1. Material feeding: based on cavity volume, including runner, gates, etc., the operator should set how much material needs to be loaded into the heated barrel per cycle. The material can now be melted in the plasticizing screw and proceed to the next phase.
2. Filling: the operator chooses injection parameters in terms of velocity and maximum pressure, and it can be set a continuous or single cycle. During this phase, the screw leads the melt towards the cavity, first applying a compression to eliminate voids and air due to empty space left after melting, and then in the zone denominated metering zone, the plastic melt moves in a spiralling motion down the screw channel to have a better homogenization. Exiting the screw, the plastic reaches the mold cavity, filling it to about 95%.
3. Packing and holding: the remaining space in the mold cavity is filled and the system continues to inject material, to compensate the shrinkage during cooling. Once the cavity is full filled and an extra amount of material has been pushed in, the pressure is hold since gate seals. For this stage, the user must set an appropriate amount of time and pressure, to obtain the desired surface finish and dimensions.
4. Cooling: after gate seals, no material can be added, and the part needs to cool down and to be hold in the mold, before opening it to avoid deformation during extraction. Since mold temperature is lower than melt temperature, the cooling is automatic, and is generally present water, or oil, runner system in the mold, to keep it at a constant temperature. Molded part is generally extracted at a temperature that is 5°C below Vicat softening temperature.
5. Mold opening: the two half of the mold are now separated, and the part can now be extracted
6. Extraction: if needed, an extractor system can be added to the mold moving half, to remove the molded part
7. System is now reset to initial condition and another cycle can be performed.

Each cycle, takes up to 10-30s, according to user setting to achieve part dimensions and based on materials involved.

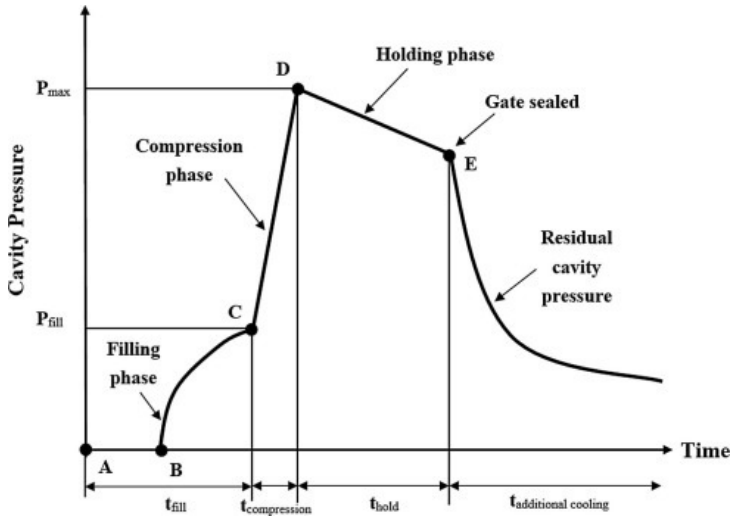

Figure 3. Typical cavity pressure profile [1]

In the filling phase, the polymer flow assumes a typical configuration in the cavity, called fountain flow (Figure 4), depending on injection velocity. The material in direct contact with mold walls solidify instantaneously, while the melt material in the core layer still flowing.
This phenomenon influences fiber orientation due to shear stresses produced during filling, and is a function of injection velocity.
Two rules of thumb exist:

- shearing flows tend to align fiber in the direction of flow;
- stretching flows tend to align fiber in direction of stretching.

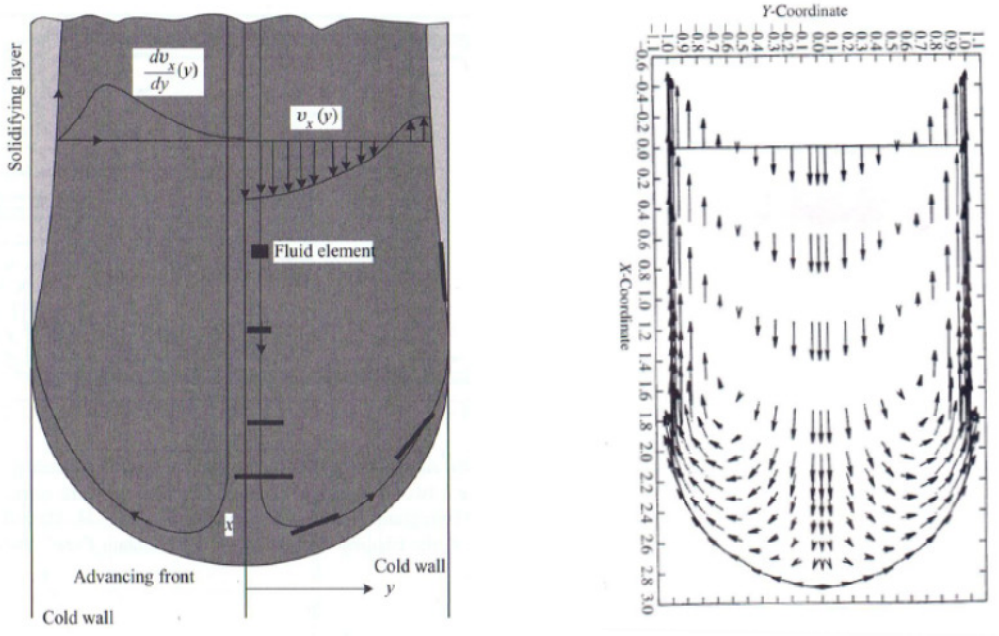

Figure 4. Fountain flow

It becomes evident that to analyze the polymer flow it is necessary to understand the relationship between the shear stress, shear rate, and viscosity. The shear stress, τ, is a measure of how much force per unit area is being exerted by the fluid as it flows. The shear rate, $\dot{\gamma}$, is a measure of the rate at which the melt velocity changes. The shear stress is related to the shear rate through the viscosity, η, which is a measure of the fluid's resistance to flow:

$$\tau = \eta\dot{\gamma} \qquad (1)$$

Shear stress is maximum at wall and is approximately zero at the centre.

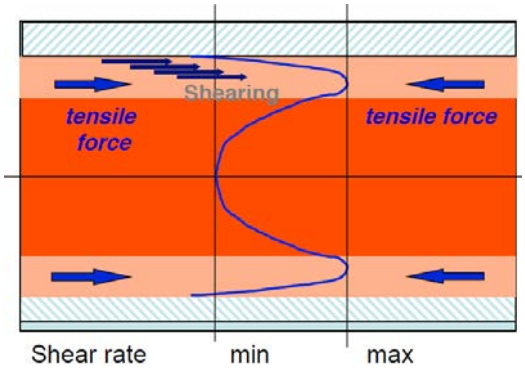

Figure 5. Shear rate trend through thickness

Considering flow between a stationary plate and a moving plate, with a stationary and fully developed flow without wall slip, the velocity profile is linear from zero at the stationary wall to a maximum velocity value at the moving plate, and the shear rate is defined as the change of velocity value through thickness, as:

$$\dot{\gamma} = \frac{dv}{dz} = \frac{v}{h} \tag{2}$$

where h is the distance between the plates.
Elongation velocity is, instead, defined as:

$$\dot{\varepsilon} = \frac{dv_y}{dy} = -\frac{dv_x}{dx} \tag{3}$$

In terms of injection velocity, it can evaluate its effect in frozen layer thickness at wall. If injection velocity is higher, as the same amount of heat is remove from the mold, the frozen layer thickness, or skin layer, will be thinner than in case of a lower injection speed. Worth to notice that the skin layer presents a flow aligned fiber orientation, which is preferable, so injection velocity should be as lower as possible, while maintaining process quality and ensure full filling.

Depending on skin layer thickness, the flow exhibit different flow velocity profiles, and therefore different shear rate distributions and fiber orientations. These distributions make it possible to distinguish three different zones through thickness, in a so called skin-shear-core structure (Figure 6).

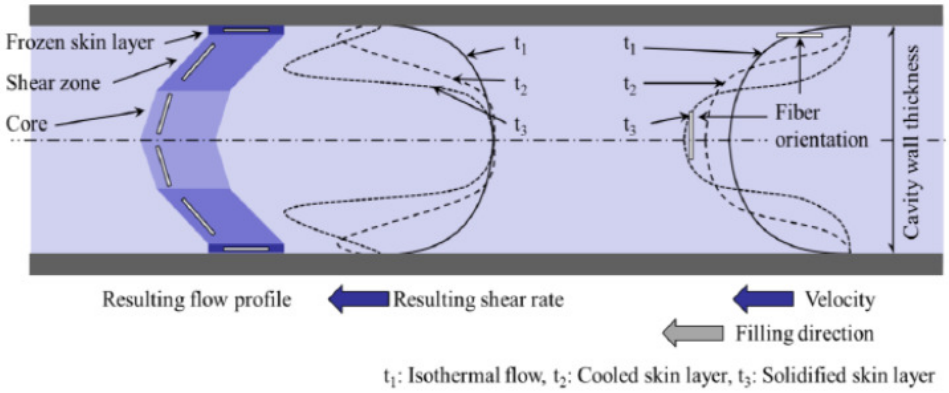

Figure 6. Skin-shear-core structure

In the previous picture is summarized the relations between shear rate, flow velocity, flow profile and fiber orientation for different process conditions, but must be remembered that also part geometry and fiber average aspect ratio and concentration contributes on orientation.

As before mentioned, in packing phase more material is added to reduce shrinkage after cooling. Polymer withdrawal is a function of PVT curves of material, and for polymers can be noticed high thermal expansions coefficients, so significant shrinkage occurs during solidification and cooling and must be compensated.

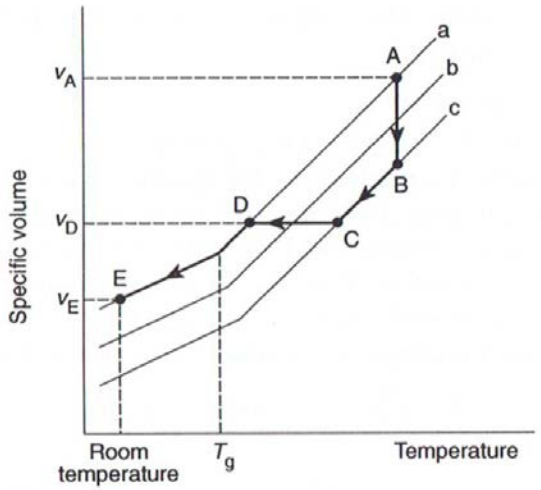

Figure 7. Polymer shrinkage during solidification and cooling (pVT diagram)

In Figure 7**,** is shown specific volume reduction of a generic polymer with temperature:
A-B) represents injection and packing phases, in which the material is injected in cavity at constant temperature and under pressure;
B-C) the polymer starts to cool and extra material is added to avoid excessive shrinkage, and pressure is kept constant;
C) represents gate closure;
C-D) material starts to cool at constant volume, and pressure reduces to ambient pressure in D;
D-E) material cools freely and can be noticed a volume contraction.
Factors affecting shrinkage are the presence of fillers, injection pressure, compaction time and molding temperature. Higher pressures force more material into the mold cavity; longer compaction time have similar effect of higher pressures; higher molding temperatures lower polymer melt viscosity, allowing more material to be packed into mold to reduce shrinkage.

In cooling phase, the objective is to cool the part in the shortest time possible, without introducing aesthetic defects or compromise properties of the product. In the figure below (Figure 8), is shown the temperature distribution of a 3mm PMMA sheet, starting from a 180°C melt temperature and letting it cools below the glass transition temperature, which is 100°C for this material.

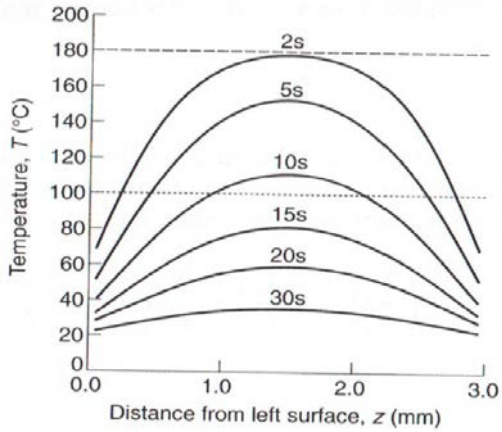

Figure 8. PMMA temperature distribution through thickness during cooling

As it can be seen, the core is the last zone that cools, but after 12s also this region has reached glass transition temperature Tg.
Cooling time can be estimated as:

$$t_{cool}[s] = \frac{h_{max}^2}{\pi^2 \alpha} * \ln \frac{4(T_i - T_s)}{\pi(T_r - T_s)} \quad (4)$$

where: t_{cool} is cooling time [s]
h_{max} is the maximum cavity thickness [mm]
α is thermal diffusivity $[mm^2/s]$
T_i is polymer injection temperature [°C]
T_s is mold recommended temperature [°C]
T_r is extraction recommended temperature [°C]

Cooling phase is the process step that generally requires more time, up to 70-80% of total cycle time. For simple geometry, it doesn't in general overcome 1 minute, but it is important to emphasize that is proportional to the square of thickness.

1.2 Compounding

Compounding consists of preparing plastic formulations by mixing or/and blending polymers and additives in a molten state.
Matrix materials can be classified as the materials used as a base for the future polymer compound, and additive or reinforcement materials, as the materials disperse and blended within the matrix to achieve the desired properties for the final compound. These reinforcements can help to strengthening component, act as UV-stabilizer or enhance electrical conductivity.
There are different critical criteria to achieve a homogenous blend of the different raw material. Dispersive and distributive mixing as well as heat are important factors.
Compounding is usually obtained by extrusion, where a hopper feeds the begin of the screw which will gradually transport the resins towards the die. The screw itself is confined in a barrel that melts the material to be extruded. The extrudate looks like a long plastic strand and it can be cooled in a water bath, or by spraying as the conveyor belt moves it to the granulator. Lastly, the granulator breaks the strand into the desired pellet sizes.

1.2.1 Matrix materials

A polymer is a substance defined as a large molecule, or macromolecule, composed of a large number of elementary units, called monomers. These macromolecules show a relative high molecular mass, and they can be obtained by homogeneous or heterogeneous subunits, which results in different mechanical properties.

IUPAC (International Union of Pure and Applied Chemistry) has adopted two different polymer nomenclatures, defining different kind of polymers on source-based or structure-based classification. In source-based nomenclature can be found:

- homopolymers: where only a kind of monomer is used;
- copolymers: where multiple kinds of monomer is used;
- non-linear polymers: monomers can be distributed also in a non-linear configuration, so they can show ramifications. In IUPAC nomenclature can be found different qualifiers, such as blend, comb, complex, cyclic, branch, network and star configuration.

In structure-based nomenclature can be distinguished regular single/double-strand organic polymers, that can be regular or irregular, in terms of repetition of the constitutional repeating unit (CRU).

When they fit into the general pattern of systematic nomenclature, some traditional names of polymers are maintained, such as polyethylene, polypropylene and polystyrene. [2]

Polymers can be either natural or synthetic. Natural polymers are, for example, protein, starch, cellulose, DNA, and make up most of the structures of living tissue. Synthetic polymers are nowadays more commonly used, thanks to the properties control they show during polymer production.
Usually when referring to polymers, they can be called plastics and this implies that synthetic polymers, elastomers, or every other artificial polymer with plastic behaviour have been considered.
Synthetic polymers can be obtained with two different techniques: polyaddition and polycondensation. Polyaddition occurs as a reaction between functional groups on molecules with low degrees of polymerization, via individual independent addition reactions. Polycondensation occurs via condensation reactions, when molecules join together producing sub-products like water or methanol.

Above all these different nomenclatures, the most interesting distinction concerning plastic processing is about thermoplastic and thermosetting materials.

- Thermoplastic materials: are plastic materials that become moldable above a specific temperature, i.e. melt temperature, and solidify upon cooling. This kind of materials can be reheated and reshaped thanks to their intermolecular forces that weaken with increasing temperature.
  This class of materials is increasingly used in automotive or aerospace applications due to low density, high elongation at break, high impact resistance, reduced cycle time and recyclability. Conversely, they have lower melting points than metals, so metal replacement can't be fully achieved, but some of their properties can be improved with filler or reinforcements in order to make them more suitable for industrial applications.
  Two thermoplastic structures can be characterized in solid state: amorphous or semi-crystalline polymers.
  In amorphous kind, materials don't show long-range order, and they have an internal structure made of interconnected structural blocks. These kinds of material can be processed after reaching glass transition temperature (Tg). In crystalline kind, polymers have an ordered arrangement of molecule, that reduce the temperature range in which the material can be processed, so they can undergo processes only after reaching melting temperature (Tm).
  Specific volume vs. temperature for these two kinds of materials can be seen in Figure 9.
  Worth noticing that there aren't materials that present pure crystalline structure, because a part of amorphous material structure still remains during solidification, therefore it is usual to refer to these materials as semi-crystalline.

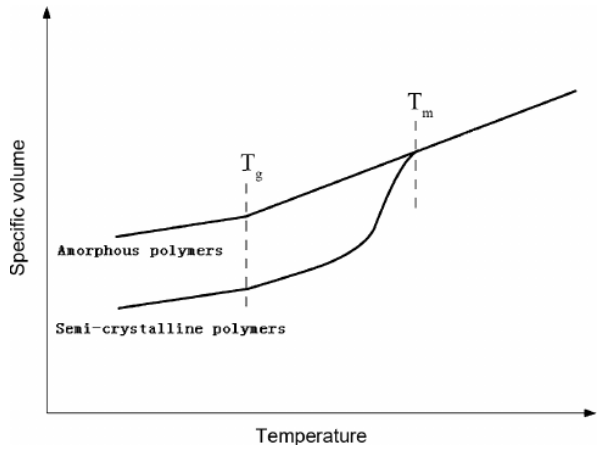

Figure 9. Specific volume vs. Temperature curves for amorphous and semi-crystalline polymers [3]

- Thermosetting materials: are characterized by irreversible chemical bonds during curing process. These materials have a liquid viscous appearance before being processed and show extensive cross-linking between polymer chains after curing, so once hardened, a thermosetting material cannot be reshaped. In opposition to thermoplastic ones, these materials show higher heat resistance and hardness.

Commonly used thermoplastic materials are ABS, nylon, Teflon, polypropylene, polystyrene and polyethylene, while for thermosetting materials most common once are polyester resin, polyurethanes, epoxy resin, polyimides and silicone.

Today's tendency is moving from thermosetting to thermoplastic materials, and this second class of materials is, indeed, the one applied in injection molding processes.

1.2.2 Reinforcement materials

Reinforcement material can be divided in fibrous and non-fibrous reinforcements, with different characteristics.

Fibrous reinforcements: increase tensile strength and modulus,
increase flexural strength and modulus,
increase deflection temperature,
decrease warpage,
decrease mold shrinkage, elongation, moisture absorption,
decrease impact resistance (in some cases)
can be used in injection molding applications
long fiber products have better mechanical properties.

Non-fibrous reinforcements: reinforcement and fillers,
increase tensile strength and deflection temperature,
good flatness properties,
lower impact resistance,
usually combined with crystalline resins.

Typical fibrous reinforcements are glass fibers, carbon fibers, aramid fibers or other thermoplastic fibers. Non-fibrous reinforcements are usually platelet shape mica, glass beads, Wollastonite, non-metallic mineral, metallic powders, calcium carbonate, kaolin and talc.

For some application could be interesting have blends with conductive fillers, such as:

- carbon fibers, mostly used for shielding application,
- nickel-coated carbon fibers to improve electrical performance,
- stainless steel fibers, widely used for EMI/RFI shielding
- aluminium flakes
- carbon powders
- nickel coated mica

Fillers can be used not only to enhance material properties, but they can also be useful in cost reduction since they reduce volume available for most expensive materials.
Following, the most common used reinforcements are listed and described.

Glass fibers: were mass produced only after the invention of finer machine tooling. To form glass fibers thin strands of silica-based glass are extruded into many fibers of desired diameter. Apart dimensions, glass fibers are classified with different names, depending on glass composition, as shown in Table 1:

Type	SiO_2 [%]	Al_2O_3 [%]	CaO [%]	R_2O [%]	MgO [%]	B_2O_3 [%]	ZrO_2 [%]
A	72.3	0.6	10.2	14.2	2.7	-	-
E	54	14.4	18.3	<0.7	3.7	8.5	-
S or R	65	25	-	-	10	-	-
AR	-	-	-	-	-	-	18-20

Table 1. Glass composition for common glass fiber

Pure silica is viable glass and glass fiber but has to be worked with at very high temperatures. In order to reduce operating temperature, other formulation has been introduced. Soda lime glass, A-glass, was the first kind to be used for fiber production. Unfortunately, this glass can't be used in environments with presence of water and humidity, so its terrestrial applications are limited, but it is widely used in aerospace. E-glass, which is alkali free, was the first used in continuous filament formation, and is one of the most used worldwide, even if it presents low elastic modulus (75 GPa) and a 2500 kg/m_3 density. E-glass was originally used for electrical applications. S-glass is used when the main goal is to ensure high tensile strength. AR-glass stands for alkali resistant, and is specifically designed for concrete applications.
There are also other two principal kind of fiber that are not listed in Table 1, C-glass and T-glass, that are used for chemical resistant and thermal insulator applications, respectively. [4]
Glass fibers are widely used thanks to being cheaper than other types of fiber, for their high density/weight ratio, impact and heat resistance and chemical stability. Used as reinforcement they increase elastic modulus and maximum load, creep resistance and fatigue behaviour and they provide lower shrinkage after injection molding process and less thermal expansion of composite matrix.

Kevlar fibers: polymeric fibers have been created to reduce composite density. It is demanding that reinforcement presents high elastic modulus, mechanical strength and resistance at high temperatures. Poly aramid are used for these goals since they are formed by a long macromolecular linear chain, with strong chemical bonds. Kevlar is synthesized in solution in a condensation reaction yielding hydrochloric acid as a by-product. The result has liquid-crystalline behaviour, and mechanical drawing orients the polymer chains in the fibers direction. Kevlar (poly paraphenylene terephthalamide) production is expensive because of the difficulties arising from using concentrated sulphuric acid, needed to keep the water-insoluble polymer in solution during its synthesis and spinning. This material presents a tensile strength of about 3620 MPa and a relative density of 1.44, it is slightly stronger in cryogenic ambient but at high temperatures tensile strength suddenly decrease by about 10-20%, and progressively reduces if high temperature is maintained.
Kevlar has many applications, ranging from bicycle tires and racing sails to bulletproof vests, because of its high tensile strength-to-weight ratio and when used as a woven material, it is suitable for mooring lines and other underwater applications. In motor vehicles applications it is used for structural components and brake pads.

Carbon fibers: is a polymer and is sometimes known as graphite fiber. It is a very strong material that is also very lightweight. Carbon fiber is five-times stronger than steel and twice as stiff, but lighter; making it the ideal manufacturing material for many parts. These properties have made carbon fiber very popular in aerospace, civil engineering, military, and motorsports, along with other competition sports. However, they are relatively expensive when compared with similar fibers, such as glass fibers or plastic fibers.
Carbon fiber is made from a process that is part chemical and part mechanical. It starts by drawing long strands of fibers and then heating them to a very high temperature without allowing contact to oxygen to prevent the fibers from burning. This is when the carbonization takes place, which is when the atoms inside of the fibers vibrate violently, expelling most of the non-carbon atoms. This leaves a fiber composed of long, tightly inter-locked chains of carbon atoms with only a few non-carbon atoms remaining.
A typical sequences used to form carbon fibers from polyacrylonitrile involves spinning, stabilizing, carbonizing, treating the surface and sizing. [5]
Depending on temperature reached during carbonizing phase, can be distinguished three different fibers:

- low modulus fiber: carbonization up to 1200°C. Elastic modulus and mechanical strength are relatively low, and for these reasons it is less expensive than the other kind.
- intermediate modulus fiber: carbonization up to 1600°C. Intermediate elastic modulus and higher mechanical strength of all kind of carbon fiber.
- high modulus fiber: carbonization up to 2000°C. Higher elastic modulus of all kind of carbon fiber, but lower mechanical strength than intermediate fiber.

Carbon fiber contributes in enhancing maximum load, electric conductibility and thermal conductivity of polymer matrix. They also reduce shrinkage after molding, thermal expansion and specific weight.

Talc: is a plate-like layered structure magnesium silicate mineral, in which the octahedral brucite layer is sandwiched between two tetrahedral silica sheets, has proved to be particularly efficient filler on the mechanical properties and macromolecular orientation of compounds and consequently an increase of the performance of reinforced polymeric matrix. At low concentrations (less than 3 weight%), talc acts as a nucleating agent, reducing spherulite size and shortening processing time. At higher concentration (10-40 weight %) it acts as a reinforcing filler, increasing tensile modulus and stiffness, but reducing strain-to break and impact strength. However, it has been highlighted that the filler nature of talc influences its reinforcement ability, depending on the surface activity, particle size, surface area, and surface functional groups. [6]

Wollastonite: is a calcium inosilicate mineral, that may contain small amounts of iron, magnesium, and manganese substituting for calcium. It is usually white. Some of the properties that make wollastonite so useful are its high brightness and whiteness, low moisture and oil absorption, and low volatile content. In plastics, wollastonite improves tensile and flexural strength, reduces resin consumption, and improves thermal and dimensional stability at elevated temperatures. Surface treatments are used to improve the adhesion between the wollastonite and the polymers to which it is added. [7]

Kaolin: is a hydrated aluminium silicate belonging to the group of clays. It comes in the form of gray-greenish or ivory powder. It has an absorbent and matting function. It is used in plastics due to its chemical resistance, electrical isolation properties, hardness and surface finish appearance.

1.3 Weld lines and present research

Weld lines are one of the most significant defects that can be encountered in producing injection molding products by multi-gates mold.
Two different kinds of weld lines can be classified referring to the contact angle between the two fronts. When the meeting involving two flows coming from opposite sides is frontal and without additional flow, a *cold* or butt weld line is formed (Figure 10), with lower mechanical strength. If the stream meeting is lateral and the fronts still have some time to flow together and under pressure, the resulting *hot* or streaming weld line is stronger than the previous one.

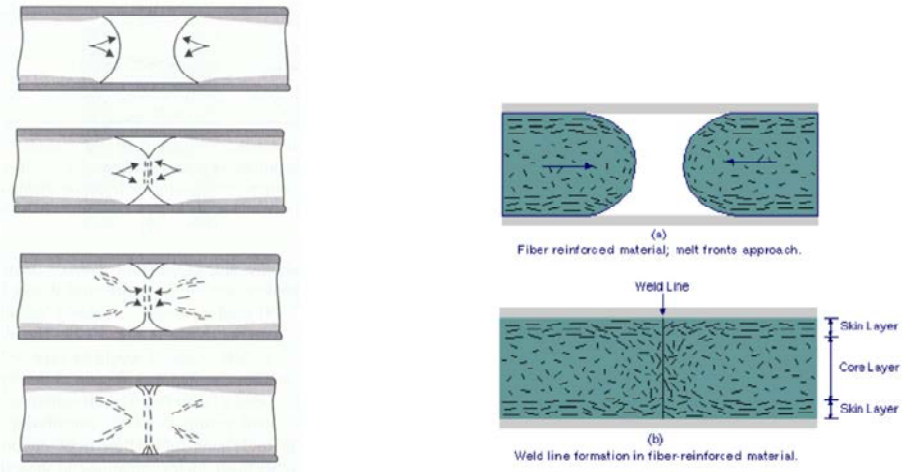

Figure 10. Formation process of a cold weld line in fiber reinforced materials

These defects are unavoidable in cases of: presence of holes or inserts, multi-gated delivery systems, significant thickness change, and so on. The effects of poor mechanical and aesthetic properties of weld lines can be summarized, referring to:

- "V"- shaped notch
- unfavourable fiber orientations
- poor bonding

When the two flow fronts collide, as in cold weld lines, a "V"- shaped notch is formed. Flow-fronts usually contain foreign substances, such as gases and moisture, which reduces good interfacial bonding and leads to the formation of this feature, deteriorating not only the surface appearance but also the mechanical strength of the molded part as it acts as stress concentrator and crack initiator during the product lifetime.
In the case of fiber-filled polymeric systems affected by shear stresses generated during the material flow within the mold, weld lines introduce molecular orientations and unfavourable fiber orientations because of the fountain-flow effect. It can be seen that in weld line region molecules and fibers result oriented perpendicular to the flow direction causing a localized anisotropic and mechanically weak structure. Moreover, at the two flow fronts interface, samples show poor bonding resulting from insufficient entanglement of the molecular chains in the weld region.

In general, the presence of weld line is responsible of a 10-60% strength reduction, depending on polymer matrix and reinforcing filler features, as its concentration. Therefore, when weld lines are likely to occur in molded products, they must be taken into account during the mechanical and technological design processes.

In the past few years, several researches have been conducted to investigate how to increase and/or improve weld lines properties.

Hsien-Chen et al. [8] designed a five-specimen cavity with different cross section, to study the influence of process parameters and cross-sectional dimensions on the tensile strength of specimen with and without a weld line. Moreover they used Taguchi method to analyze the influence of testing parameters on tensile strength of UHMWPE (ultra-high molecular weight polyethylene) samples. Six molding factors were selected for the larger-the-better case, namely: melt temperature, mold temperature, injection velocity, packing pressure, pacing time and cooling time.

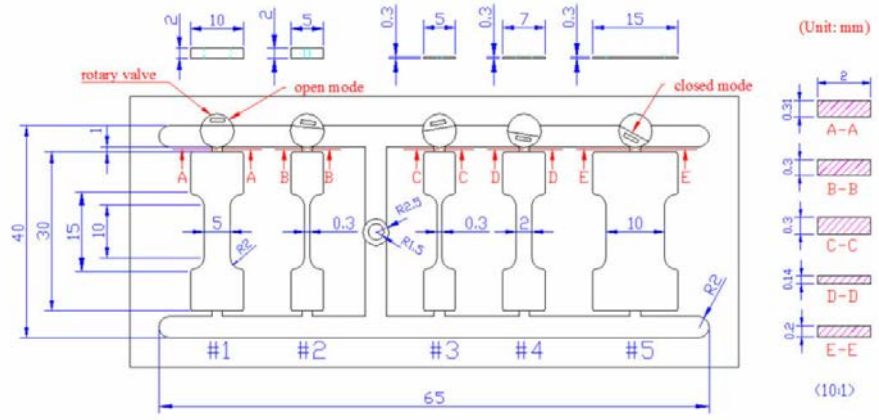

Figure 11. Dimensions of tensile specimen

The five specimen design is the one reported in Figure 11. They found that in specimen with weld lines the process parameters create greater influences than the cross-sectional dimension of the dog-bone region. Given that the width and thickness of the cross-section of the dog-bone region are smaller (e.g. specimen #4), the tensile strength of the specimen drops at a more significant range, compared with the specimen without a weld line. Contrarily, given that the width and thickness of the cross-section are bigger (e.g. specimen #1), the tensile strength of the specimen drops within a less significant range. There are two possible reasons leading to such phenomenon. First, the orientation of molecules at melt front is usually parallel to each other, which creates less molecular bonding at weld line and further weakens the tensile strength of weld line. As a result, a specimen with smaller cross sectional dimensions presents less molecular bonding than the one with bigger cross-sectional dimensions. The other reason involves the thickness of a specimen. With smaller specimen thickness, the melt temperature drops faster in the process when melt fronts from the two sides meet, thus incomplete bonding of the molecular chains at the meeting point of melt fronts appears. Moreover, in thicker specimen, the frictional heating in the filling process leads to an increased molecular bonding and self-diffusion of the UHMWPE.

Guo et al. [9] used two different blends, a PS/PMMA (30/70) and a PS/PMMA (70/30). Two dog-bone specimens were produced at a time and weld line morphology and mechanical strength of sample, as well as effects of viscosity ratio and injection parameters on them were studied. They found that tensile strength of (30/70) blend is higher than the (70/30) one. The ratio of weld line tensile strength σ_w, and no-weld line

tensile strength σ_b has been found to be higher in PS/PMMA (70/30), and it also increases with injection temperature, while it hardly increases in (30/70) composition. Studying weld line morphology, they stated that the key for increasing weld line strength is the elimination of the oriented domains and dispersed phase concentration gradients at the weld line. The molecular diffusion of polymer blends across the weld line would be advantageous to achieve a strong weld line, so the viscosity of blends and melt flow front temperature will have a great influence on the weld line strength. The weld line morphology of PS/PMMA (70/30) is quite different from that of PS/PMMA (30/70). In the PS/PMMA (30/70) blend, the viscosity of the dispersed PS phase is lower than that of the PMMA matrix, the PS phase is absent at the weld line, and PS particles are highly oriented parallel to the weld line. In the PS/PMMA (70/30) blend, the PMMA dispersed domains at the core of weld line are spherically shaped, which is the same as bulk.

Nguyen-Chung [10] conducted a non-isothermal simulation of the weld line formation due to collision of two flow fronts. It was shown that the high orientation at the weld line is a result of rather the local deformations along the interface than of the general deformation at the flow front. Fountain flow, which leads to high deformations at the mold wall (Nguyen-Chung and Mennig 2001) producing pronounced molecular orientation parallel to the wall, affects only the regions far away from the weld line. As the two flow fronts meet, the extension along the weld line can be considered to be the main source for the molecular orientation perpendicular to the wall.

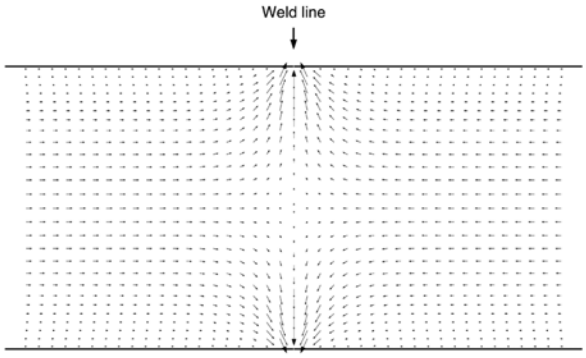

Figure 12. Increasing velocity at the last filled region due to decreasing effective cavity

The reason for the increasing extension rates towards the wall was the increasing velocity, which occurred due to the small effective cavity remaining in the last filled region while the average flow rate was kept constant (Figure 12). As a consequence of this local flow situation a high degree of molecular orientation perpendicular to the wall can be expected near the cavity surface which is therefore assumed to be the most sensitive area of the weld line region.

Zhai et al. [11] paper presents an approach to position the weld line to the non-critical region of an injection moulded part so as to reduce its effects on the part quality. They studied the gate optimal positioning based on the one which gives minimum injection pressure. Since injection pressure reflects the work required in mould filling, lower resistance for melt flow leads to lower injection pressure. Hence, the candidate gate location should be searched along the direction of decreasing flow resistance which is equivalent to negative pressure gradient. Once the gate is positioned the runner layout must be designed to create weld lines where desired via iteration process. Flow leaders and flow defectors are commonly used to achieve weld line positioning, however they change dimensions of the parts, creating non-uniform wall thickness and as a consequence, non-uniform cooling. Thus, runner re-sizing has been proven to be a valid alternative in this paper.

.

Hashemi [12] tested the effect of fibre concentration, strain rate, temperature and the type of loading on strength of single and double-gate injection moulded polybutylene terephthalate (PBT) reinforced with 0, 10, 20 and 30% by weight short glass fibre. It was found that tensile strength of double-gate mouldings increased initially with increasing fibre volume fraction but decreased as fibre concentration exceeded 10%v/v, increased linearly with increasing strain rate and decreased linearly with increasing temperature. Weld line integrity factor strength decreased with increasing fibre volume fraction but showed no significant variation with respect to temperature, strain rate or the type of loading. A linear dependence was obtained between the natural logarithm of weld line integrity factor and (fibre volume fraction)$^{2/3}$ for both tensile and flexural strength.

Xie and Ziegmann [13] developed one injection mold with four micro tensile sample cavities to study gate dimension effect on micro injection molded weld line strength, using PP and HDPE, in different process conditions. Gate design and samples configuration is reported in Figure 13.

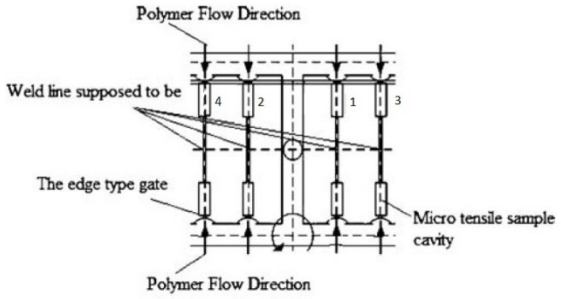

Gate Nr.	1	2	3	4
Width (mm)	1.5	1.0	1.0	0.5
Depth (mm)	0.1	0.1	0.05	0.1
Length (mm)	0.5	0.5	0.5	0.5

Figure 13. Gate design and dimensions in the experimental mold

The results showed that the width of the gate has a consistent influencing trend on the weld line strength for these two materials respectively, when the depth of gates are constant for PP, whatever the processing parameter varying, Gate Nr.2 always responds to the strongest weld line strength, and for HDPE, Gate Nr.4 causes best weld line strength, but the depth of the gate does not always affect the strength of the weld line in the positive way, and bigger gate size does not contribute to stronger weld lines all the time, which is different from the results in normal scale injection molding process. When cross sectional areas are equal, the gate with larger width and smaller depth is the best to use in term of weld line strength.
Based on results for the correlation of weld line strength, gate size, and processing parameters, a trend curve to describe it was proposed like in Figure 14.

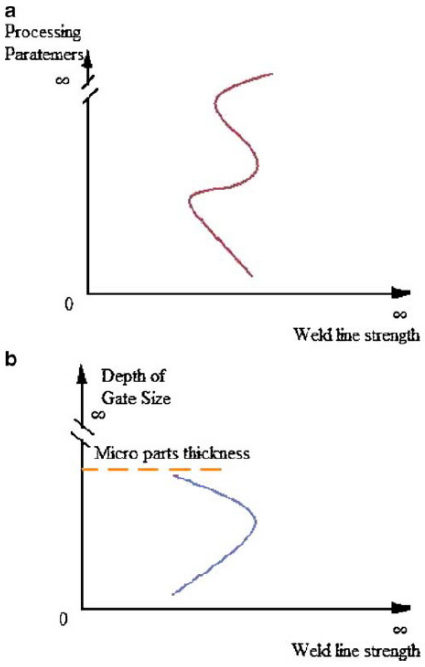

Figure 14. Trend curve describing the correlation between process parameters (a) and gate size (b) to weld line strength

"Multi-S wave" profile means that the optimal point for processing parameters will not be unique and fixed; and the depth of edge gate relates to the weld line strength by a parabola profile.

Kagitci and Tarakcioglu [14] studied injection pressure, injection time and packing pressure influence on weld line quality in a glass fiber reinforced polyamide (PA 6 GFR 30). Results showed an increase in tensile strength with mold temperature, an increase in weld line resistance with injection pressure and time and packing pressure and it was found that mechanical performance is a function of mold temperature, melt temperature, clamp and hold pressure, hold and cooling time and thickness of interphase. Positive effects are seen on weld line width when injection pressure is increased from 600 to 1200 bar. A 12% of increase in tensile load is observed. Considering weld line tensile load, injection conditions appropriate for 30 % glass

fiber reinforced polymer composite joint are as follows: injection pressure should be 1200 bar, injection time should be 2 s, and packing pressure should be 1000 bar.
Wenig and Stolzenberger [15] presented a study on sandwich structure of injected polypropylene parts with and without weld line. This sandwich structure shows three distinct layers: a "structureless" skin, a spherulitic core, and an oriented transition zone between skin and core. It was found that the skin-layer thickness is strongly dependent on whether the mould is injected through one gate or through two gates. Samples containing a weld line show a much lower skin-layer thickness than samples without a weld line. This difference, however, depends strongly on the molecular weight of the polypropylene. The skin-layer thickness also varies along the flow path and decreases with increasing mold temperature. Moreover, several crystal modifications have been found in the samples.

Ozcelik et al. [16] studied optimization of the effect of injection parameters such as melt temperature, packing pressure, cooling time and injection pressure on the mechanical properties of acrylonitrile-butadiene-styrene (ABS) moldings. An experimental plan for four parameters with three levels was organized by the Taguchi method. Results showed that the most important parameter affecting the elasticity module, tensile strength and tensile strain at yield, tensile strain at break was melt temperature and the other parameter affected by flexural module was injection pressure. The elasticity module, tensile strength at yield, flexural module and izod impact strength for steel and flexural module for aluminium mold materials gave linear relationships (based on values of r^2) with injection parameters whereas other mechanical properties resulted in non linear relationships. Values of elasticity module and tensile stress at yield for Al mold were higher than that of steel mold when melt temperature and cooling time were high. There was hardly any difference observed for values of tensile strain at yield and at break. Value of flexural modules and izod impact strength were found to be higher for Al mold when melt temperature and cooling time were low.

Sreedharan and Jeevanantham [17] considered injection molding parameters to minimize weld line and sink mark defects in ABS molded parts, focusing on melt temperature, mold temperature, injection pressure, holding pressure, cooling time, back pressure, holding time and ambient temperature. They take into account single parameter effects but not collaboration effect, via Taguchi method based on Grey relational analysis. Major effect was due to loading time trailed by back pressure, melt temperature, mold temperature, ambient temperature, holding pressure, cooling time and injection pressure. In this work weld line width and sink mark were taken as multiple response variables which are converted by GRA to a single GRG which clearly helps in getting an ideal process parameter to minimize the weld-line and sink-mark defects and by getting the ideal combination of the molding parameters. It was evidenced a reduction of weld line depth of 56.4% and sink mark depth of 68.9%.

Xie and Ziegmann [18] tested mechanical properties of weld line in micro injection molded parts in PP filled with CNFs and TiO_2, at weight fractions of 10, 20, 30 and 35%wt. Regarding CNFs (Carbon Nano Fibers), they found that elastic modulus increase with filler fraction, but also did weld line extension, instead for fiber concentration over 10%wt tensile strength of sample became lower than neat PP. Thus, 10%wt carbon fiber content has been found the best choice. Regarding TiO_2, it presents lower density than CNFs at same concentration, and elastic modulus first decreased to then increase over 10%wt content. Tensile strength also increased over 10%wt and weld line extension is optimized at the same weight fraction, showing no further improvement increasing filler concentration. Elastic modulus and tensile strength showed a decreasing trend for concentration under 30%wt, to then invert trend and increase. The morphological properties of all nano composites were characterized by WXRD, whose results imply the adding nano fillers did not change the crystal form of PP, but the crystallites size and distance between lattices of crystals were changed with various nano fillers and loading fractions. They concluded that for functional nano filled polymer composites, the mechanical properties of micro weld lines were obviously influenced by nano fillers' shape and loading fractions. The E modulus of micro weld line was increased due to loading CNFs in PP matrix, while the elongation of the micro tensile samples with weld line is considerably decreased comparing with those of unfilled PP samples.

Azieatul Azrin Dzulkipli and Azuddin [19] focused their study on effects of injection molding process parameters varying melt temperature, material and mold design. Three different molds with different design were fabricated and injected with molten polypropylene and polypropylene with glass fiber.

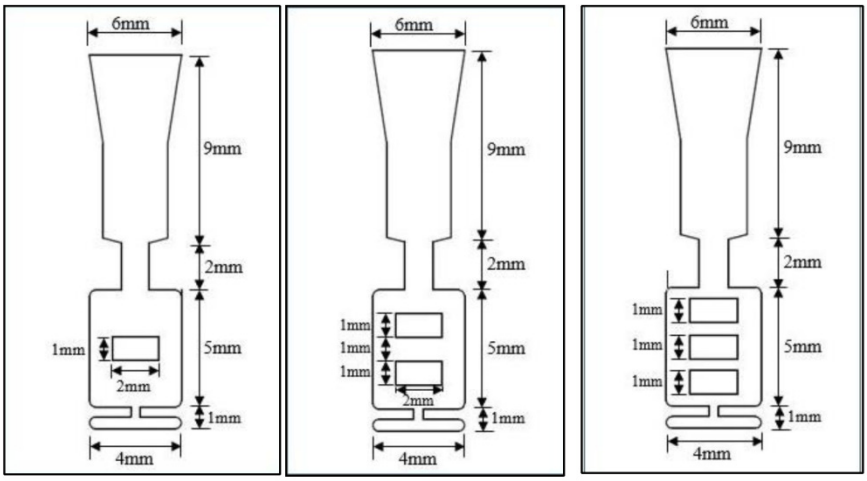

Figure 15. Different cavity design

In Figure 15, is shown cavity design used in their study, manipulating the number of same sized barriers. The experimental result of the length, angle and location of the weld line were compared to the result from Autodesk Simulation Moldflow Adviser software. They concluded that melt temperature influences weld line formation and when higher melt temperature is used, the formation of weld line decreases. Moreover, composition of fiber material must be taken into account in weld line formation as with higher filler weight weld line length is shorter and weld line angle is larger. Dedicated software is useful to preliminary test, but users must check on results experimentally because software sometimes gives different result.

Yizong et al. [20] wanted to investigate processing parameters of injection molded polystyrene samples using Taguchi method. Six parameters were selected for the injection molding process which includes, number of gate, injection speed, injection pressure, mold temperature, melt temperature and hold pressure. It can be seen from their results that the introduction of weld line onto the PS samples will have the most reduction towards the tensile strength. The other parameters had about the same degree of influence onto the tensile strength of dumbbell samples, but the polymer melt temperature had a slightly higher impact compared to the rest. Taking into account weld line thickness, mold temperature and melt temperature had much effect with inverse relationship; instead the injection pressure was directly proportional to the weld line thickness, but not having much effect onto the tensile strength. They proved that higher melt temperature and mold temperature can reduce the residual stress presented in the samples, making the weld line thinner and stronger.

Ozcelik [21] studied optimization of the effect of injection parameters such as melt temperature, packing pressure, cooling time and injection pressure on the mechanical properties of polypropylene (PP) moldings. Taguchi method was used and analysis of variance (ANOVA) was performed to study melt temperature, packing pressure and injection pressure effects. The most important parameter affecting the maximum tensile load and the extension at break (without/with weld line) was injection pressure and melt temperature, respectively. The other important parameters affecting the maximum tensile load for specimens with both without weld line and with weld line were packing pressure and melt temperature, respectively. The other parameters affecting the extension at break (without/with weld line) were closed to each other. The most important parameters for charpy impact strength (notched) (without/with weld line) were melt temperature and injection pressure, respectively. The other important parameters for charpy impact strength of the both specimens were packing pressure. The results of the mechanical tests were high under optimum conditions, in general. All mechanical properties gave linear relationships (based on values of r^2) with injection parameters.

Boyanova et al. [22] performed a micro indentation hardness (H) study to characterize the influence of processing conditions on the weld line, investigating samples in glassy polycarbonate (PC) and polystyrene (PS). Precisely they studied effect of processing parameters on the H-value across cold weld line. Indentations were taken with the diagonals parallel and perpendicular to the injection direction, since the melt flow induced orientation may affect the diagonal sizes and thus the micro hardness values too. They concluded that microhardness can be useful to define the region across weld line that the broadening of the weld depends primarily on the mutual chain diffusion from the two polymer fronts coming from opposite

sides and it was shown that the main factors affecting the quality of the welding on the line z=0 are, on one hand, the Tg of the polymer under investigation, and on the other hand the melt and the mold temperatures.

Ozcelik et al. [23] designed polypropylene specimen to be molded in cavities with obstacle having edge angle of 0°, 15° and 45° (Figure 16), located in the center of the mold. Mechanical properties such as tensile strength and izod impact strength (notched) of the specimens were measured by test methods.

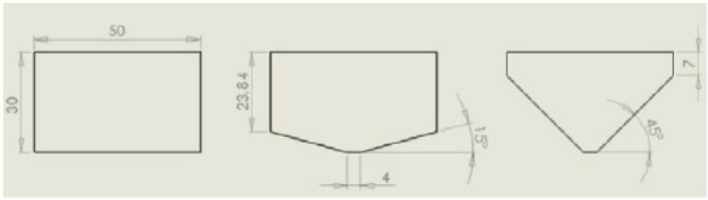

Figure 16. Design of obstacles

Molecular orientation was simulated in *Moldflow*, to give a better comprehension of experimental outcome, and to elaborate faster multiple cases (Figure 17).

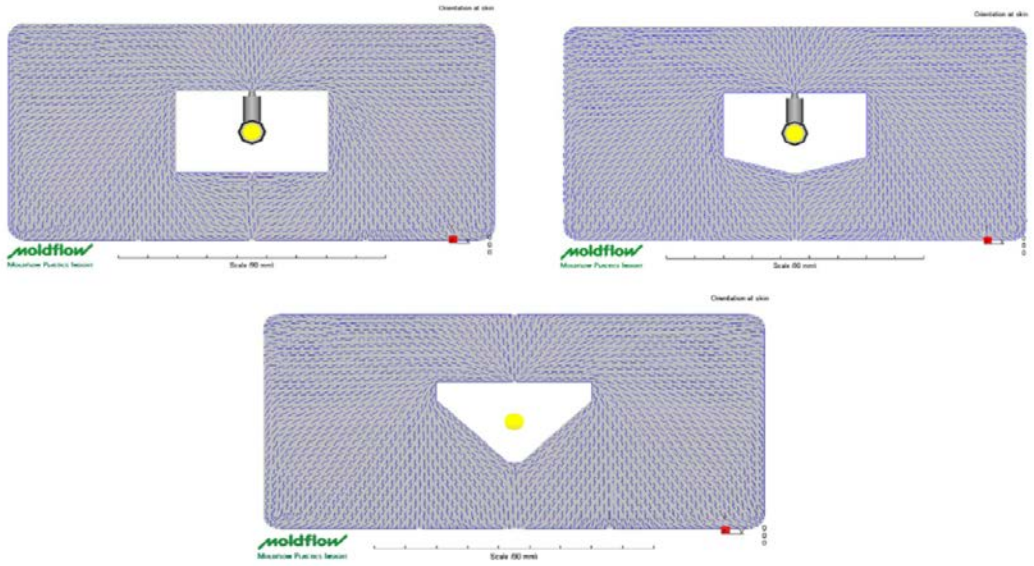

Figure 17. Moldflow analysis

This study was conducted varying melt temperature and packing pressure. The tensile and impact strength of specimens having a weld line were lower than the values obtained from specimens without a weld line. The impact strength of specimens revealed more significant change than the tensile strength. The impact strength for the specimen without a weld line tended to increase as the packing pressure increased from 14 to 20 MPa. But, this result was not valid for the specimen with a weld line. When the melt temperature and packing pressure increased, the tensile strength of specimen with weld line and without weld line did not show any major changes. But the impact strength of the specimens decreased in important ranges for both the conditions. Weld line tensile strength of injection molded specimens having obstacle edge angle (OEA) of 15° was obtained higher than the other obstacle edge angles.

Morelli et al. [24] test a polypropylene-ethylene copolymer (PP_{cop}-PX) filled with 20 and 30% by weight of talc, varying injection temperature and injection time. It was found that the impact strength of talc-filled polypropylene composites is influenced by the filler content and the processing conditions that affect orientation. The influence of the weld lines in the toughness of PP/talc composite moldings can be assessed by tensile-impact tests on samples punched off from the moldings at room temperature. The tensile-impact strength of the weld lines depends on the injection temperature and the injection rate, the influence of the latter being more pronounced at lower injection temperatures. Nevertheless, the main factor influencing the tensile-impact resistance is the orientation of the talc particles in the weld-line plane.

Janko et al [25] proposed a technique that acts when weld line forms using a flow obstacle placed in the cavity to redirect the melt streams in the weld line area. The change in flow direction alters the fiber orientation of PEEK+30% GF and so improves the mechanical properties.

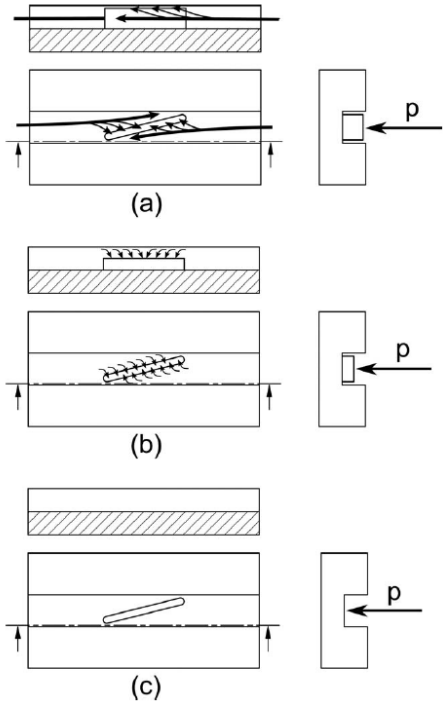

Figure 18. Janko et al. flow obstacle operation

In Figure 18 is described flow obstacle operation: (a) As the obstacle diverts the melt flows entering the mold from left and right, material also begins to enter the narrow gap between the top surface of the obstacle and the opposite mold face. (b) Rising pressure on the top surface starts to push the obstacle out of the mold.
(c) The obstacle in its fully withdrawn position. Once the part is ejected, a spring moves the obstacle back into the cavity in preparation for the next shot. Worth mentioning that because the obstacle is inserted and ejected from one side of the mold, the fiber orientation varies across the thickness of the specimen, so flexural tests must be performed from both sides. The flexural results for the specimens with modified weld lines showed significant differences according to which side was uppermost in the test rig, but overall showed a big improvement in both flexural strength (up to 66%) and flexural strain at strength (up to 92%) compared with specimens with standard weld lines. The reason for the dependence on the tested specimen side is found in the presence of so called “side weld lines,” which are created during the filling phase, that provide points for fractures to start. The limitations of the modified weld line technique become apparent under pure tensile testing, where the improvement compared with standard weld lines is about 20% for tensile strength. Once a crack has formed, the load-bearing area decreases instantly, increasing the stress in the remaining cross-section and leading to complete failure.

Park et al. [26] used high frequency induction to heat mold surface over glass transition temperature of PC with the aim to eliminate weld lines, producing a cell phone cover. This technique has been proven capable to achieve an heating rate of 40°C/s, and applied to the case in object weld depth was greatly reduced with the aid of induction heating, from 2.943 μm to 0.298 μm at most, proving its effectiveness without significant increase in cycle time.

Cheng et al. [27] used electromagnetic induction heating combined with coolant cooling to create a mold surface temperature control system, with the aim to eliminate weld line surface mark and increase weld line strength. They also operated a computer simulation, that gave slightly different results, but consistent with measured values. Their experimental set up provides a 3s heating to take plate central temperature from 110°C to 180°C, and 21s to return to 110°C. Then a second cycle was performed to take plate central temperature from 110 to 210°C, in 4s, with a following 21s cooling to return to 110°C. Their results indicated this technique to be effective, eliminated weld line mark and enhancing weld line strength for injection molded ABS tensile bars.

Wang et al. [28] investigated the effects of cavity surface temperature on mechanical properties of molded specimens in rapid heat cycle molding. Thanks to rapid heat cycle molding (RHCM) the cavity surface should be thermally cycled in a relatively large temperature range by rapid mold heating and cooling technologies, avoiding premature freezing and eliminating frozen layer. In their study was used general purpose polystyrene, polypropylene, high gloss ABS, high gloss ABS/PMMA, ABS/PMMA/nano-$CaCo_3$ and PP with 20% short fibers (FRPP). The main processing parameters in RHCM include melt temperature, cavity surface temperature just before filling, injection speed or time, packing pressure, packing time and cooling time. In their experiments, only T_{cs} (cavity surface temperature just before filling) was changed. It was found that, considering tensile strength, the weld line factor or weld line integrity of PS can be improved while that of FRPP can be conversely decrease by increasing T_{cs}. For PP, ABS, ABS/PMMA and ABS/PMMA/nano-$CaCO_3$, the weld line factor is always close to 1.0 although it tends to increase with the increase of T_{cs}. The weld line factor of FRPP is, instead, less than 0.4. Considering impact strength, the weld line factor of PS fluctuates in the range of 0.8–1.0, but for PP are over 1.0 indicating a positive effect. For ABS, ABS/PMMA and ABS/PMMA/nano-$CaCO_3$ instead, a negative effect was noticed. For FRPP, the weld line factor on impact strength varies in the range of 0.5–0.8, the lowest value of which is much higher than the weld line factor on tensile strength. It indicates that the negative influence of weld line on the impact strength for FRPP is much smaller than that on tensile strength.

Wang et al. [29] also tested the effect of RHCM on surface appearance and tensile strength of molded specimen. In this study they implemented thermal cycling experiments to investigate cavity surface temperature responses with different heating time and cooling time, and how these affects the aforementioned specimen properties. In this case, only ABS/PMMA and PP with 20% glass fibers (FRPP) were used. The results showed a slightly tensile strength reduction for ABS/PMMA, but a slightly increase for FRPP. Surface appearance was significantly improved eliminating weld line and jetting marks and giving a glossy finish.

Sorgato et al. [30] investigated the effect of a nano structured mold surface on PET molded samples. They used laser-induced periodic surface structures (LIPSS) to induce the slip of polymer melt over mold surface in an open flow channel, using a micro injection molding machine. Results showed a reduction in filling flow resistance using LIPSS oriented aligned to flow direction, which allowed a maximum pressure reduction of 23%, due to the high values of slip velocity. As a consequence, lower resource consumption and shorter cycle times were required, reducing cost and environmental impact. A test on polypropylene was also conducted by Masato et al. [31], using different LIPSS orientation. It was shown that orienting ripples in the direction parallel to the flow favours the bending of the adsorbed chain loops, and thus promoting the disentanglement from those adsorbed in the bulk. The highest drag reduction was obtained with intersecting ripples (13%), and smaller but still significant reductions were observed in parallel (8%) and transversal flow ripples (3%).

Shia-Chung Chen et al. [32] studied the effects of TiN and Teflon coatings of various thicknesses on cavity surface, molding a tensile bar specimen designed with double gate. The aim of their study was to test the effect of lower thermal conductivity coatings on mold surface, to maintain the melt temperature higher during filling stage, to obtain better part properties. It resulted that, with 4 μm thick TiN coating, the initial contact temperature was nearly identical to that of regular injection molding without any surface, thus it didn't help to eliminate weld line and showed no significant improvement in part quality. Conversely, with 10 μm thick Teflon coating, the initial contact temperature was nearly identical to that of regular injection molding without any surface coating. As a result, its effect on weld line mark elimination and tensile strength increased significantly. When Teflon surface coating is combined with IR heating, the heating rate, the initial contact temperature, and the associated tensile strength were all further increased.

Pengcheng Xie et al. [33] also used surface coatings to realize rapid thermal cycling (RTC) in injection molding. They used carbide-bonded graphene coating, which was deposited on surface of the silicon cavity through chemical vapour deposition, which allowed depositing a 3.5 μm thickness. The coating was applied on two different silicon molds, with different surface roughness. In their tests four different mold temperatures were used to identify its effect on weld line, and other four different cavity temperature were performed to discuss effects on residual internal stress and replication fidelity. This new RTC setting allowed an improvement in product surface quality and narrowed the weld mark or even eliminated it completely, enhancing average tensile strength by 37.77%.

Masato et al. [34] used diamond-like carbon (DLC), chromium nitride (CrN) and chromium titanium niobium nitride (CrTiNbN) coatings for thin wall small parts injection. They produced PP specimens in an open flow channel and tested coatings application to promote filling through melt flow resistance reduction, due to wall

slip. The results showed that the DLC deposited on chrome substrate is the coating that most significantly reduces the cavity pressure drop for the selected polystyrene (−28% compared to the uncoated insert). Limited effects were observed with CrN (−3%) and CrTiNbN (−2%) coatings, while an increase flow resistance (+6%) was observed with the DLC deposited on chromium nitride. It was observed that cavity pressure drop is inversely dependent on the slip velocity, thus indicating the importance of selecting a proper mold surface coating.

Lu et al. [35] tested the effects of ultrasonic oscillation and ultrasonic oscillation-induced modes on weld line strength. They used polystyrene and a blend of polystyrene (PS) and high density polyethylene (PS/HDPE 90/10). During injection molding, the ultrasonic oscillation induced modes are Mode I – ultrasonic oscillations were induced into mold at the whole process of injection molding and Mode II – ultrasonic oscillations were induced into mold after injection mold filling. They reported that ultrasonic oscillations have great influence on weld line strength of PS, especially with Mode II settings, thanks to an enhanced molecular diffusion in the weld line zone. Even if molecular diffusion is promoted, at the skin still poor bonding at the interface and ultrasonic oscillations caused a wider skin than in their absence. For PS/HDPE blend, ultrasonic oscillations still increase weld line strength, with improvement similar to PS. Worth to mention that they noted, that in case skin layer at weld line is removed, Mode I resulted more effective than Mode II.

Xie et al. [36] also tested ultrasonic oscillation efficiency on weld line strength, but they made microinjection molded polypropylene (PP) samples. Mode I and II are the same as described in the previous study. Their research confirmed the effective improvement in weld line strength using this technique, but they found that Mode I gave better effects in all ultrasonic output power varying range. With the ultrasonic oscillation function, the weld line appeared as a curve which means one flow front flew into the other flow front. Additionally, the ultrasonic oscillation almost erased the V notch in weld line area according to the AFM test and optical microscope observation.

Shuai et al. [37] used gas counter pressure (GCP) technology to contrast negative fountain flow effect. GCP can impose a reverse pressure acting on the melt at flow front, that inhibit the fountain effect in the melt filling process, decreasing the dimensional shrinkage of molded samples, increasing dimensional accuracy of samples, and effectively improving impact property of samples. The schematic process used in their study is shown in Figure 19.

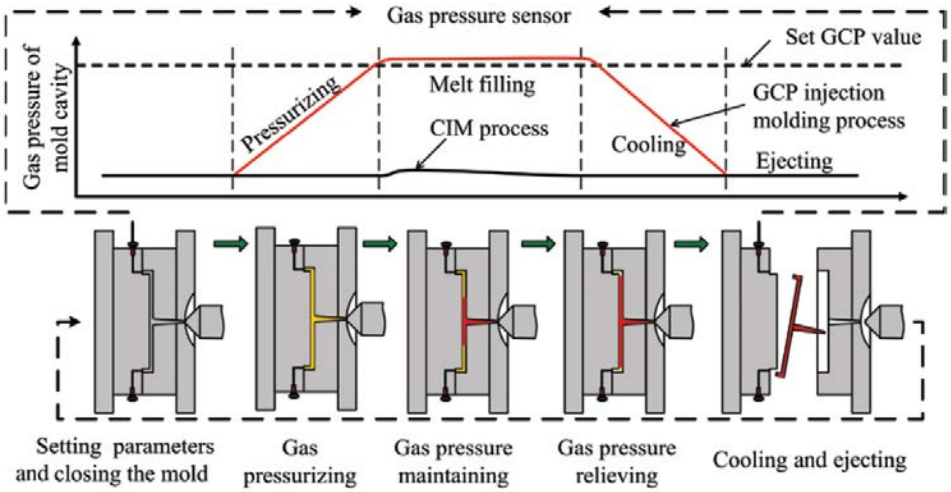

Figure 19. GCP injection molding process and comparison between CIM and GCP gas pressure curves

In their paper, they respectively used short shot and full shot injection molding to investigate the effect of GCP and GCP holding time in molding process on melt filling process and qualities of molding plastic parts. Results showed that GCP process obviously affects melt filling process. The higher the GCP in melt filling process, the smaller the "fountain effect" of melt flow front, the smoother the surface of melt flow front, and the smaller the volume of short shot molding samples. Moreover, GCP process decreased the dimensional shrinkage of molded samples and increased the dimensional accuracy of samples. Impact value was also improved, as well as tensile strength and flexural strength of samples.

Kikuchi et al. [38] developed a vibration assisted injection molding (VAIM) setup, based on the concept of using motion of the injection screw to apply mechanical vibration to polymer melt during the injection and packing stages of injection molding process, to control the polymer behaviour at a molecular level to improve/alter mechanical behaviour of molded products. In this study, influence of delay time to begin vibration (t_{del}), vibration duration (t_{dur}), vibration frequency (f), intracycle compression duration (t_{com}), and intracycle decompression duration (t_{dec}) was studied. It was found that VAIM processing can significantly strengthen molded polymer samples and improve product uniformity from cycle to cycle. The actual degree of strength improvement depends on at least four parameters; which are vibration frequency, vibration amplitude, vibration duration, and the delay time between the injection start and the vibration start. When these parameters were optimized for polystyrene, as much as a 28% strength improvement can be achieved. The toughness of the products manufactured was also increased.

Cao et al. [39] patented an injection molding process based on a spinning device. After the mold is filled and the polymer adjacent to the walls of the mold has begun to solidify, a pin located in the middle of the cavity is spun transversely to the direction of the polymer melt flow. It was found that this application increases energy at yield of about 20% in the circumferential direction because of drag flow induced orientation resulting from core pin rotation.

Rawson et al. [40] explored the combination of Shear Controlled Orientation Injection Molding (SCORIM) and Bright Surface Molding (BSW) to remove surface weld lines in highly reflective aluminium pigmented polypropylene. This two technique in series are called SBM, and it consists in a first stage (MODE A) were a reciprocating piston movement to realign the filler along flow direction, followed by a stage when holding pressure is maintained until gate freeze (MODE C). The process is shown in Figure 20.

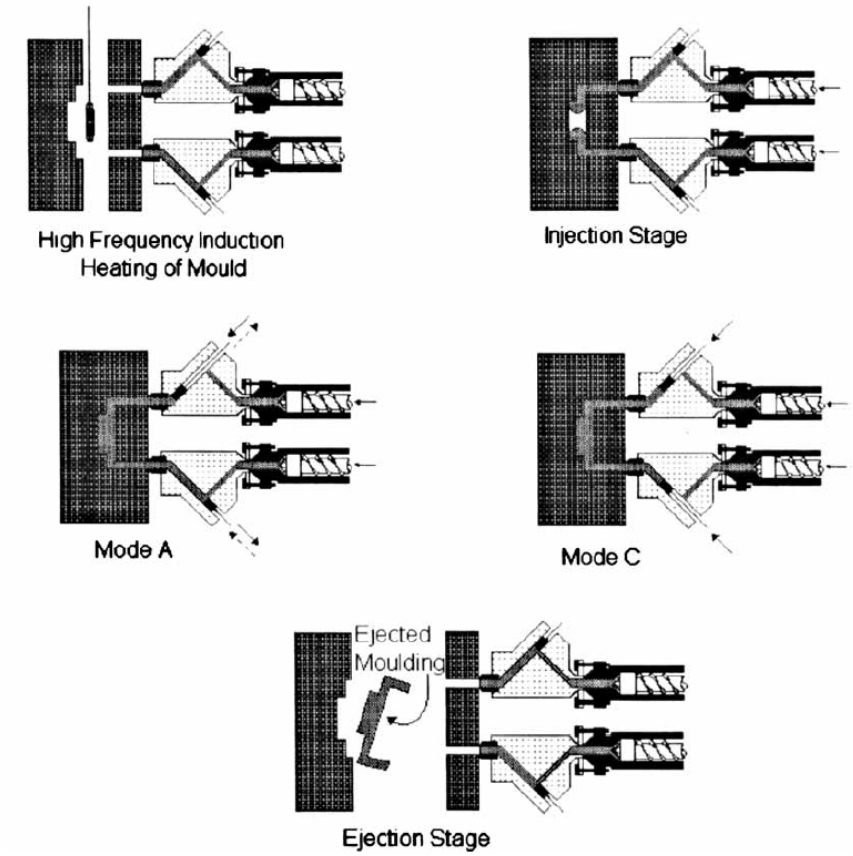

Figure 20. Schematic representation of the significant stages of the SBM process

Weld line removal was tested using BSM and then using SCORIM. Neither technique has been found completely useful in weld line elimination when used alone, however, when SBM was used, weld line removal was successful and moldings showed a high quality of surface finish. The high temperature of the mold cavity surface induced by BSM, was able to prevent any solidification of a skin layer for a sufficient time to enable SCORIM to realign the Al flake and polymer molecules at the molding surface in the direction of flow. In conclusion, with the use of the SCORIM and BSM technologies (SBM) in series with an adapted

conventional molding machine, and with the informed application of shear to the mold cavity melt, it was possible to reproducibly remove surface weld lines to an acceptably high quality of surface finish.

Waschitschek et al. [41] studied the influence of push-pull injection molding technique on fiber reinforced polypropylene. PPP (push-pull processing) enables control of shear rate and temperature history during solidification. While melt is solidifying, an alternate injection is applied from two nozzles, moving the polymer back and forth the cavity. Thus, after filling from one side, PPP replaces or postpones packing and injection start from the other nozzle while pressure is taken from the previous nozzle. Then an alternating injection is applied, until cavity is filled with oriented and solidified polymer. This process enables control of the flow during cooling and solidification and hence allows orienting reinforcing fibers in flow direction. Injection pressure and fiber length have more influence on fibre orientation than the frequency of oscillation. The interlaminar shear strength tests show only a small effect of PPP on fiber reinforced thermoplastics.

1.4 Focus on techniques used in this work

1.4.1 In-flow

Kazmer and Roe [42], [43] presented a new technique that could lead to a weld line strength improvement without process or cost further expenses, which exploit the material possibility to re-orient fibers and modify weld line surface during packing phase.

Di Tocco et al. [44] designed a cavity with an 11x11 array of holes on a 2.54 mm spacing for use as a pin grid array zero insertion force socket. They used neat and 40% talc filled polypropylene through two tab gates located on opposite ends of the same side wall. Their purpose was to show the effects of in-flow and process parameters on weld lines strength in different sample regions. In-flow is defined as the below-frozen-skin flow in the cavity, after filling, and considering that this flow can differ from the principal one involved during filling, it has been considered as a way to re-orient fibers and change properties in the weld line area.

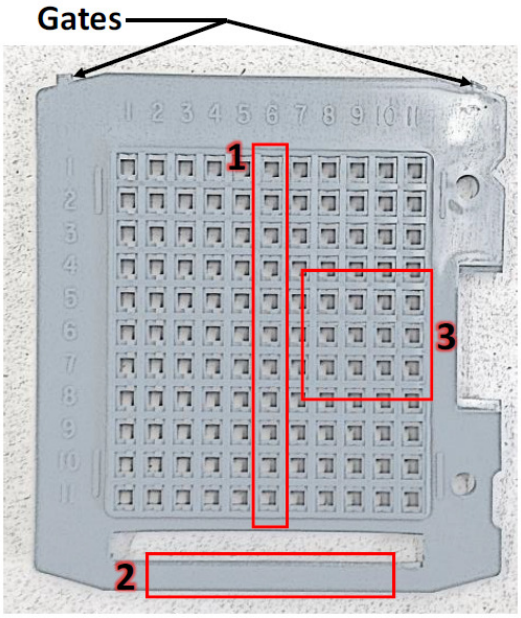

Figure 21. Cavity with 11x11 arrays of holes

In Figure 21, is shown cavity design and are highlighted the three regions considered to evaluate weld line properties. In region 1, weld line is formed by the two flow fronts meeting each other in the middle of the sample; in region 2, weld line is formed by the two flow fronts colliding at the very end of flow; in region 3, weld lines are formed after the flow is separated because of hole

presence, and then rejoined, allowing testing of the hypothesis that subsequent in-flow during filling improves the weld line performance.
A first run was necessary to set the zero for weld lines positions to provide reference results for the tests, and was obtained via process settings listed below (Figure 22).

Processing Condition	Setting
Feed Throat (°C)	40
Nozzle (°C)	230
Zone 1 (°C)	225
Zone 2 (°C)	210
Zone 3 (°C)	205
Zone 4 (°C)	200
Zone 5 (°C)	190
Mold (°C)	40
Injection Velocity (mm/s)	20
Pack Pressure (MPa)	20

Figure 22. Reference processing conditions

A series of four design of experiments (DOE) run was implemented to evaluate the effects of high and low temperature, injection velocity, and packing pressure were centered around the reference process described above, with the injection velocity.

	Design of Experiments Run			
Processing Condition	**1**	**2**	**3**	**4**
Zone 1 Temperature (°C)	260	260	210	210
Coolant Temperature (°C)	21	21	54	54
Injection Velocity (mm/s)	20	70	20	70
Pack Pressure (MPa)	15	25	25	15

Figure 23. Design of experiments

Each DOE presented in Figure 23 was repeated for the neat and talc-filled polypropylene.
Results on twin-gated bar specimens are shown in Figure 24.

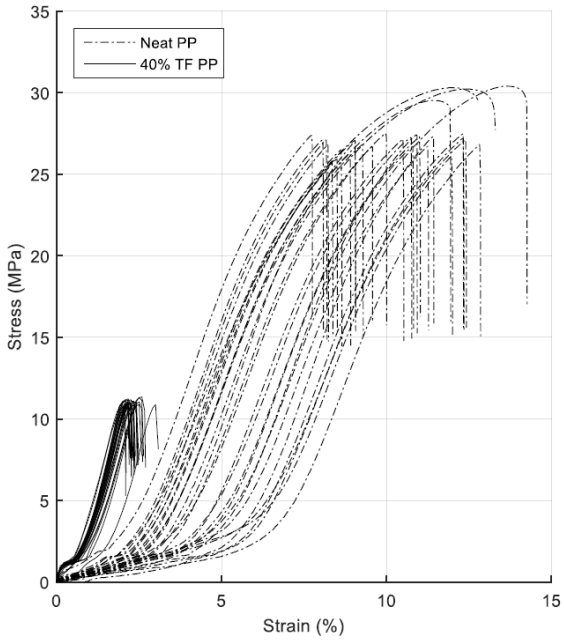

Figure 24. Stress-strain behaviour of twin-gated tensile bars molded of neat and 40% talc-filled PP

They observed that the neat PP has a modulus of 273 MPa (standard deviation of 70 MPa) and weld line strength of 25.4 MPa (standard deviation of 2.1 MPa). By comparison, the 40% TF PP has a higher modulus of 492 MPa (standard deviation of 41 MPa) but lower weld line strength of 9.9 MPa (standard deviation of 0.5 MPa).

Considering the different regions and plotting stress-strain behaviour at DOE run condition 1, results are shown in Figure 25, respectively on the left for neat polypropylene, and on the right for talc filled polypropylene.

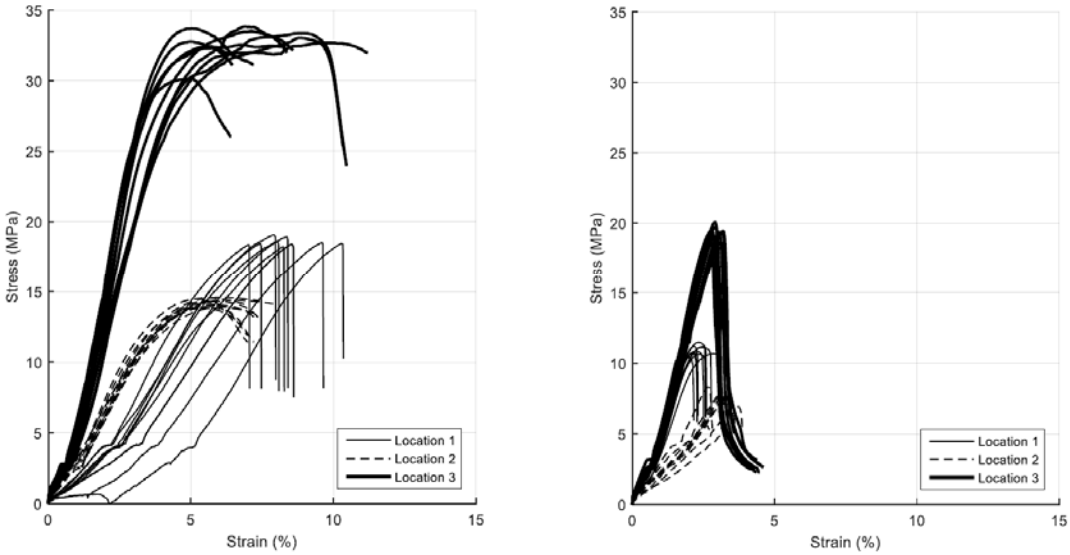

Figure 25. Stress-strain curves for neat (left) and talc-filled (right) polypropylene

For neat PP:

- at location 1, weld line has an ultimate strength of 18.2 MPa, a little lower that reference;
- at location 2, weld line has a lower ultimate strength of 14.3 MPa that may be caused by the lower pressure and faster cooling at the end of the flow, leading to a reduced interfacial healing;
- at location 3, instead, ultimate strength is of 32.3 MPa, higher than reference, suggesting that in-flow can e useful to improve weld line properties in the flow direction.

For talc-filled PP:

- at location 1, weld line has an ultimate strength of 10.9 MPa, closed to reference value;
- at location 2, weld line has a much lower ultimate strength of 7.2 MPa, due to poor interfacial healing. Fracture surface examination showed a talc filler agglomeration at the interface;
- at location 3, the ultimate strength of 19.1 MPa is significantly higher than in location 1 and 2, suggesting that in-flow can be used also in filled polypropylene application to improve weld line properties.

To further understand in-flow outcome, they performed analysis of variance (ANOVA) to verify the statistical significance of the investigated factors. The results indicate that the two most significant factors are the material being talc-filled (TF) followed by the presence of in-flow. The temperature, injection velocity, and pack pressure of themselves were not found to be statistically significant at the 95% confidence level while their interactions with the material and type of flow were found to be significant. These results imply that the effect of the processing parameters is dependent on the type of material and flow forming the weld line.

Based on the ANOVA results, a multiple regression model was fit to the 230 strength observations as a function of interactions, and the results suggest that the effect of in-flow is not only statistically significant but physically dominating, with the presence of in-flow increasing the weld line strength by 14.1 MPa. Adding the 40% talc-filler reduces the weld line strength by 7.0 MPa. The process conditions have been found to be less significant.

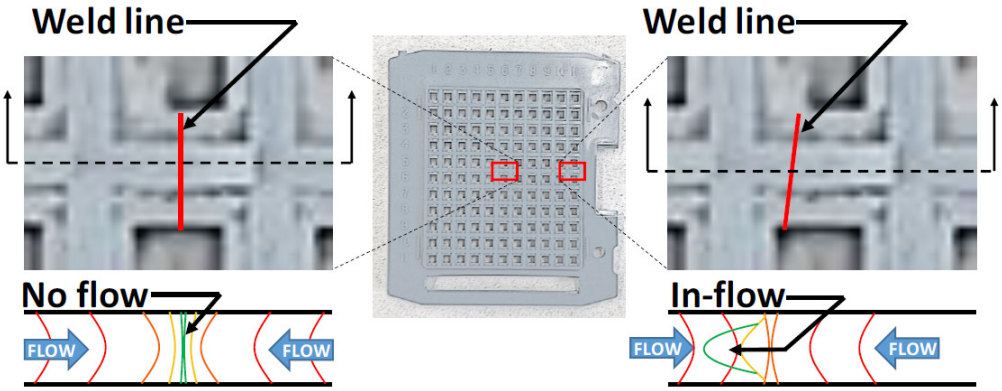

Figure 26. Weld line formation with no flow (left) and in-flow (right)

In Figure 26, the in-flow phenomenon is shown. It can be seen that the in-flow associated with ongoing process, let the polymer melt to continue stream across the initial weld line interface. Thus, in-flow not only causes a larger interfacial area but also conveys additional heat by melt convection that serves to delay cooling and foster greater intermolecular diffusion to increase the weld strength.

At the end of their article, simple guidelines for products and mold design using in-flow are lists, and here summed:

- Considering an object like the one in Figure 27, it is suggested to place the gate with an offset from the plane of symmetry, to improve weld lines strength inducing in-flow.

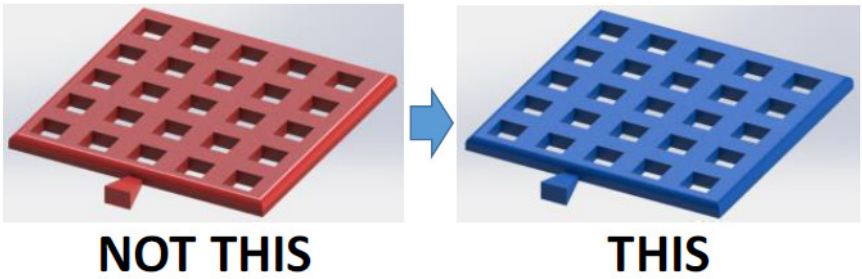

Figure 27. Edge gate placement off plane of symmetry

- Considering an object like the one in Figure 28, placing the gate on the side than on the top will produce stronger weld lines, thanks to in-flow.

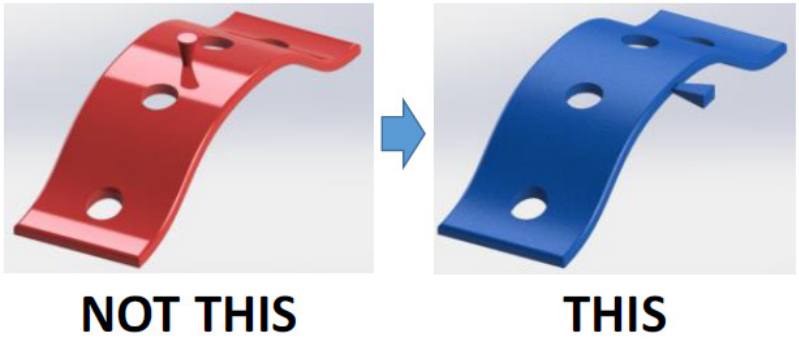

Figure 28. Edge gate preference over centered pin gate

- Considering an object like the one in Figure 29, a central gate may cause knit-line issues. The use of an off-centered over-flow as shown at right will tend to improve the weld line performance due to post-filling in-flow. The over-flow is designed to minimize melt pressure imbalances while also being designed with a gate to easily remove and recycle

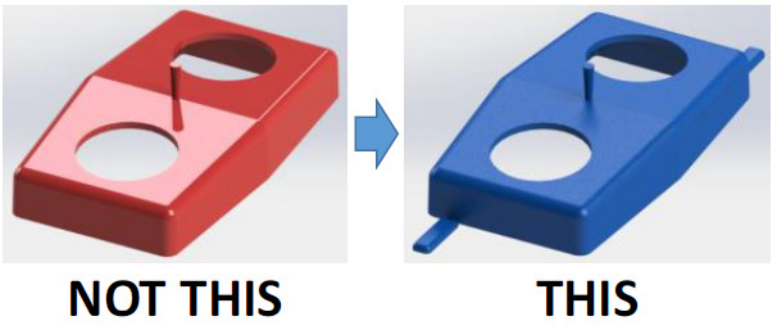

Figure 29. Use of over-flows to induce in-flow

Scantamburlo et al. [45] produced a cavity to promote in-flow phenomena via pressure gradient due to material hesitation during filling phase. In Figure 30, is shown cavity geometry. The side features will be filled during packing phase and they are positioned near weld line formation section, to induce a material and fiber re-orientation, modifying local morphology and mechanical properties.

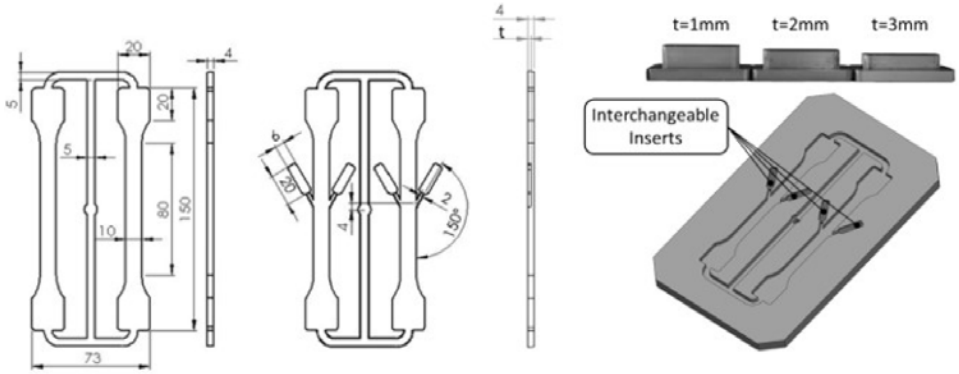

Figure 30. In-flow and no in-flow cavity and removable inserts to vary in-flow entity

Thanks to short shot, shown in Figure 31, it can be noticed that lateral appendixes are actually filled due to pressure gradient after switch over.

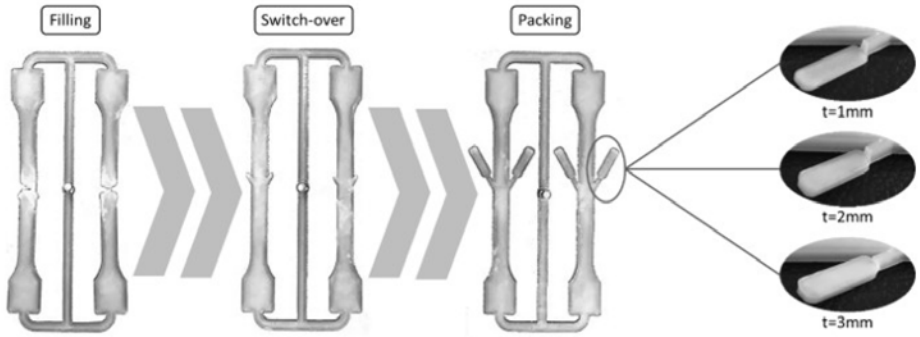

Figure 31. Cavity filling pattern

After molding, appendixes have been removed and tensile tests have been performed at 1mm/min constant speed, until specimen failure occurred. Fracture surfaces are then analyzed with Scanning Electron Microscope (SEM) to evaluate fracture surface, fiber orientation and failure mode at weld lines.

Moreover, a numerical simulation has been performed via *Autodesk Moldflow Insight 2019®*. In Figure 32, the comparison between numerical and experimental data shows how in-flow can effectively modify weld line position and morphology.

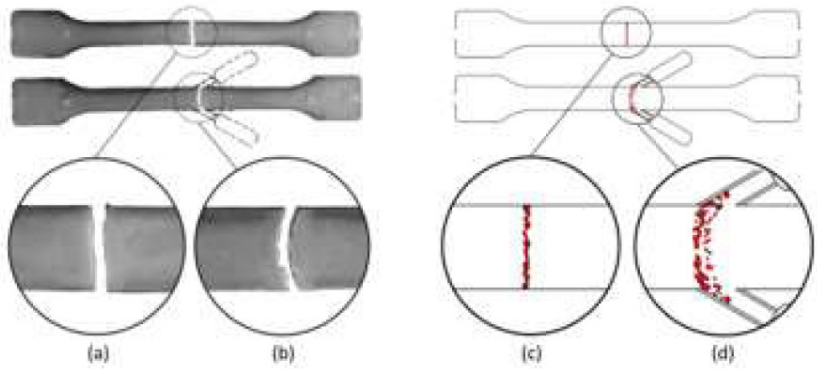

Figure 32. No in-flow (a, c) and in-flow (b, d) weld lines morphology both experimental (left) and numerical (right)

SEM analysis showed a better fiber distribution in the weld line area, with enhanced interfacial bonding. Results showed a 19% stress at failure increment and a 15% tensile strength.

1.4.2 Variotherm

The basic principle behind variotherm systems is trying to be as close as possible to ideal molding condition, in terms of having a hot mold during the injection stage and a cold mold during the cooling stage. To achieve this objective, starting from 1960s, different methods have been proposed, such as electric heating, induction heating, gas heating, flame heating and infrared heating [46].
The heating method used in a variotherm system is different based on requirements for injection molding process, and they can be classified into four principal categories by the type of heat supply.

- For mold heating by convection, a distinction is made between direct and indirect heating of the cavity surfaces. Dry hot air can be blown directly into a mold and fluids are used to heat the mold indirectly via fluid channels such as water, oil or steam. Different kinds of convective heating methods are used in industry, principally gas and liquid. Heating oil is the most widely used medium in injection molding processes.

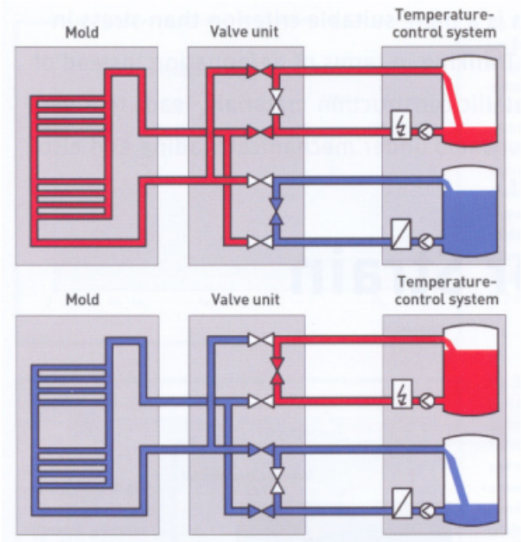

Figure 33. Example of convection temperature control system via fluid coolant

- Radiation heat is transmitted rapidly to objects in the form of rays and waves. Different studies have been conducted using infrared rapid heating system, external infrared radiation sources, infrared lamps, electromagnetic radiation, high frequency proximity heating, dielectric hating and laser.

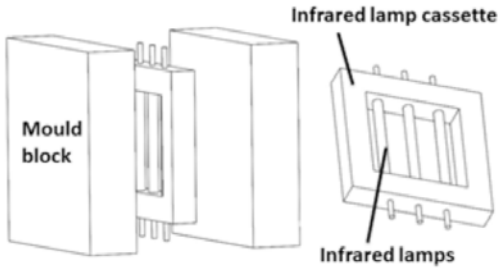

Figure 34. Example of radiation heating via infrared lamps

- Electrical resistance heating and heating cartridges can be directly integrated into the injection mold; the generated heat reaches the cavity surface by conduction. Among heating methods, electrical resistive heating is the most widely used in variotherm systems. It is quick and energy efficient to control the mold surface temperature in this way. However, heat conduction is a diffusion process, heating a thick mold would take considerable time, so this method is only suitable for heating thin shells, in which the geometry is simple and the mold material has a high thermal conductivity.

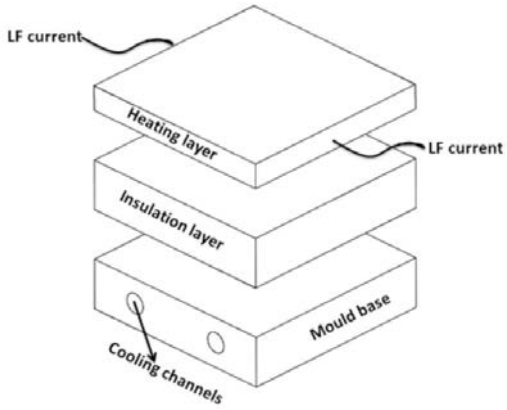

Figure 35. Schematic of electrical resistive heating

- Induction heating is the result of eddy current losses in the conductive metal mold cavity, which are generated with an alternating current field. The heat is generated directly in the mold; very high heating rates are possible. Induction heating combined with water cooling is also used widely in the variotherm systems in micro injection molding. The biggest difference from electric resistive heating is that this method is much more flexible when heating the mold, the heating coil does not contact the mold surface, and its energy is also focused onto the mold surface rather than the mold base. Inductors can be internally or externally positioned, each with its pros and cons. An ultrasonic molding method was also tested, but it was designed specifically for manufacturing small and precise plastic parts.

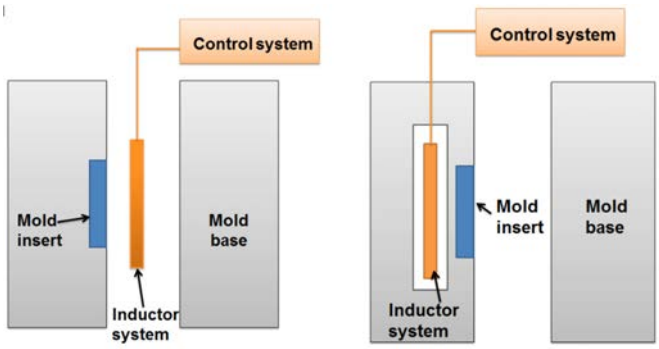

Figure 36. Schematic of external (left) and internal (right) induction heating

Each of the precedent categories has produced improved molded parts, but it must be taken into consideration also the temperature uniformity and cycle time of the different techniques while designing mold geometry and molding process, to chose the one suitable for the desired application. Moreover, energy consumption of some of the aforementioned heat supply may lead to additional costs. In terms of weld line improvement, when using a variotherm system during the injection process, this defect occurs less frequently.

The attention has been focused on heating methods because they are much more challenging than cooling methods in designing a variotherm system. Typical cooling design suitable for variotherm applications are limited and water still the most widely coolant used. Moreover, compared with the heating stage, the cooling stage can be conducted at a slower rate, which is often sufficient for some thick parts.

1.4.3 Bi-injection molding

Bi-injection molding is a process in which two different resins are simultaneously injected at different locations in the same mold. As the materials flow into the mold, they meet along a common interface and cross-polymerize. Bi-injection is relatively simple and is only used to produce simple, low-tolerance parts. The interfaces naturally formed when the separate resins meet are usually very simple planar surfaces. In Figure 37, a schematic illustration of bi-injection molding machine and process is illustrated.

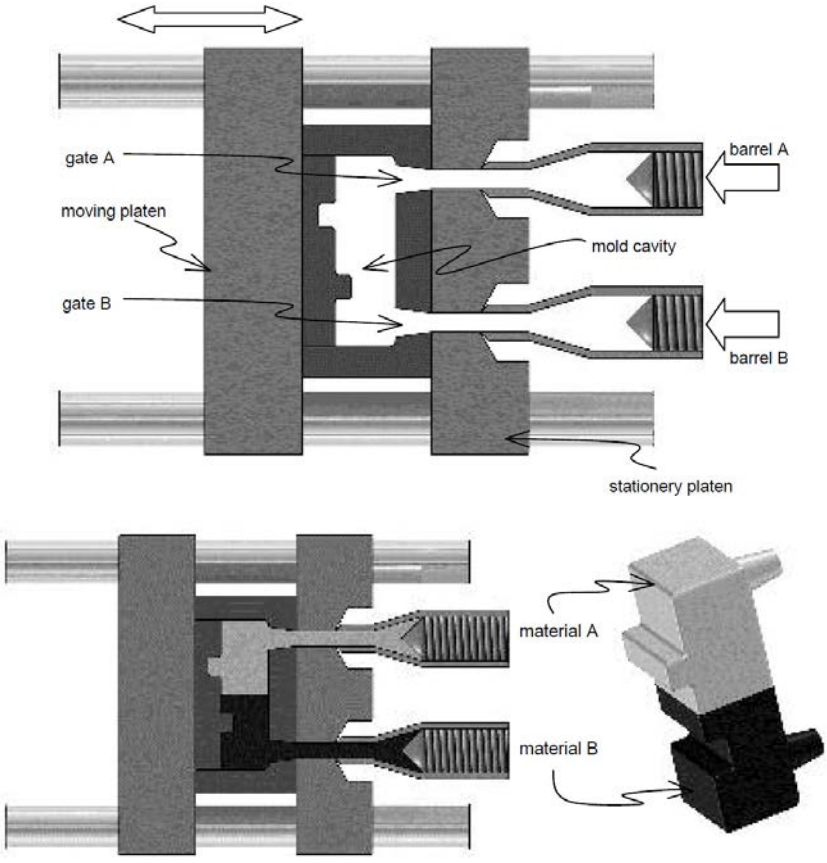

Figure 37. Bi-injection molding machine and process illustration

Kiyotaka Tomari et al. [47], using SCI (Simultaneous Composite Injection), reported that weld line is strengthen by "back flow" during the holding stage. The back-flow is expected to occur when there is a difference of holding pressure between two cylinders of the SCI molding machine. In their tests, they used fiber reinforced polycarbonate and neat polycarbonate to evaluate the effect of pressure difference between two injection cylinders on the back-flow phenomena.

They examined three pairs of injection combinations: PCGF/PCGF, PCGF/PC, PC/PC. One material in each pair was coloured to identify weld lines.
In Figure 38, results for PCGF/PCGF at different pressure gradients are shown.

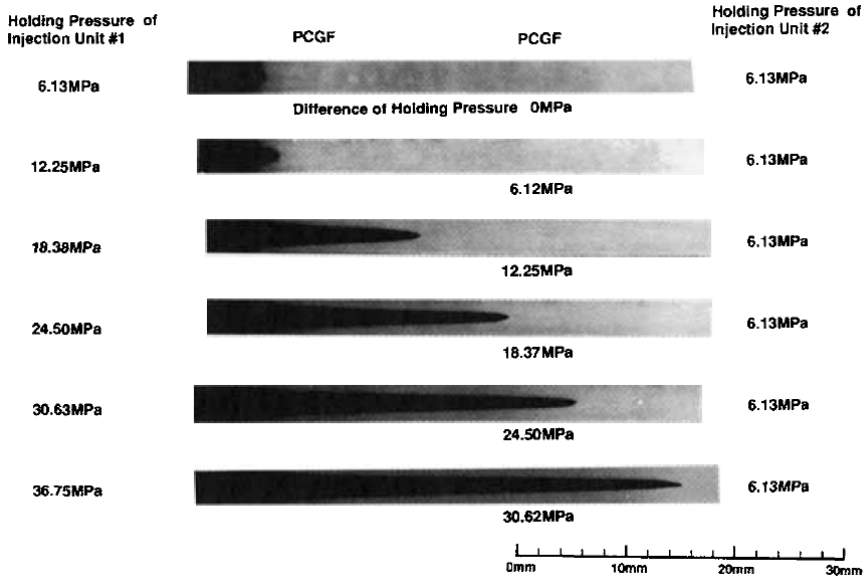

Figure 38. Weld line geometries of PCGF/PCGF

It is clear that as the pressure difference between the two injection units increases, weld lines are subjected to increasing axis deformations. Weld line formed on mold surface, instead, doesn't move with increasing pressure gradients. Results for PCGF/PC and PC/PC show similar trends, but lower inclinations due to the fact that unfilled PC is difficult to flow n the holding stage.
Submitting obtained specimens to tensile tests, using as reference the one molded when the pressure difference was 0 MPa, they found that the fracture position was changed by pressure difference. These results were obtained for PCGF/PCGF samples, as the other combinations yielded before they broke at the weld line.
In terms of weld line strength, it shows an increasing trend with increasing pressure differences for PCGF/PCGF. For differences above 20 MPa, weld strength was nearly 100% of non-weld strength. Weld line strength trend with difference of holding pressure is illustrated in Figure 39.

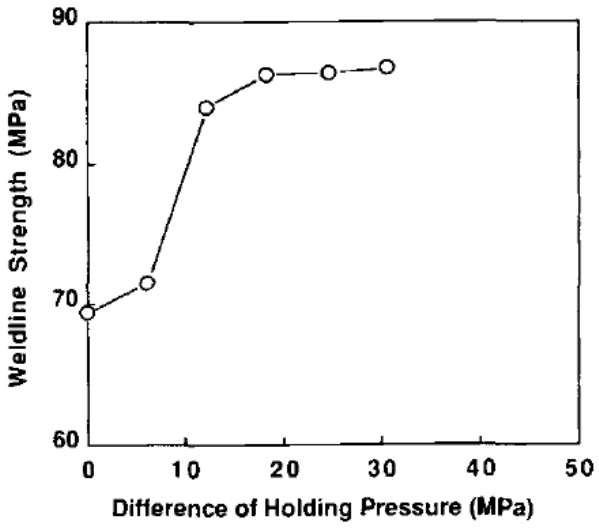

Figure 39. Pressure difference dependence of weld line strength for PCGF/PCGF

The weld line strength of unfilled polymers could not be improved even when back-flow occurred, considering that there was not the same effect of molecular reorientation due to the back-flow as in the case of fiber filled materials.

1.5 Objectives of present study

In this study, dog-bone specimens (Figure 40) will be molded in 50% wt glass fiber reinforced polypropylene. This material has been chosen in order to evaluate the process effects on a material that would fit a structural application.
A double-injector equipped injection molding machine has been used to operate filling phase with both injectors active but packing phase uses a single injector active.

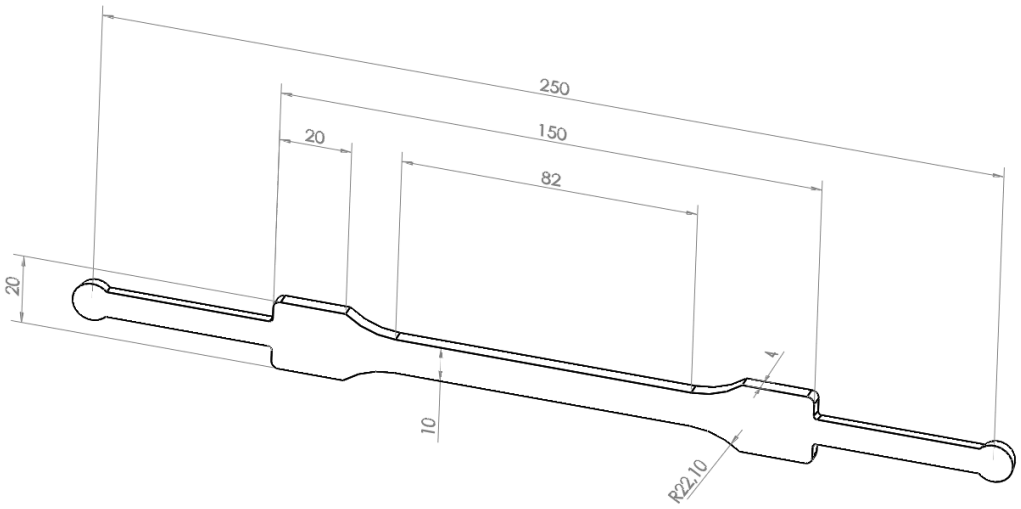

Figure 40. Cavity design used

The purpose is to evaluate how the present design of experiment (DOE) can be effective in enhancing weld line properties and geometry with the present material. The idea behind the design (similarly at Kiyotaka Tomari et al. [47] described in the previous section) is to provide a mechanical movement of weld line surfaces by the generation of a pressure gradient and an associated flow, to re-orient fibers and obtain a better orientation in flow direction. Moreover, the resulting flow is expected to have effect on weld line geometry, enhancing local properties.

As previously explained, weld lines represent one of the major causes of structural weakening, and their effect is emphasized in reinforced polymers, in particular in presence of highly loaded material. Fiber reinforced polymers are nowadays used in an increasing number of applications, thus it is of fundamental importance to ensure that the components made of polymeric material, especially if used in the metal replacement perspective, possess the qualities and reliability that is guaranteed by metals.

To test the proposed process improvement outcomes, a first study using a single nozzle configuration was performed, both numerical and experimental, to validate numerical model. Then, numerical analysis of a double nozzle configuration has been implemented. Comparison between the results of the two configurations will be evaluated in order to prove the DOE effectiveness.

In the following chapters, the steps to obtain the information mentioned above will be widely exposed. Starting from material characterization and the relative tests, followed by experimental setup in terms of equipment, mold and cavity design and concluding with tests on specimen and simulation output verification, the processes and test peculiarity will be discussed, and conclusions will be drawn.

CHAPTER 2

Material characterization

This chapter focus on the material used in this study and its characterization. In particular, capillary rheometer, rotational rheometer and a differential scanning calorimetry (DSC) were used to determine viscosity curves, pVT diagrams, transition temperature and specific heat capacity.

2.1 Polymeric materials rheological behaviour

Thermoplastic polymers are characterized by primary bonds (covalent) that hold the atoms and secondary molecular bonds that hold group of polymer chains together. The last mentioned bonds are the weaker ones, and they are responsible of the overall resistance the material offers. If temperature increases, these bonds can be broken and the long polymeric chains can be moved easily when subjected to deformation forces. If cooled, the polymer returns to its original hardness and resistance, so the process is reversible, even if attention must be paid as multiple repeated cycles can cause material degradation.

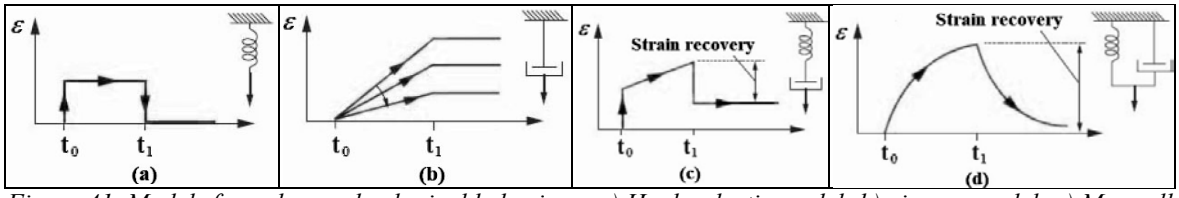

Figure 41. Models for polymer rheological behaviour: a) Hooke elastic model; b) viscous model; c) Maxwell viscoelastic model; d) Kelvin-Voigt viscoelastic model

Thermoplastics materials can exhibit each behaviour shown in Figure 41, e.g. if in solid state (under Tg) they show an elastic behaviour, described by Hooke law, but if the temperature is raised around Tg the behaviour is viscoelastic. Thus, the models in Figure 41 must be applied for the specific case to have an accurate output. Since all models have a viscous component depend on viscosity, it is important to understand how viscosity affects polymer response to different load conditions. There are two kinds of behaviour, namely Newtonian and no-Newtonian. In Newtonian behaviour, viscosity is a function of pressure and temperature only. In no-Newtonian behaviour, viscosity depends also on shear rate.
For some polymers, as polypropylene, viscosity highly decreases with shear rate, assuming a pseudo-plastic behaviour. The relation between viscosity and shear rate can be expressed as:

$$\eta = A\dot{\gamma}^{1-n} \tag{5}$$

where A is the consistency index and n is the power law index.
Temperature effect on η can be described with the following equation:

$$\eta(t) = \eta_0 \, e^{E/kT} \tag{6}$$

where η_0 is a constant depending on material; k is the Boltzmann's constant (13.8×10^{-24}[J/K]) and E is the activation energy.

Considering the case in which shear is applied, the relation between load and deformation, i.e. shear stress and shear rate, for solids is:

$$\tau = G\gamma \tag{7}$$

where G is the shear modulus.

Increasing temperature, elastic modulus and strength decrease and polymers exhibit viscoelastic behaviour. In case of viscous fluids, shear stress is proportional to shear rate with viscosity, and the corresponding equation is:

$$\tau = \eta\dot{\gamma} \tag{8}$$

In between, there are all that materials that exhibits viscoelastic behaviour. Maxwell was the first to investigate the relation for these materials in 1868. The idea behind his equation is to combine elastic and viscous properties of storing and dissipating energy, as in a spring-damper system (Figure 41c). As a spring and a dumper are in series, they are subjected to the same tension, so the deformation is the sum of the single elastic element and viscous element ones. Denoting with σ the tension and with ε the deformation, and using subscript e for the elastic element and the subscript η for the viscous one, it can be written:

$$\varepsilon_e = \frac{\sigma}{E} \tag{9}$$

$$\frac{d\varepsilon_\eta}{dt} = \frac{\sigma}{\eta} \tag{10}$$

where E is the elastic modulus (constant with time), thus Maxwell viscoelastic model is described by:

$$\frac{d\varepsilon}{dt} = \frac{1}{E}\frac{d\sigma}{dt} + \frac{\sigma}{\eta} \tag{11}$$

It can be defined even a viscoelastic modulus, which represents a time dependant elastic modulus, which can be calculated as:

$$E_r = \frac{\sigma}{\varepsilon_e + \varepsilon_\eta} \tag{12}$$

To characterize the fluidity of materials under specific flow conditions, a dimensionless number, named Deborah's number has been introduced, in which the numerator is the relaxation time, which is the time needed for a reference amount of deformation to occur under a suddenly applied reference load, while the denominator is the material time, that is the amount of time required to reach a given reference strain.

$$De = \frac{t_c}{t_p} \tag{13}$$

2.2 **Material**

The material used in this study is commercially named *Dafnelen HP 1003S*®, and it is produced by Sirmax S.P.A. It consists in a polypropylene glass fiber compound, with 50%wt of glass fibers.

Figure 42. Dafnelen HP 1003S® pellets

2.2.1 Polypropylene

Polypropylene, generally indicated with PP, is a plastic material derived from propylene.
It was first polymerized in 1951 by Paul Hogan and Robert Banks and later by Italian and German scientists Natta and Rehn. It became prominent in a very short time, as commercial production began after only three years since when the Italian chemist, Professor Giulio Natta, first polymerized it. By 1957, its popularity had exploded and widespread commercial production began across Europe. Today it is one of the most commonly produced plastics in the world.

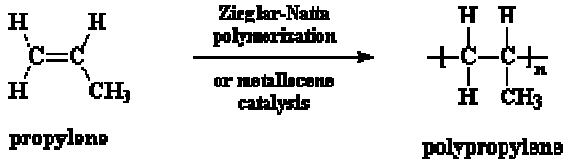

Figure 43. Polypropylene structure and derivation

In Figure 43, is shown the polypropylene structure and it is indicated the process to obtain this polymer from propylene. The subscript n indicates that the monomer in brackets is repeated several times.

During polymerization, methyl groups in polypropylene can result oriented in three different configurations (Figure 44):

atactic (aPP): irregular methyl group (CH_3) arrangement
isotactic (iPP): methyl groups (CH_3) arranged on one side of the carbon chain
syndiotactic (sPP): alternating methyl group (CH_3) arrangement

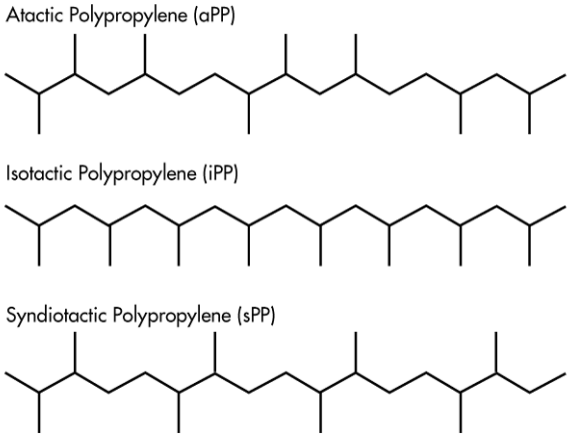

Figure 44. Polypropylene configurations

Isotactic polypropylene is the only one used in industrial applications thanks to its strength, stiffness and high melting temperature respect to other polyolefins.
Industrial polypropylenes can be created with different properties, in terms of molecular structure and weight, crystallinity and spherulitic structure. Moreover, polypropylene properties can also be modified according to needs with additives, fillers and reinforcing materials in compounding phase.

For the specific material used in this study, *Dafnelen HP 1003S®*, matrix of polypropylene is a blend of different homopolymer PP with different fluidity index, then reinforced with E-glass fibers to enhance mechanical and impact resistance. Glass fibers used are known commercially as *Chopped Strands CS 7952®* and they are provided by Lanxess (Figure 45).

Figure 45. CS 7952® glass fiber

In this reinforcing material, fibers have an average diameter of 14 μm, and a nominal length of 4.5 mm.

Dafnelen HP 1003S® is produced via extrusion process, in three principal stages. The process setup phases are different in terms of weight mass, screw rotational speed and fiber percentage loaded. In Table 2 are summarized the different stages parameters, and in Table 3 the extruder temperature profile.

	weight mass [Kg/h]	**screw rotational speed [RPM]**	**fiber percentage loaded [%]**
First stage	600	400	30
Second stage	800	500	40
Third stage	1200	400	50

Table 2. Dafnelen HP 1003S® production parameters process

T_0	T_1	T_2	T_3	T_4	T_5	T_6	T_7	T_8	T_9	T_{10}	T_{11}	T_{12}	T_{13}	T_{14}
230	230	230	250	260	250	250	250	250	250	240	230	240	240	240

Table 3. Extruder temperature profile for Dafnelen HP 1003S® production

The final compound shows the physical, rheological, thermal and mechanical properties summed in Table 4 from Sirmax S.P.A. datasheet.

PHYSICAL AND RHEOLOGICAL PROPERTIES					
Property	**Melt flow rate**		**Density**		**Shrinkage**
Test parameters	230 °C – 2.16 Kg		23 °C		-
Unit of measure	g/10’		g/cm3		%
Value	3.0		1.32		0.1 – 0.3
THERMAL PROPERTIES					
Property	**Vicat**	**Vicat**	**HDT**	**HDT**	
Test parameters	A50	B50	1.80 MPa	0.45 MPa	
Unit of measure	°C	°C	°C	°C	
Value	166	144	152	160	
MECHANICAL PROPERTIES					
Property	**Flexural modulus**	**Flexural strength**	**Tensile modulus**	**Tensile strength at break**	**Tensile elongation at break**
Test parameters	23 °C 2 mm/min	23 °C 2 mm/min	23 °C 1 mm/min	23 °C 5 mm/min	23 °C 5 mm/min
Unit of measure	MPa	MPa	MPa	MPa	%
Value	10500	170	11500	110	4.0
IMPACT MECHANICAL PROPERTIES					
Property	**Izod impact resistance**	**Charpy impact resistance**	**Charpy impact resistance**		
Test parameters	23 °C with notch	23 °C with notch	23 °C without notch		
Unit of measure	KJ/m^2	KJ/m^2	KJ/m^2		
Value	12	12	50		

Table 4. Dafnelen HP 1003S® datasheet

2.3 Characterization tests

Materials choice is a fundamental step in product design that will determine part performance and behaviour during operative life. Thus, it appears crucial to determine material properties in terms of chemical, physical, mechanical and technological response.

- Chemical-physical properties are bonded to chemical structure and composition of the material investigated. The main ones are: density, melting temperature, boiling temperature, specific heat, thermal conductivity, electric conductibility, thermal expansion, resistance to corrosion, permeability and opacity.
- Mechanical properties identify material response to mechanical solicitation, that can be static, dynamic, concentrated, distributed, periodic or by friction. Among all mechanical properties, principal ones are: tensile strength, compressive strength, flexural strength, shear strength, torsion resistance, resiliency, hardness, fatigue resistance and friction resistance.
- Technological properties define the material behaviour under processing, such as ductility, malleability, fusibility and extruding, drawing, bending, welding, casting, hardening, machining and polishing behaviour.

Most of the aforementioned properties can be found in material datasheet, but sometimes further tests are required to have a full comprehension of material nature.
In this section rheological tests done for the specific material used in this study will be described and the relative results will be displayed.

2.3.1 Capillary rheometer test for viscosity curves determination

This test is based on ASTM D3835 regulations [48] and it permits to measure rheological properties of polymeric materials at various temperatures and shear rates common to processing equipment. It covers measurement of melt viscosity, sensitivity, or stability of melt viscosity with respect to temperature and polymer dwell time in the rheometer, die swell ratio (polymer memory), and shear sensitivity when extruding under constant rate or stress. The techniques described permit the characterization of materials that exhibit both stable and unstable melt viscosity properties.
This method is useful to perform quality control tests on reinforced and un-reinforced polymers, and it is sensitive to molecular weight and polymer distribution, thermal and rheological stability, shear sensitivity and additive presence.

Capillary rheometer main parts are:

- Rheometer: polymer melt is forced through a capillary orifice and it is possible to control temperature, applied force, exiting speed and capillary dimension.
- Polymer reservoir: equipped with temperature sensors at wall, it consists in a cylindrical hole with diameter spacing from 6.35 and 19 mm.
- Capillary: an insert to be fixed under polymer reservoir, presents a capillary hole with a reservoir diameter to capillary diameter from 3 to 15. Rate between reservoir length and capillary length is from 15 to 40.
- Piston: made in metal with Rockwell hardness over 45 HRC, must have a diameter 0.0254 ± 0.007 mm less than reservoir, and be 6.35 ± 0.13 mm less in length.
- Heating and temperature control: temperature needs a strict control (± 0.2°C) and due to shear stresses and chemical/physical melt behaviour it could be possible to exceed this range. Solution to overcome this scenario must be applied.

Figure 46. Capillary rheometer

To proceed with test, piston must be removed and reservoir must be filled with polymer. During filling, not all the polymer is loaded at a time because air voids must be eliminated. Thus, after some polymer is loaded, a manual compression is applied to compact the material before other polymer is added. How many times this procedure must be applied depends on polymer and its form (platelet, powder, pellet, etc.). When all polymer is filled, piston is positioned back in the reservoir and heating system is started. A timer is set to let the polymer melt and then a first load is applied until regime functioning is achieved. Test can now start and data are collected to evaluate flow rate exiting the capillary (Q).
All polymer must be extruded and piston and capillary must be cleaned after test.

This test let the user have information about different material properties. Equations for shear rate $\dot{\gamma}$, shear stress τ and viscosity η for Newtonian fluids are listed below.

$$\tau\ [Pa] = \frac{Pr}{2L} = \frac{Fr}{2\pi R^2 L} \tag{14}$$

$$\dot{\gamma}\ [s^{-1}] = \frac{4Q}{\pi r^3} = \frac{4V}{\pi r^3 t} \tag{15}$$

$$\eta\ [Pa\ s] = \frac{\tau}{\dot{\gamma}} = \frac{p\pi r^4}{8LQ} = \frac{Fr^4 t}{8R^2 LV} \tag{16}$$

Where: P is load pressure [Pa]
F is load force [N]
r is capillary radius [m]
R is reservoir radius [m]
L is capillary length [m]
Q is volumetric exiting flow rate [m^3/s]
V is extruded volume [m^3]
t is total extrusion time [s]

For non-Newtonian fluids, equations are:

$$\tau\ [Pa] = \frac{(P - P_c)D}{4L} = \frac{D}{4LA_B} \tag{17}$$

$$\dot{\gamma}\ [s^{-1}] = \frac{(3n-1)}{4n}\,\dot{\gamma}_a \tag{18}$$

Where: P is melt pressure [Pa]
P_c is the intercept of curve aspect ratio vs. pressure, at a certain $\dot{\gamma}$ (Figure 47)

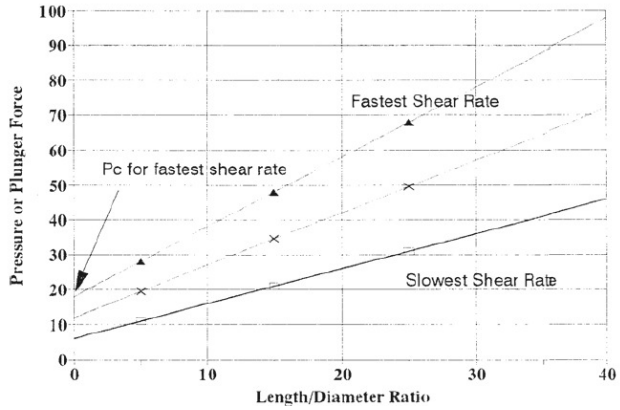

Figure 47. Aspect Ratio vs. Pressure

D is capillary diameter [m]

L is capillary length [m]

F is the force exerted by piston [N]

F_c is force intercept on Bagley diagram [N]

A_B is reservoir section area [m^2]

n is a power law factor derived from the graph below (Figure 48)

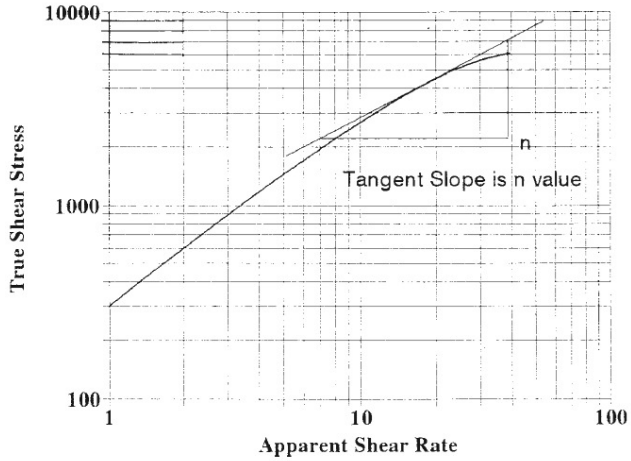

Figure 48. True shear stress vs. apparent shear stress

$\dot{\gamma}_a$ is the shear velocity for Newtonian fluid, derived above in Eq. *(15)* [s^{-1}]

For non-Newtonian fluids, viscosity still Shear stress on shear rate ratio.
Eq. *(18)* is commonly referred as "Rabinowitsch correction"

Density is calculated by:

$$\rho\,[g/mL] = \frac{m}{tQ} \qquad (19)$$

where: m is the mass of extruded material [g]
t is total extrusion time [s]
Q is volumetric exiting flow rate [mL/s], calculated as product of piston speed [cm/s] and is reservoir section area [cm^2]

Test performed on the material used in this study, gave the following output, for test temperatures of 200, 220, 240°C.

D=1, L=30		Shear rate [s^-1]									
		50	75	100	150	200	500	1000	2000	3000	5000
200°C	Δp [MPa]	5,322	6,323	6,982	7,849	8,557	10,681	12,219	13,659	14,599	15,747
220°C	Δp [MPa]	4,638	5,444	6,042	7,043	7,727	10,07	11,779	13,403	14,404	15,649
240°C	Δp [MPa]	4,113	4,858	5,444	6,408	7,104	9,484	11,401	13,000	14,16	15,344

Table 5. Pressure drop at different shear rate varying temperature

D=1, L=30		Shear rate [s^-1]									
		50	75	100	150	200	500	1000	2000	3000	5000
200°C	τ [Pa]	44350	52691	58183	65408	71308	89008	101824	113825	121658	131224
220°C	τ [Pa]	38650	45366	50349	58691	64391	83916	98158	111691	120033	130408
240°C	τ [Pa]	3475	40483	45366	53400	59200	79033	95008	108333	117999	127866

Table 6. Shear stress at different shear rate varying temperature

Capillary dimensions are 1 mm diameter and 30 mm length, so that Bagley correction isn't necessary. Thus, Eq. *(14)* is the one to be used for real shear stress calculation. However, for real shear rate, Rabinowitsch correction should be applied, so Eq. *(18)* is used. The power law factor n is derived as described above, and in the following tables (Table 7-Table 8-Table 9) power law factor *n*, real shear rate *SRre* and real viscosity *ηre* are listed for several apparent shear rate at the three different aforementioned temperatures.

200°C	Apparent shear rate [s^-1]									
	50	75	100	150	200	500	1000	2000	3000	5000
n	0,359	0,336	0,320	0,296	0,280	0,227	0,188	0,148	0,125	0,095
SRre [s^{-1}]	72	112	153	239	329	925	2083	4884	8273	16875
ηre [Pa*s]	613,45	470,22	379,67	273,58	219,92	96,22	48,88	23,31	17,71	7,78

Table 7. SRre, n and ηre at different apparent shear rate at 200°C

220°C	Apparent shear rate [s^-1]									
	50	75	100	150	200	500	1000	2000	3000	5000
n	0,405	0,380	0,362	0,337	0,319	0,261	0,218	0,175	0,149	0,117
SRre [s^{-1}]	68	106	144	224	307	853	1896	4361	7270	14393
ηre [Pa*s]	565,64	429,68	349,54	262,18	209,84	98,37	51,76	25,61	16,51	9,06

Table 8. SRre, n and ηre at different apparent shear rate at 220°C

240°C	Apparent shear rate [s^-1]									
	50	75	100	150	200	500	1000	2000	3000	5000
n	0,440	0,413	0,394	0,366	0,647	0,285	0,239	0,192	0,165	0,130
SRre [s^{-1}]	66	102	139	215	294	813	1798	4107	6811	13364
ηre [Pa*s]	520,25	398,3	327,55	248,54	201,29	97,18	52,84	26,38	17,33	9,57

Table 9. SRre, n and ηre at different apparent shear rate at 240°C

The main output of this test is real viscosity vs. real shear rate curves, obtained by above data.

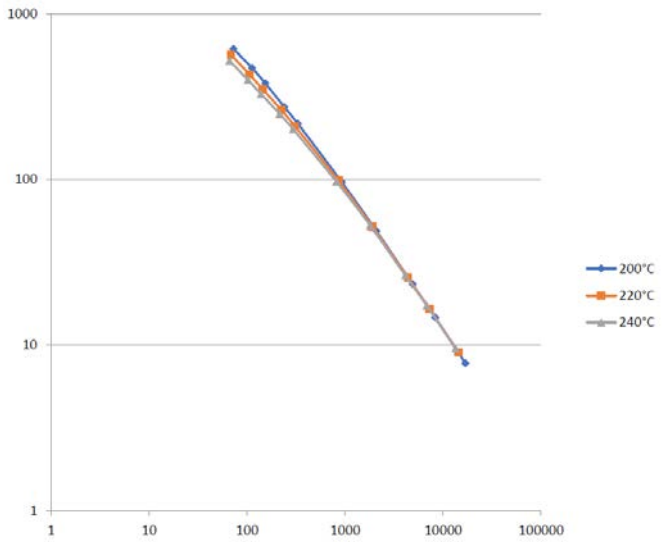

Figure 49. Real viscosity vs. real shear rate curves for capillary rheometer

Graphs in Figure 49 shows real viscosity versus real shear rate curves for each test temperature.

In order to use material viscosity in *Autodesk Moldflow Insight*®, Cross-WLF viscosity model is implemented. Cross-WLF model is based on the following equation (Eq. *(20)*):

$$\eta = \frac{\eta_0}{1 + \left(\frac{\eta_0 \dot{\gamma}}{\tau^*}\right)^{1-n}} \tag{20}$$

Where: η is melt viscosity [Pa s]
η_0 is the zero shear rate viscosity [Pa s]
$\dot{\gamma}$ is the shear rate [s^{-1}]
τ^* is the critical shear stress value for shear thinning [Pa]
n is the power law factor

Zero shear rate viscosity can be calculated with Eq. *(21)*:

$$\eta_0 = D_1 \exp\left[-\frac{A_1(T - T^*)}{A_2 + (T - T^*)}\right] \tag{21}$$

Where: T is temperature [K]
T^* is glass transition temperature [K]
$A_2 = A_3 + D_3\, p$
p is pressure [Pa]
D_1, A_1, A_3 and D_3 are fitting coefficient

Glass transition temperature T^* is calculated by:

$$T^* = D_2 + D_3 p \tag{22}$$

Real viscosity vs. real shear rate curves obtained with this model is then compared with experimental data. As can be seen in the graphs below (Figure 50), numerical and experimental data are in good agreement.

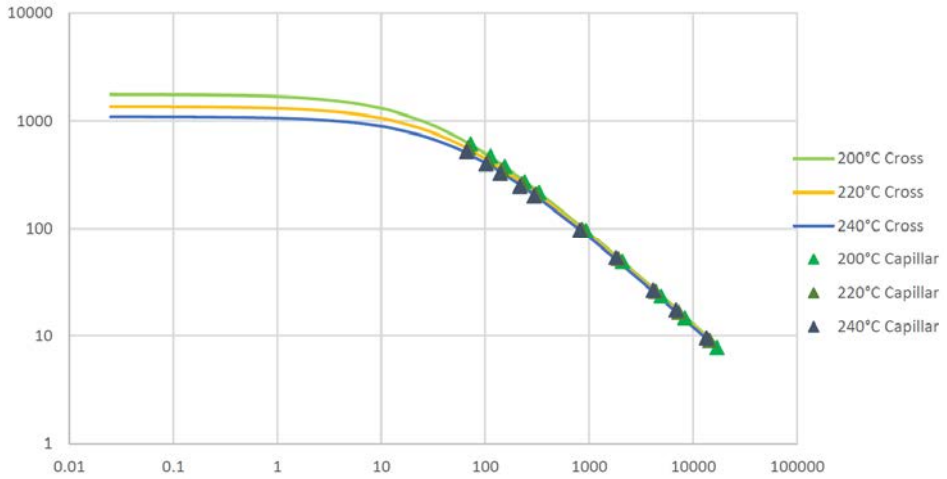

Figure 50. Comparison between experimental and Cross-WLF model data

2.3.2 Rotational rheometer test for viscosity curves determination

Rotational rheometer *ARES-G2* by TA Instruments let the user investigate independently shear stress and normal stress, thanks to a Torque Rebalance Transducer (TRT) and a Force Rebalance Transducer (FRT), and it is also provided with a dedicated deformation sensor. This rotational rheometer is recognized as the industrial standard for rheological investigation instrument by rheological community, and it is used to compare accuracy with other rotational rheometer measures.

For high viscosity polymers it is suggested to use plate-plate test design, in which the material is confined between two shearing plates by capillary force. The gap between the disks must be between 0.5mm and 1mm. Disks available for PP characterization space from 8mm to 50mm diameter, from steel to titanium.

Oscillatory shear measurement is commonly used in viscoelastic properties investigations and it is performed imposing a small amplitude oscillatory shear of shear amplitude γ_0 and angular frequency $w = 2\pi f$ [rad s^{-1}], where f [s^{-1}] is the frequency oscillation. Typical w values are in a range from 0.1 rad/s to 500 rad/s.

In this test, temperature and frequency has been kept constant and properties have been investigated for different shear rate, to evaluate linear viscoelastic region. As for previous viscosity curves determination test, temperature used are 200, 220, 240 °C. Tests are conducted at least two times, to ensure good repeatability.

Figure 51. Rotational rheometer

Sensor on the upper plate measure the change in position of the plate, and the signal is valuated as deformation γ. The sensor in the lower plate measure the force applied to maintain it in his position, and the signal is valuated as shear stress τ. The real viscosity η^* is then calculated as:

$$\eta^* = \frac{\tau}{\gamma} \qquad (23)$$

η^* is a vector quantity, combination of elastic contribute η' and viscous contribute η". If one of the contributes is unknown, it can e determined by Pitagora's theorem, as:

$$\eta^{*2} = \eta'^2 + \eta''^2 \qquad (24)$$

In Table 10 values of real viscosity η^* vs. shear rate are listed, for each test temperature.

Using this data, at low shear rate a bi- logarithmic graph is displayed. Typically under 1 s^{-1} curves in this region shows a plateau, and the corresponding value is called η_0. In Figure 52 curves obtained during tests are shown.

T=200°C	
shear rate	eta star
0,1	19558,09
0,12589255	15261,88
0,15848933	12537,542
0,19952625	10551,824
0,25118867	9075,6943
0,31622779	8014,2046
0,3981072	7131,1528
0,50118726	6376,2095
0,63095742	5785,8164
0,79432833	5275,0503
1,0000001	4831,9414
1,2589256	4444,1069
1,5848935	4107,1758
1,9952627	3810,0845
2,5118871	3540,8691
3,1622787	3295,5264
3,9810731	3067,8276
5,0118742	2852,238
6,309576	2647,1301
7,9432859	2455,4458
10,000005	2272,5264
12,58926	2096,5688
15,84894	1930,1345
19,952633	1768,5786
25,118877	1615,6008
31,622793	1469,9552
39,810738	1333,4152
50,118752	1204,6584
63,095772	1083,7112
79,432869	971,41254
100,00006	865,67725
125,89262	767,69916
158,48943	679,03644
199,52637	598,16089
251,18881	523,9411
316,228	450,90967
398,10748	380,20929

T=220°C	
shear rate	eta star
0,1	12650,638
0,12589255	10093,165
0,15848933	8285,4316
0,19952625	6974,8394
0,25118867	5913,9453
0,31622779	5135,5718
0,3981072	4507,1519
0,50118726	3992,1428
0,63095742	3557,7937
0,79432833	3213,2183
1,0000001	2915,4917
1,2589256	2667,2004
1,5848935	2450,4163
1,9952627	2261,1284
2,5118871	2094,2371
3,1622787	1945,9542
3,9810731	1812,1783
5,0118742	1689,0848
6,309576	1574,6353
7,9432859	1468,6788
10,000005	1367,9791
12,58926	1272,3044
15,84894	1181,5038
19,952633	1093,1428
25,118877	1008,9197
31,622793	927,48346
39,810738	850,97784
50,118752	777,96887
63,095772	708,40228
79,432869	642,73236
100,00006	579,79272
125,89262	520,33185
158,48943	465,64304
199,52637	414,89935
251,18881	367,66733
316,228	321,33957
398,10748	274,02774

T=240°C	
shear rate	eta star
0,1	7472,4473
0,12589255	6385,9312
0,15848933	5431,0073
0,19952625	4635,0996
0,25118867	3984,2542
0,31622779	3445,4058
0,3981072	3003,4209
0,50118726	2632,4414
0,63095742	2310,457
0,79432833	2056,3779
1,0000001	1840,0381
1,2589256	1658,6837
1,5848935	1507,1637
1,9952627	1375,9023
2,5118871	1263,6942
3,1622787	1165,0396
3,9810731	1078,3489
5,0118742	1001,3436
6,309576	931,83215
7,9432859	869,46417
10,000005	811,23846
12,58926	756,59802
15,84894	706,15533
19,952633	657,23676
25,118877	610,73901
31,622793	566,16406
39,810738	523,64398
50,118752	482,94989
63,095772	443,94025
79,432869	406,55258
100,00006	370,36685
125,89262	336,00681
158,48943	304,02777
199,52637	273,74939
251,18881	245,31422
316,228	217,11389
398,10748	187,42261

Table 10. Rotational rheometer real viscosity vs. shear rate output

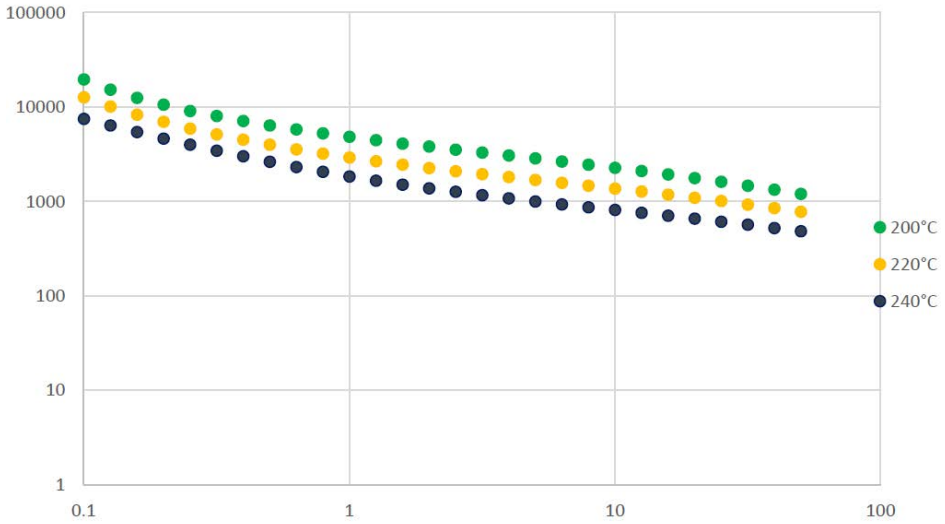

Figure 52. Real viscosity vs. real shear rate curves for rotational rheometer

2.3.3 Capillary rheometer test for pVT diagram determination

The pVT diagram, already described in 1.1 (Figure 7), can be determined with a capillary rheometer. Knowing sample mass and varying pressure and temperature, it is possible to evaluate specific volume, and track its trend with temperature at different pressures.
This diagram let the user define the volumetric shrinkage of the molded part as:

$$Shrinkage = \frac{V_D - V_E}{V_D} \qquad (25)$$

Where: V_D is the specimen volume in the cavity
V_E is the specimen volume at room temperature

Tests were conducted on a mass sample of 6.42g at 20, 40, 75, 110, 145 and 180MPa. For each pressure, data were collected at 80, 110, 130, 140, 145, 150, 155, 160, 165, 170, 180, 200, 230, 245, 260, and 290°C. Worth mentioning that it is demanding that material Tg is included in test temperature range.

pVT diagrams obtained using the previous parameters are shown in Figure 53.

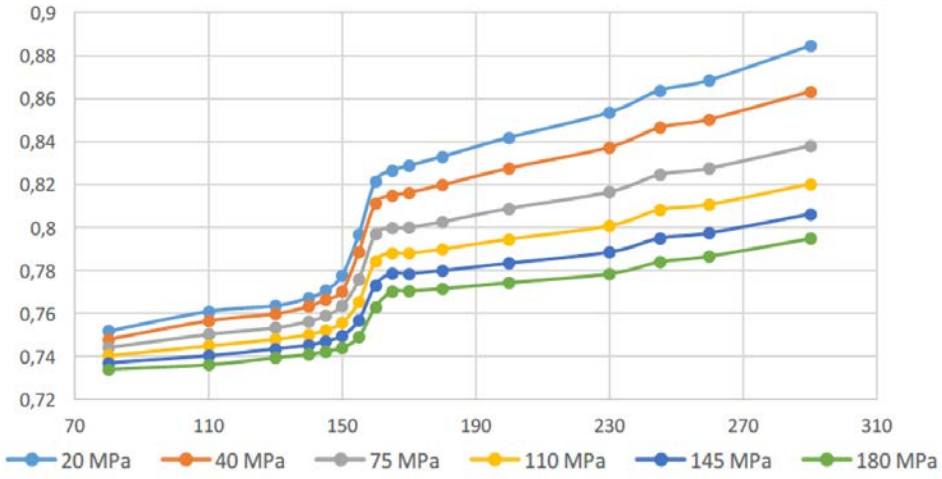

Figure 53. pVT diagrams obtained during tests

In order to use material pVT diagrams in *Autodesk Moldflow Insight®*, pVT 2-domain Tait model is used. Main governing equation for this model is:

$$v(T,p) = v_0(T)\left[1 - C\ln\left(1 + \frac{p}{B(T)}\right)\right] + v_t(T,p) \quad (26)$$

where: v (T, p) is the specific volume at certain pressure and temperature [m^3/kg]
v_0 is the specific volume at pressure defined as zero [m^3/kg]
T is temperature [K]
p is pressure [Pa]
C is a constant, which value is 0.0894
B is a factor that takes into account material sensitivity to pressure

To determine B value, the procedure is the following:

- The region when temperature is high, i.e. material melting temperature Tm is lower than working temperature T, is described by:

$$v_0 = b_{1m} + b_{2m}(T - b_5) \quad (27)$$

Thus:

$$B(T) = b_{3m}e^{[-b_{4m}(T-b_5)]} \quad (28)$$

$$v(T,p) = 0 \quad (29)$$

where b_{1m}, b_{2m}, b_{3m}, b_{4m} and b_5 are fitting coefficients.

- The region when temperature is low, i.e. material melting temperature Tm is higher than working temperature T, is described by:

$$v_0 = b_{1s} + b_{2s}(T - b_5) \quad (30)$$

Thus:

$$B(T) = b_{3s}e^{[-b_{4s}(T-b_5)]} \quad (31)$$

$$v(T,p) = b_7e^{[(b_8(T-b_5))-(b_9p)]} \quad (32)$$

where b_{1s}, b_{2s}, b_{3s}, b_{4s}, b_5, b_7, b_8 and b_9 are fitting coefficients.

Dependence of Tm with pressure is described by:

$$Tm(p) = b_5 + b_6p \quad (33)$$

Comparing pVT curves obtained by rheological tests with pVT curves obtained via numerical model, a good agreement can be found, as shown in Figure 54.

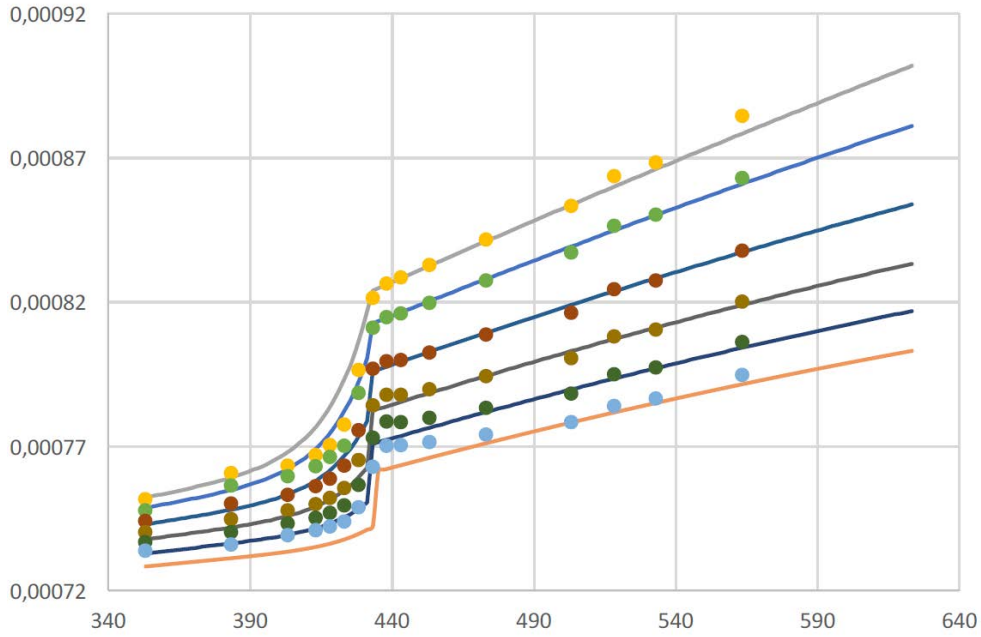

Figure 54. Comparison between experimental and Tait model pVT curves

Dotted data represents test value, respectively for:
20MPa (yellow)
40MPa (green)
75MPa (red)
110MPa (light brown)
145MPa (dark green)
180MPa (light blue)

Lines are Tait model generated curves, for the same value of pressures.

2.3.4 DSC analysis for transition temperature evaluation

DSC (Differential Scanning Calorimetry) analysis to determine transition temperatures and enthalpies of fusion and crystallization of polymers is based on ASTM D3418 regulations [49]. This test method consists of heating or cooling the test material at a controlled rate, under a specified purge gas at a controlled flow rate and continuously monitoring, with a suitable sensing device, the difference in heat input between a reference material and a test material due to energy changes in the material. A transition is marked by absorption or release of energy by the specimen resulting in a corresponding endothermic or exothermic peak or baseline shift in the heating or cooling curve. Areas under the crystallization (exothermal) or fusion (endothermic) of the test materials are compared against the respective areas obtained by the treatment of a well characterized standard.
Thermal analysis provides a rapid method for measuring transitions due to morphological or chemical changes, in a polymer as it is heated/cooled through a specified temperature range. Change in specific heat capacity, heat flow and temperature values are determined for these transitions. Differential scanning calorimetry is used to assist in identifying specific polymers, polymer alloys, and certain polymer additives, which exhibit thermal transitions. Chemical reactions that cause or affect certain transitions have been measured with the aid of this technique; such reactions include oxidation, curing of thermosetting resins, and thermal decomposition. This method is applicable to polymers in granular form, or o any fabricated shape, and can be performed from cryogenic temperatures to 600°C, but range can be extended if special equipment is used.

In Figure 55, an example of a DSC analysis on Nylon is shown and characteristics first order picks (melting and crystallization transitions) can be seen.

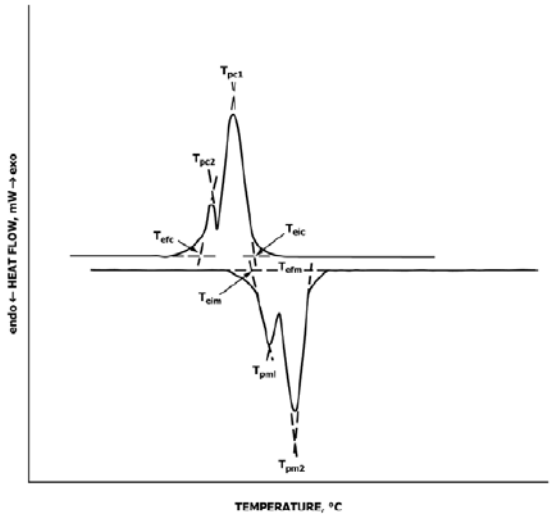

Figure 55. First-order transition of Nylon

Where: T_{eim} = melting extrapolated onset temperature [°C]
T_{efm} = melting extrapolated end temperature [°C]
T_{pm} = melting peak temperature [°C]
T_{eic} = crystallization extrapolated onset temperature [°C]
T_{pc} = crystallization peak temperature [°C]
T_{efc} = crystallization extrapolated end temperature [°C]

In Figure 56, is shown an example of glass transition of PMMA.

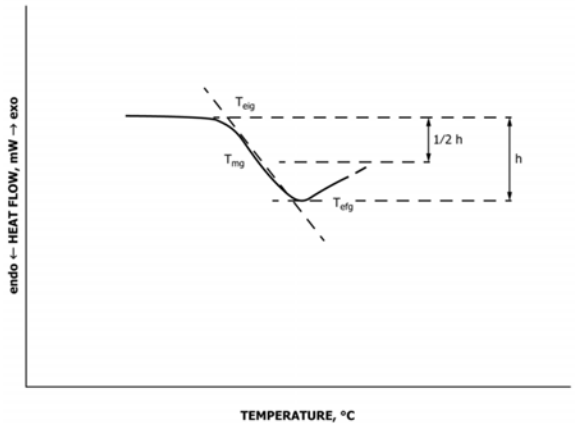

Figure 56. Glass transition of PMMA

Where: T_{eig} = extrapolated onset temperature [°C]
T_{mg} = midpoint temperature [°C]
T_{efg} = extrapolated end temperature [°C]

The essential instrumentation required to provide the minimum differential scanning calorimetric capability for this test method includes:

- DSC Test Chamber, composed by:
    1. *Furnace(s),* to provide uniform controlled heating (cooling) of a specimen and reference to a constant temperature or at a constant rate;
    2. *Temperature Sensor,* to provide an indication of the specimen temperature to ±0.01°C;
    3. *Differential Sensor,* to detect heat flow difference between the specimen and reference equivalent to 1 mW.
    4. *Means of Sustaining a Test Chamber Environment* of purge gas at a purge flow rate of 10 to 50 ±5 mL/min.

- *Temperature Controller,* capable of executing a specific temperature program by operating the furnace(s) between selected temperature limits at a rate of temperature change of 0.5 to 20°C/min constant to ±0.1°C/min or at an isothermal temperature constant to ±0.1°C.
- *Recording Device,* capable of recording and displaying any fraction of the heat flow signal (DSC curve) including the signal noise as a function of temperature.
- *Software,* for integrating areas under endothermic valleys or exothermic peaks, or both.
- *Containers* (pans, crucibles, and so forth) that are inert to the specimen and reference materials; and that are of suitable structural shape and integrity to contain the specimen and reference in accordance with the specific requirements of this test method.
- Cooling capability to hasten cool down from elevated temperatures, to provide constant cooling rates of 0.5 - 20 ºC/min to obtain repeatable crystallization temperatures, to achieve sub-ambient operation, or to sustain an isothermal sub-ambient temperature, or combination thereof.

Moreover, a *balance* capable of weighing to ±0.0001 grams for transition temperatures and to ±0.00001 grams for determining enthalpies, is required.

Figure 57. DSC equipment

In this study, a heating rate of 10°C/min is applied, producing the graph below (Figure 58).

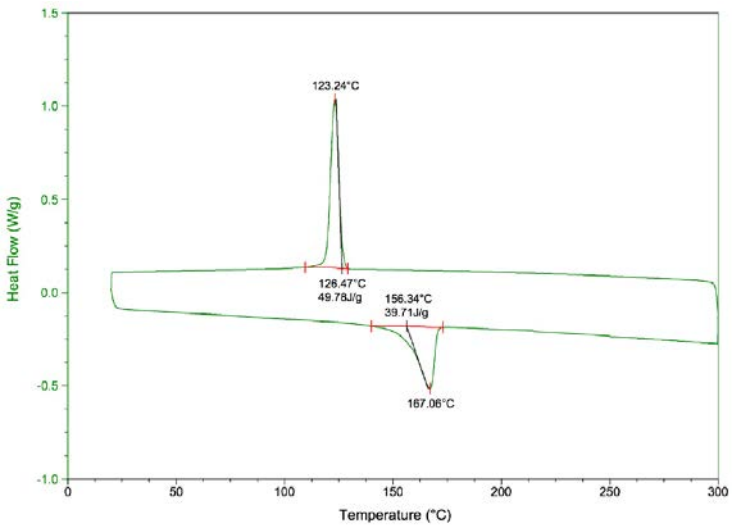

Figure 58. DSC analysis on Dafnelen HP 1003S®

Two characteristics picks can be noticed:

– The first pick, starting from left, at nearly 123°C, represents an exothermic reaction, corresponding to material crystallization. Long-range order structures forms releasing energy in terms of heat.

– The second pick, nearly at 167°C, is an endothermic reaction corresponding to material melting. Bonds between molecules are broken absorbing energy, in terms of heat.

2.3.5 DSC analysis for specific heat capacity evaluation

DSC (Differential Scanning Calorimetry) analysis to determine material specific heat capacity is based on ASTM E1269 regulations [50]. This test method consists of heating the test material at a controlled rate in a controlled atmosphere through the region of interest. The difference in heat flow into the test material and a reference material or blank due to energy changes in the material is continually monitored and recorded. Specific heat capacities are important for reactor and cooling system design purposes, quality control, and research and development. This method can be applied to thermally stable solids and liquids, within a test temperature range from 100 to 600°C, than can be extended if special equipment is used. As for the previous test using DSC, the apparatus still the same.
To run this test, the DSC apparatus is purged with dry nitrogen, or another inert gas, at a flow rate of 10 to 50 ±5 mL/min throughout the experiment and specimen holder plus lid must be weighted with a precision of ±0.01 mg and recorded as tare weight before start. Then the user can proceed positioning the empty specimen holder plus lid and a reference specimen holder plus lid (weight-matched, if possible) in the DSC apparatus. Then DSC test chamber is heated/cooled at 20°C/min to the initial test temperature, and kept at this temperature for 4min to establish equilibrium, and heat curve starts to be recorded. Test can now start and specimen can be heated at 20°C/min to final test temperature. The apparatus can now be cooled and the same procedure is applied to standard synthetic sapphire disk sample, to be used as reference.

In Figure 59, an example of obtained curve is displayed.

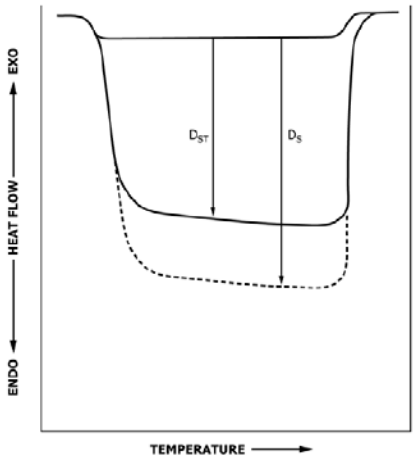

Figure 59. Specific heat capacity thermal curve of standard sapphire and unknown specimen

To evaluate specific heat capacity of the sample, the distance between the empty sample holder and the standard sapphire at temperature T is measured (D_{st}). Specific heat capacity is calculated as:

$$C_{p(s)} = C_{p(st)} \frac{D_s W_{st}}{D_{st} W_s} \quad (34)$$

where: $C_{p(s)}$ = specific heat capacity of the specimen [*J/(g*K)*]
$C_{p(st)}$ = specific heat capacity of the sapphire standard [*J/(g*K)*]
D_s = vertical displacement between the specimen holder and the specimen DSC thermal curves at a given temperature [mW]
D_{st} = vertical displacement between the specimen holder and the sapphire DSC thermal curves at a given temperature [mW]
W_s = mass of specimen [mg]
W_{st} = mass of sapphire standard [mg]

In this study, room temperature was set as initial temperature, and 300°C was set as final temperature. Sapphire sample was used as reference, so that Eq. *(34)* is the one used to determine material specific heat capacity.

In Figure 60, is shown C_p trend with temperature for the specific material used in this study.

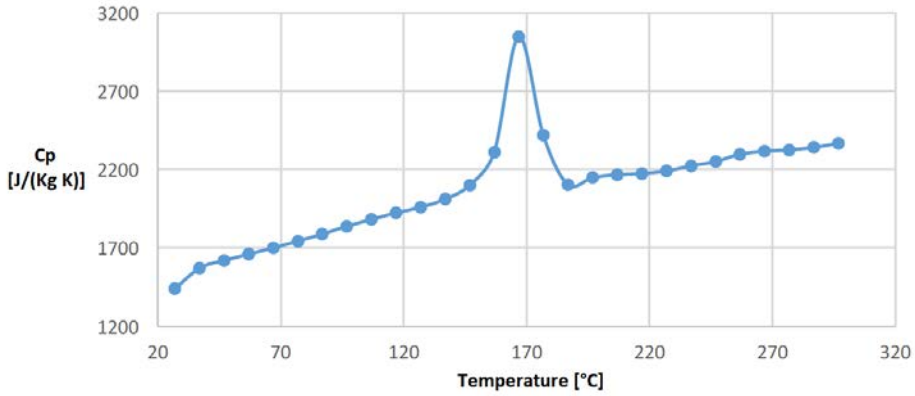

Figure 60. Specific heat capacity with temperature for Dafnelen HP 1003S®

CHAPTER 3

Experimental setup

In this chapter the focus will be on the experimental setup used to create specimens via injection molding, equipment and parameters used to set injection molding machine as well as molds design will be exposed and geometry of molded samples will be described.
A numerical analysis has been performed using *Autodesk Moldflow Insight*® to simulate process parameters and expected output, and *Ansys*® to simulate tensile test output. These results along with stress vs. strain curves of specimens milled from a square plate at 0°, 45° and 90° with respect to the flow direction, will then be submitted to *Helius PFA* analysis to extrapolate the principal mechanical properties.
A first set of specimen will be simulated and actually molded with a single-nozzle configuration, to validate numerical simulation over experimental outputs and to obtain no-in-flow weld line morphology and properties. Will follow the double-nozzle process simulation, which will be compared with previous results to proof effectiveness in enhancing weld line properties of this configuration, thanks to in-flow phenomena.

3.1 Injection molding machine

The injection molding machine used in this experimental analysis was the *BATTENFELD HM 110/525H/210S*®, in Figure 61.

Figure 61. BATTENFELD HM 110/525H/210S®

H and S in the machine name define how injection unit are positioned. In particular it means that the injection molding machine is provided with a second injection unit mounted diagonally (S) above the horizontal (H) aggregate. Both injections take place through the fixed platen, and the two injection units are thermally separated. Each injection unit is also equipped with its own travelling cylinders for independent linear movement. Each hopper will be loaded with the same material, *Dafnelen HP 1003S*®. Process parameter must be set, and the machine will be ready to use in a few minutes. First series of cycles will be used to set the optimum parameters in order to avoid short shot and flashes. Once optimum parameters are set, a continuous molding cycle is started and the first samples are discarded. The following molded products are collected in a sufficient number of specimens in order to obtain a statistically representative sample.

Clamping force [kN]	1100
Screw diameter [mm]	35
Screw stroke [mm]	200
Max. screw speed [min^{-1}]	318
Specific injection pressure [bar]	2743
Theoretical shot volume [cm^3]	193

Table 11. BATTENFELD HM 110/525H/210S ® performances

3.2 Single-nozzle configuration

3.2.1 No-in-flow specimen design

In order to produce no-in-flow specimen, the injection molding machine described above, in 3.1, has been used, but only the central nozzle was active. As it can be seen in Figure 62, a double dogbone specimen has been molded in each cycle. The cavity geometry presents a single injection point, and a runner system that lead the melt material in the desired-shaped sample.

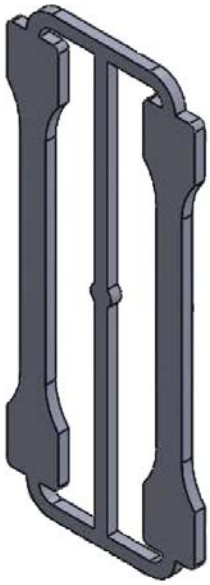

Figure 62. Single-nozzle configuration cavity geometry

Mold insert used to model the cavity present two plates, one to be fixed on the fixed half-mold, and the other one to be fixed on the mobile half. On the plate to be positioned on the fixed half, only fixing screw and gate hole were drilled, while on the plate to be positioned on the mobile half, along with holes due to fixing screw and ejector pins passage, the cavity has been designed.

3.2.2 Injection molding process parameters

According to *BATTENFELD HM 110/525H/210S*® and *Dafnelen HP 1003S*® specifics, process parameters have to be set. Main process values to be considered are temperature and pressure for each phase and cooling time. In Table 12 are listed the parameters used in this case.

Filling					Packing			Cooling
Flow rate [cm^3/s]	Vol. [cm^3]	Pressure [bar]	Mold temp. [°C]	Melt temp. [°C]	Velocity vs. pressure switch-over [% filling]	Pressure [bar]	Time [s]	Time [s]
33.6	24.05	1000	50	260	98	400	12	50

Table 12. Injection molding process parameters

In filling phase flow rate control is applied to then switch to pressure control when the cavity is nearly full filled.

3.2.3 Tensile test

Using polymer materials, tensile tests must be conducted following ASTM D638 [51] regulations. Tensile test is a fundamental materials science and engineering test in which a sample is subjected to a controlled tension until failure. Properties that are directly measured via a tensile test are ultimate tensile strength, breaking strength, maximum elongation and reduction in area. From these measurements the following properties can also be determined: Young's modulus, Poisson's ratio, yield strength, and strain-hardening characteristics. It can be performed via hydraulic or electromagnetic powered machines (Figure 63).

Figure 63. Tensile test machine

Tensile test can be used to:

- Select a material or item for an application
- Predict how a material will perform in use: normal and extreme forces.
- Determine if, or verify that, the requirements of a specification, regulation, or contract are met
- Demonstrate proof of concept
- Demonstrate the utility of a proposed patent
- Provide standard data for other scientific, engineering, and quality assurance functions
- Provide a basis for technical communication
- Provide a technical means of comparison of several options
- Provide evidence in legal proceedings

In ASTM D638 [51] for reinforced composites the specimen geometry is the one used to define the cavity in this study. The procedure to operate the test comprises:

– Place the specimen in the grips of the testing machine, taking care to align the long axis of the specimen and the grips with an imaginary line joining the points of attachment of the grips to the machine;

- Attach the extension indicator. When modulus is being determined, a Class B-2 or better extensometer is required;
- Set the speed of testing at the proper rate, and start the machine;
- Record the load-extension curve of the specimen;
- Record the load and extension at the yield point (if one exists) and the load and extension at the moment of rupture.

During test, the load-extension curve is recorded, but it takes into account the specimen geometry dependence, so it is convenient to convert this information to engineering tensile stress σ_{eng} and strain ε_{eng}.

$$\sigma_{eng} = \frac{F}{A_0} \tag{35}$$

$$\varepsilon_{eng} = \frac{L - L_0}{L_0} = \frac{\Delta L}{L_0} \tag{36}$$

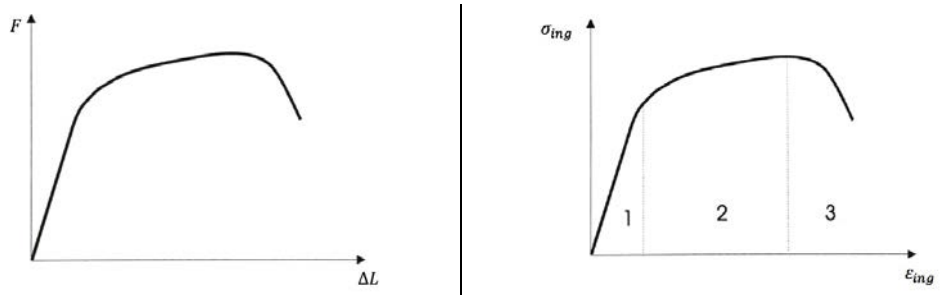

Figure 64. Load-extension (left) and stress-strain (right) curves

As it can be seen in Figure 64, load-extension and stress-strain curves are homothetic, which means that they show the same trend as they are referred to the same quantities by means of constants. Even if each material shows its own curves, the three regions highlighted in stress-strain curve are typically present.
Zone 1 is the one in which the material shows a linear trend, as it has an elastic behaviour, which means that the material is able to recover deformation obtained under load conditions.
Zone 2 represents the strain hardening region. This region starts as the strain goes beyond yielding point, and ends at the ultimate strength point, which is the maximal stress shown in the stress-strain curve. In this region, the stress mainly increases as material elongates, except that there is a nearly flat region at the beginning.
Zone 3 is the necking region. Beyond tensile strength, a neck forms where the local cross-sectional area becomes significantly smaller than the average. The necking deformation is heterogeneous and will reinforce itself as the stress concentrates more at small section. Such positive feedback leads to quick development of necking and leads to fracture. Note that though the pulling force is decreasing, the work strengthening is still progressing, that is, the true stress keeps growing but the engineering stress decreases because the shrinking section area is not considered. This region ends up with the fracture.

Tensile strength calculation is achieved dividing the maximum load sustained by the specimen in Newtons by the average original cross-sectional area in the gage length segment of the specimen in square meters. Express the result in Pascals, and report it to three significant figures as tensile strength at yield or tensile strength at break, whichever term is applicable. When a nominal yield or break load less than the maximum is present and applicable, it is often desirable to also calculate, in a similar manner, the corresponding tensile stress at yield or tensile stress at break and report it to three significant figures.

Modulus of elasticity is calculated by extending the initial linear portion of the load-extension curve and dividing the difference in stress corresponding to any segment of section on this straight line by the corresponding difference in strain. All elastic modulus values shall be computed using the average original cross-sectional area in the gage length segment of the specimen in the calculations. The result shall be expressed in Pascals and reported to three significant figures.

For engineering stress and strain (σ_{eng}, ε_{eng}) the original gage dimensions of the specimen are employed, but in plastic region, length and cross-sectional area change. For this reason, true stress σ_{true} and strain ε_{true} are used for accurate definition of plastic behaviour of ductile materials by considering the instantaneous dimensions. Considering A the actual cross-sectional area:

$$\sigma_{true} = \frac{F}{A} \tag{37}$$

$$\varepsilon_{true} = \ln\frac{L}{L_0} \tag{38}$$

Correlation between engineering and true values can be found considering the constancy of volume:

$$Volume = A * L = A_0 * L_0 \tag{39}$$

Thus:

$$\sigma_{true} = \frac{F}{A} = \frac{F}{A_0 \frac{L_0}{L}} = \frac{F}{A_0}\frac{L}{L_0} = \sigma_{ing}\left(\frac{L}{L_0} - 1 + 1\right) = \sigma_{ing}(1 + \varepsilon_{ing}) \tag{40}$$

$$\varepsilon_{true} = \ln\frac{L}{L_0} = \ln\left(\frac{L}{L_0} + 1 - 1\right) = \ln(1 + \varepsilon_{ing}) \tag{41}$$

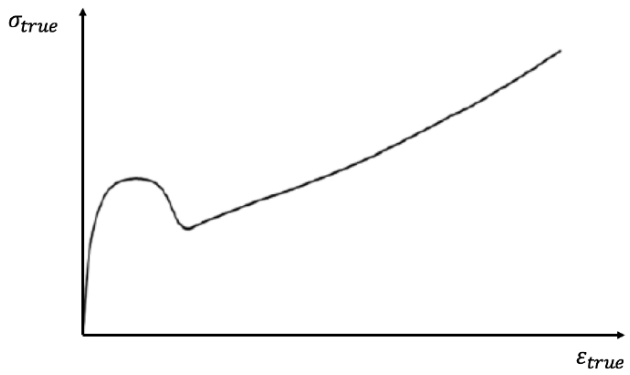

Figure 65. True stress vs. true strain curve

In this study, the test was conducted at 23°C with humidity percentage of 50% and applying a 0.01 mm/s clamp movement.

3.2.4 Numerical process parameters simulation via Autodesk Moldflow Insight®

A numerical analysis has been implemented using *Autodesk Moldflow Insight*® software. This software is often use to simulate and predict plastic injection molding output, indeed processes simulation is nowadays commonly used to cut design costs to achieve the final configuration (lower than with trial and error method) and to improve the overall production process and mold and product design. Moreover, with this software it is possible to predict fiber orientation when using reinforced materials.
Below, the main stages implemented in this study to obtain a numerical response will be listed and described. The analysis to be used is called "Thermoplastics injection molding".

First of all, a CAD file has been generated with *SolidWorks*®, which contains cavity geometry to be imported in *Moldflow*. In this study a 3D importing option was preferred to midplane or dual domain options in order to obtain enhanced accuracy. As the part produced comprises sprue, it has to be added to evaluate the real process conditions.

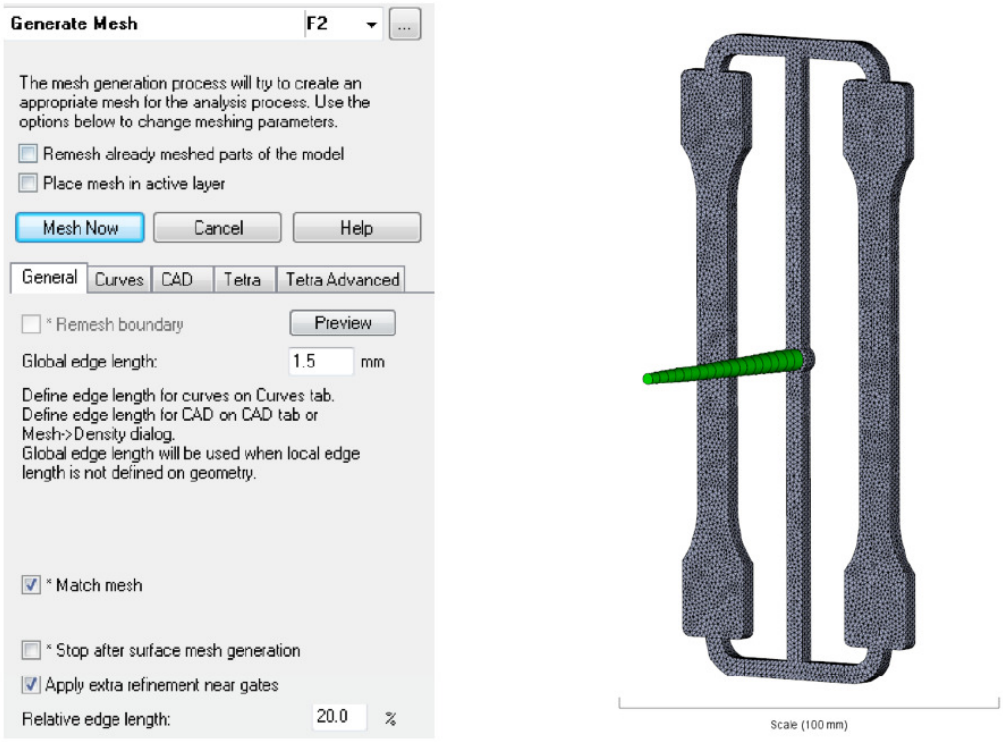

Figure 66. Moldflow part to be analyzed and mesh generation parameters

Secondly, the object has been meshed using tetrahedral elements, with a global edge length of 1.5 mm (Figure 66). Then, injection was set (Figure 67).

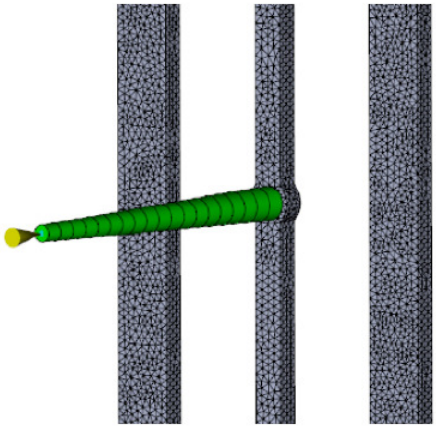

Figure 67. Injection position detail

Once that geometry of cavity and mold features are defined, analysis sequence has to be chosen. For this process, it was performed a "Fill+Pack+Warp" analysis.

Material parameters has to be specified, and it was chosen from database the *Dafnelen HP 1003S®* file (Figure 68).

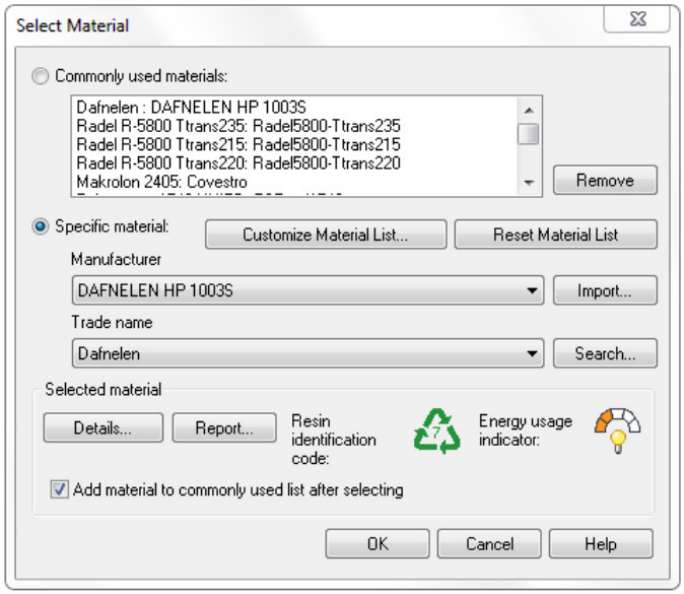

Figure 68. Material selection window

Before running analysis, process parameter needs to be set for the injection location.

- Melt temperature: 260°C
- Mold temperature: 50°C
- Cooling time: 50 s
- Flow rate: 33.6 cm^3/s

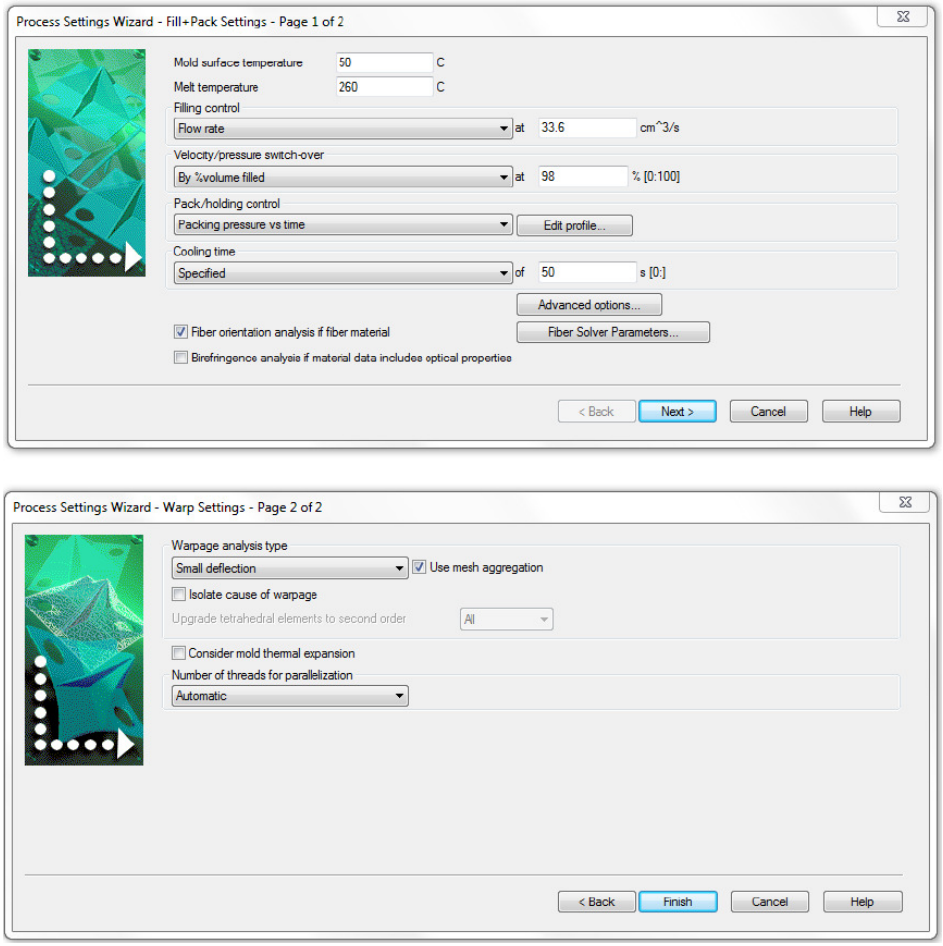

Figure 69. Process parameters setting

Now that all is set, the analysis can be performed. In particular will be analyzed weld line area and fiber orientation tensor.

3.2.5 Uniaxial tensile test simulation via Ansys®

Using *Ansys*® it is possible to simulate an uniaxial tensile test on dogbone specimens. As for *Autodesk Moldflow Insight*®, first the CAD model of the specimen has to be imported (Figure 70).

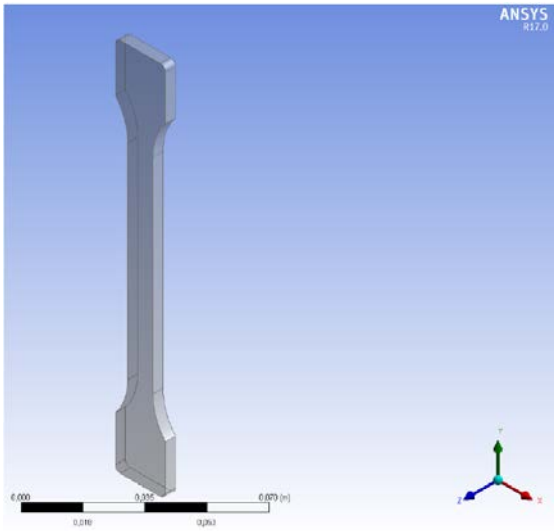

Figure 70. Specimen CAD imported

The second step consists in creating a mesh over the proposed geometry, which nodes and elements are shown in Figure 71.

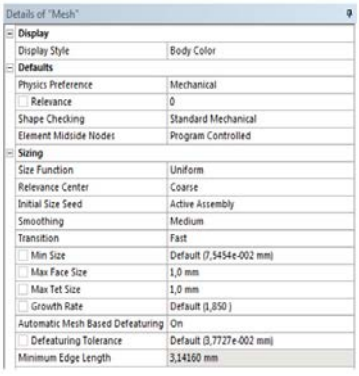

Details of "Mesh"	
Display	
Display Style	Body Color
Defaults	
Physics Preference	Mechanical
Relevance	0
Shape Checking	Standard Mechanical
Element Midside Nodes	Program Controlled
Sizing	
Size Function	Uniform
Relevance Center	Coarse
Initial Size Seed	Active Assembly
Smoothing	Medium
Transition	Fast
Min Size	Default (7,5454e-002 mm)
Max Face Size	1,0 mm
Max Tet Size	1,0 mm
Growth Rate	Default (1,850)
Automatic Mesh Based Defeaturing	On
Defeaturing Tolerance	Default (3,7727e-002 mm)
Minimum Edge Length	3,14160 mm

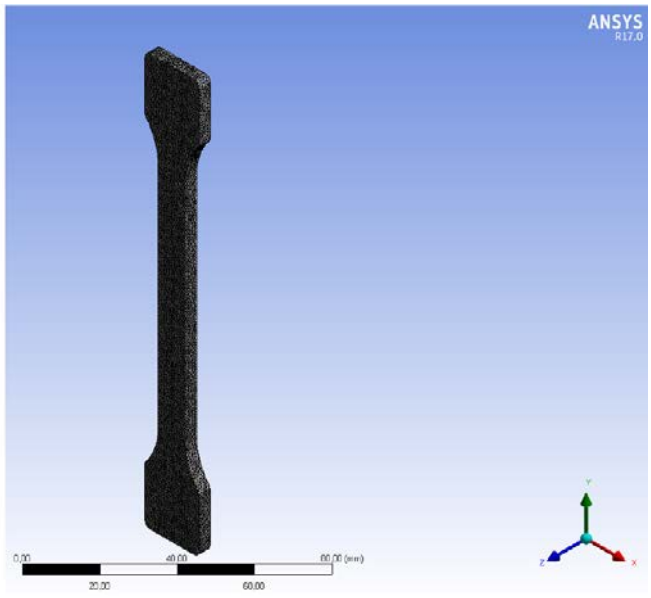

Figure 71. Mesh parameters and resulting output

To proceed with tensile test, constraints must be set. The clamping zones are constrained differently: one, that is denoted with FIX, cannot move in any direction, while the other, denoted with DEF, can only stretch 0.6mm along Y-axis, while the other two directions still fixed, as shown in Figure 72.

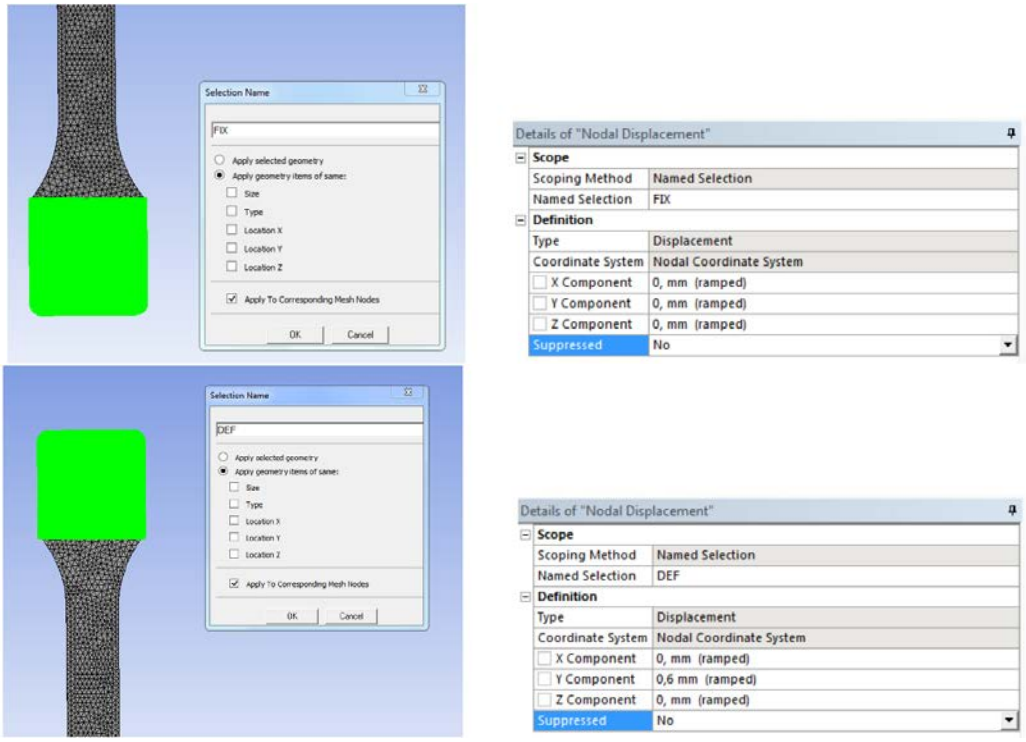

Figure 72. FIX (above) and DEF (below) nodal displacement setting

Parameters shown in Figure 73 are set to run the analysis. The obtained results along with *Moldflow* output will be used as *Helius PFA*® analysis inputs.

Details of "Analysis Settings"	
Step Controls	
Number Of Steps	1,
Current Step Number	1,
Step End Time	1, s
Auto Time Stepping	Off
Define By	Substeps
Number Of Substeps	100,
Solver Controls	
Solver Type	Program Controlled
Weak Springs	Off
Solver Pivot Checking	Program Controlled
Large Deflection	On
Inertia Relief	Off
Restart Controls	
Nonlinear Controls	
Output Controls	
Analysis Data Management	
Visibility	

Figure 73. Tensile test analysis parameters

3.2.6 Autodesk Helius PFA® modelling

Autodesk Helius PFA® software uses *Moldflow*® and *Ansys*® results as input files to determine some of the principal tensile-tested specimen mechanical properties. Besides these input files, stress and strain curves must be provided for reinforced materials at 0°, 45° and 90° compared to the pulling direction.
It is possible to take into account a weld line strength reduction factor that for this study has been set as 0.65.
Before running the analysis by *Command Shell*, the "enable rupture" flag has been activated.

3.2.6.1 Stress-strain curves at 0°, 45° and 90° to be used in Helius PFA®

To determine which parameter set gave the best fiber orientation along flow direction, four simulations were conducted using *Moldflow*. Cavity geometry is shown in Figure 74.

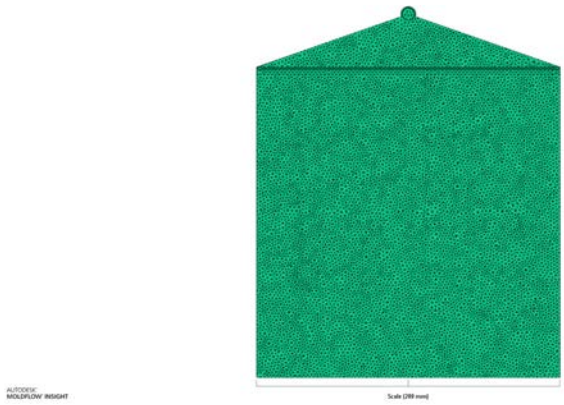

Figure 74. Cavity geometry and mesh

The four analysis are conducted to determine which combination of volumetric flow rate and mold temperature to use, and they are conducted with the following settings:

1) high volumetric flow rate (110 cm^3/s) and mold temperature (100°C);
2) low volumetric flow rate (34 cm^3/s) and high mold temperature (110°C);
3) high volumetric flow rate (110 cm^3/s) and low mold temperature (50°C);
4) low volumetric flow rate (34cm^3/s) and mold temperature (50°C)

Fiber orientations for each simulation are shown below (Figure 75).

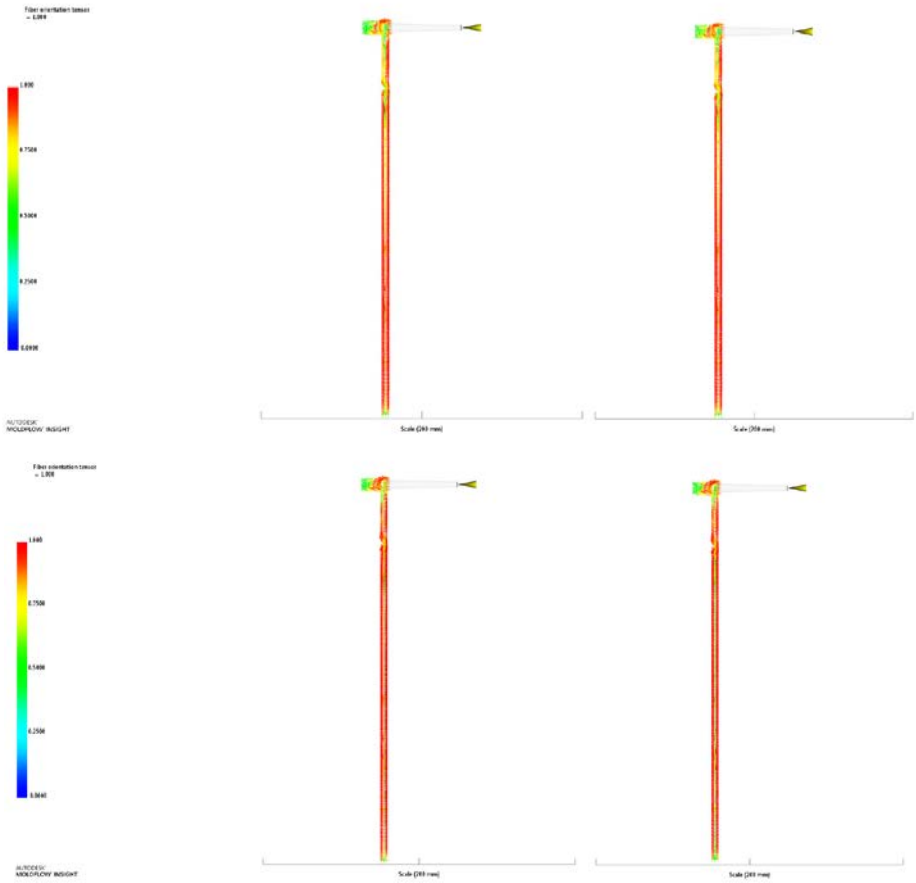

Figure 75. First (up, left), second (up, right), third (down, left) and forth (down, right) simulations fiber orientation outputs

Figure 75 shows how the forth simulation parameters are the one that suits better the scope, as hotter molds reduce the frozen skin layer (red), thus providing less oriented section.

Forth simulation parameters are now used to actually produce the injection molded plates, from which differently-oriented dogbone specimen will be obtained. A total of 9 plates have been molded.
Mold cavity geometry is shown in Figure 76, to mold 20x20 mm plates with a 4 mm thickness. Above the rectangular part, a triangle part of 4 mm height has been provided, and the upper vertex coincides with the injection point.

Figure 76. Mold cavity geometry

Parameters set for injection molding machine are listed in Table 13. As the total plate volume is higher than the maximum molding volume, a pre-extrusion has been performed.

Filling				Packing		Cooling	Cylinder temperature profile			
Vol. flow rate [cm^3/s]	Vol. [cm^3]	Pressure [bar]	Mold temp. [°C]	Pressure [bar]	Time [s]	Time [s]	$T_{0.1}$ [°C]	T_1 [°C]	T_2 [°C]	T_3 [°C]
33.67	192.42	1000	50	380	20	120	240	230	220	210

Table 13. Injection molding parameter setting for plates

To get the different specimens from the injection molded plates, it is necessary to proceed with the milling by means of a micro-milling machine. In this way, it is possible to make the samples that will be subsequently submitted to uniaxial traction, highlighting the differences given by the different orientations of the fibers. In particular, the stress-strain curves will be derived, necessary as input data for Autodesk Helius PFA software, elastic modules, elongations and fracture stresses.

The micro-milling machine used to obtain the differently oriented specimens was the KUGLER MICROMASTER 5X®, in Figure 77.

Figure 77. KUGLER MICROMASTER 5X®

It is a high precision, CNC controlled, 5-axis machining center with oil bearings, which is specially designed and optimized for micromachining and microstructuring use thanks to micro chip removal. According to the selection of tool and process parameters, a wide variety of materials can be machined and structured with the highest precision in optical quality. In combination with the rotary and swivelling unit, CNC give the machine 2.5/3D and freeform surfaces, thanks to the 5-axis simultaneous motion. The base of the unit is made of solid, fine-grained granite, which guarantees the highest long-term thermal and mechanical stability and eliminates vibrations in combination with passive air friction damping elements. Together with the high precision of the individual axis, this guarantees high precision for the entire unit. [52]
Below are shown some micro-milling machine details (Figure 78).

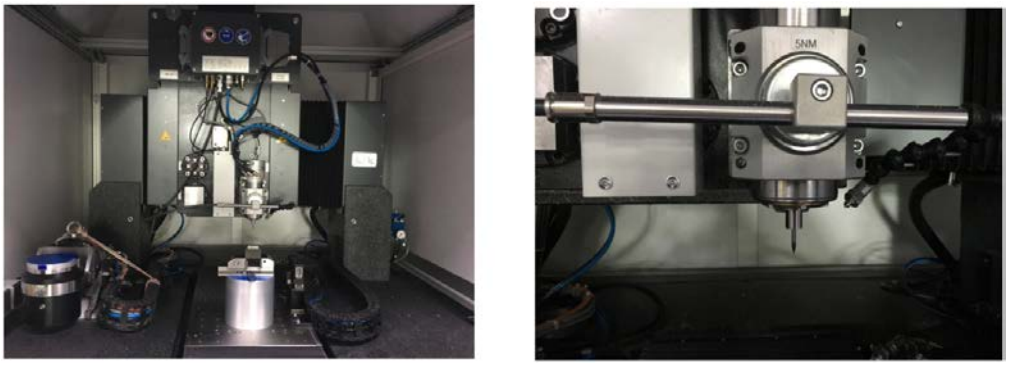

Figure 78. KUGLER MICROMASTER 5X® details

To cut desired specimens from plates, a particular designed support must be used, in order to allow the milling machine operate in the three cutting directions. Clam used is shown in Figure 79, and simply changing installation orientation, it is possible to cut 0°, 45°and 90° oriented samples.

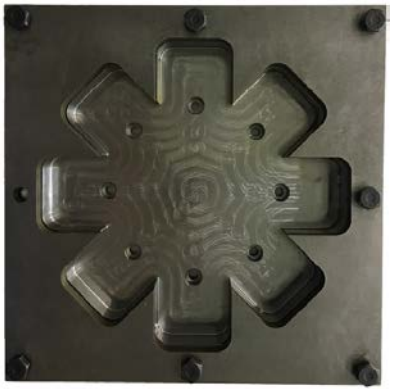

Figure 79. Clamp design for 0°, 45° and 90° sample milling

Positioning the plate on the support, the three oriented samples can be milled (Figure 80). Each sample has a total length of 16.5 mm, thickness of 4 mm, gage length of 1.6 mm and grips length of 2.5 mm.

Figure 80. 0° (left), 45° (centre) and 90° (right) samples

Using these samples and performing tensile tests on them, stress-strain curve for the three different orientations are obtained, and these data will be used as inputs for *Helius PFA* analysis. Stress-strain curves for this study, acquired from 9 samples, are shown below (Figure 81).

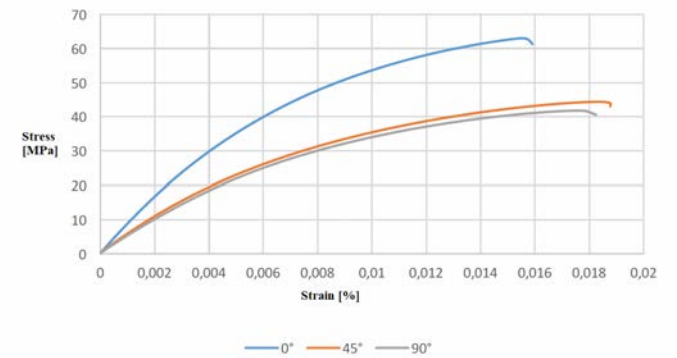

Figure 81. Stress vs. strain curves at 0°, 45° and 90°

For a good matching between experimental and numerical curves, Romberg-Osgood model has been used. Eig= 0.69 is the maximum eigenvalue of fiber orientation tensor.

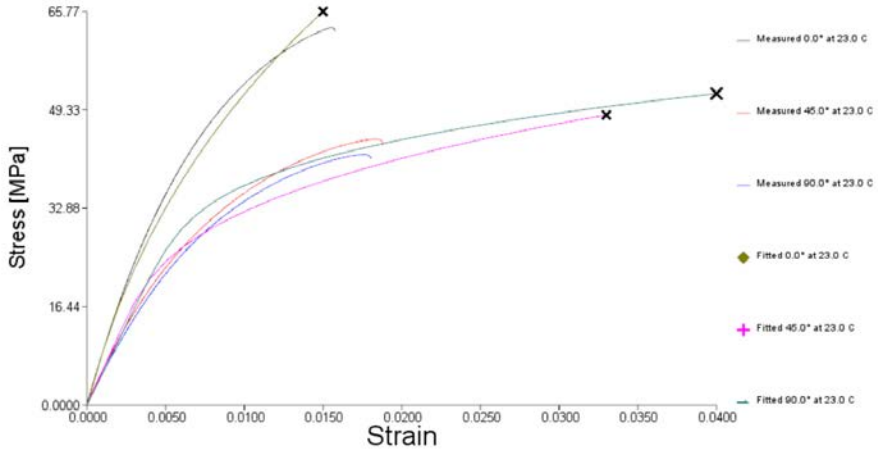

Figure 82. Experimental and numerical stress vs. strain curves

Curves in Figure 82 are obtained applying the Eig value, which scales the represented quantities to take into account that not all the fibers are actually oriented along specimen thickness.

Moreover, elastic modulus and stress and strain at break are acquired and listed in Table 14.

Fiber orientation	Sample	Elastic modulus [MPa]	Stress at break [MPa]	Strain at break [%]
0°	1	8349.73	60.77	1.55
	2	8498.47	62.54	1.58
	3	8602.43	62.36	1.51
	Average	8483.54	61.89	1.55
	STD	127.01	0.97	0.03
45°	1	5562.20	43.53	1.88
	2	5089.89	42.80	1.98
	3	5244.42	43.08	2.19
	Average	5298.84	43.14	2.02
	STD	240.81	0.37	0.16
90°	1	5443.49	41.09	1.75
	2	5107.42	41.14	1.81
	3	5236.85	38.21	1.53
	Average	5262.59	40.15	1.70
	STD	169.51	1.68	0.14

Table 14. Elastic modulus and stress and strain at break at 0°, 45° and 90°

3.2.7 Fracture surface analysis and result validation via SEM

The scanning electron microscope (SEM) uses the generation of a high energy electron beam in a vacuum, focusing it thanks to a system of lenses and deflectors to scan sample area. Beam-sample interaction generates various signals that are acquired by appropriate detectors and then processed to generate a greyscale 3D image.

In a typical SEM, an electron beam is thermionically emitted from an electron gun fitted with a tungsten filament cathode. The electron beam, which typically has an energy ranging from 0.2 keV to 40 keV, is focused by one or two condenser lenses to a spot about 0.4 nm to 5 nm in diameter. The beam passes through pairs of scanning coils or pairs of deflector plates in the electron column, typically in the final lens, which deflect the beam in the *x* and *y* axes so that it scans in a raster fashion over a rectangular area of the sample surface. When the primary electron beam interacts with the sample, the electrons lose energy by repeated random scattering and absorption within a teardrop-shaped volume of the specimen known as the interaction volume, which extends from less than 100 nm to approximately 5 µm into the surface. The size of the interaction volume depends on the electron's landing energy, the atomic number of the specimen and the specimen's density. The energy exchange between the electron beam and the sample results in the reflection of high-energy electrons by elastic scattering, emission of secondary electrons by inelastic scattering and the emission of electromagnetic radiation, each of which can be detected by specialized detectors. The beam current absorbed by the specimen can also be detected and used to create images of the distribution of specimen current. A scheme is proposed in Figure 83.

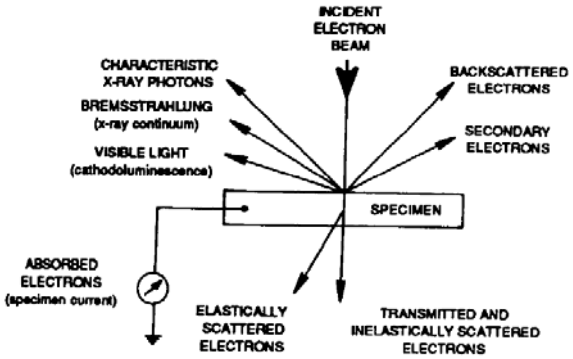

Figure 83. Effect of incident electronic beam interaction with specimen

Information that can be acquired are:

- surface morphology
- chemical-physical composition
- electrical defectiveness
- surface contamination
- surface electrical potentials

In this study, SEM has been used to analyze fracture surfaces of specimen that break after tensile test. Fracture surface morphology and fiber orientation in this area has been investigated to validate numerical model prediction.

3.2.7.1 SEM structure

SEM structure can be seen in Figure 84. It is composed by:

- Electron beam generator in 10^{-2} Pa vacuum ambient to avoid bombardment of the emission region by molecular ions;
- Vacuum generator system to ensure that the average free path of electrons is higher than the source-sample distance;
- Electromagnetic lenses;
- Deflection yoke;

- Signal detectors: the secondary electron detector is on the side of the sample, eccentric with respect to the electro-optical axis to confer three-dimensionality; the detector of the back-diffused is perforated, coaxial to the electro-optical axis and placed above the region of observation; the X-ray detector is placed at the side and is inclined so as to have a wide collection angle;
- Signals converter and transmitter;
- Sample chamber.

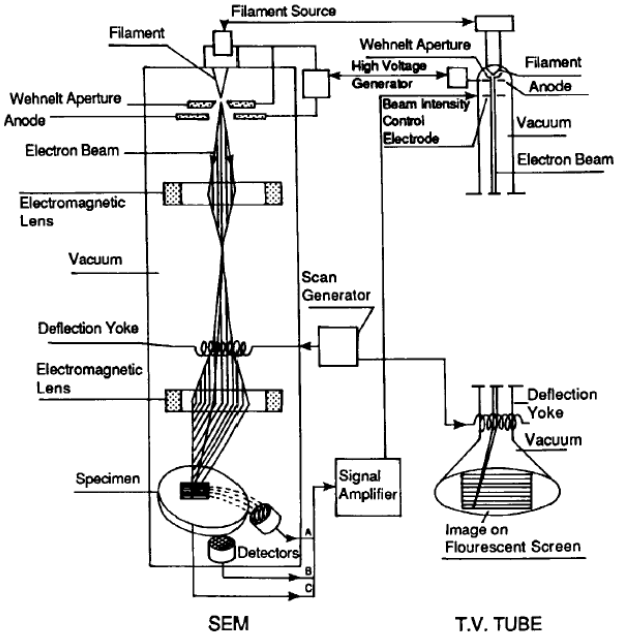

Figure 84. SEM structure scheme

3.2.7.2 Sample preparation

The electron beam is a current of electrons that generates, on an electrically non-conductive sample, the accumulation of a negative static charge which causes difficulties in image formation. Insulating materials, therefore, come covered with a conductive film, which can generally be of gold or carbon, with thicknesses that are so small that they don't alter the surface, in terms of morphological structure. The choice of material depends on the type of investigation to which the sample will be submitted: gold is used for the investigation of exclusively morphological character, carbon for those concerning the constitution chemistry.
The recommended geometry for the sample is a parallelepiped with maximum dimensions of 2.5 cm x 2.5 cm x 1.0 cm.

3.3 Double-nozzle configuration

3.3.1 Mold design

In the following figures (Figure 85-Figure 86) are displayed the main configuration features used in this study.

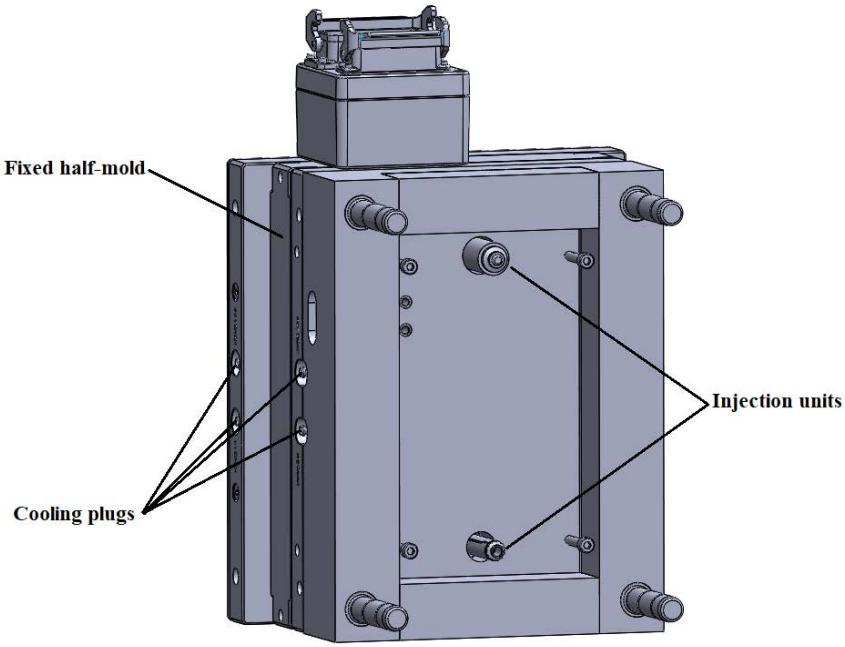

Figure 85. Fixed half-mold principal features

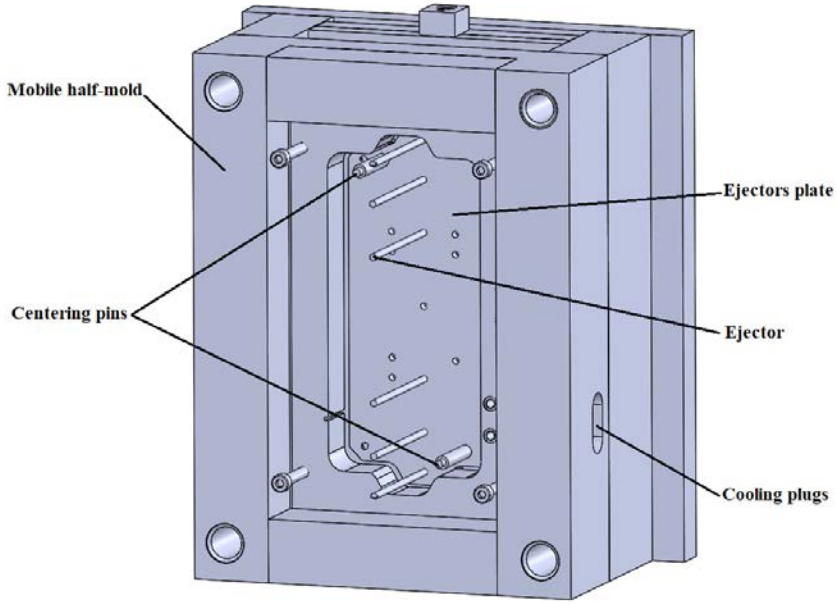

Figure 86. Mobile half-mold principal features

Centering pins are used to correctly assemble the various parts.
The ejector system is used to extract the molded piece once the mold is reopened. Ejector pins are designed so as to provide sufficient force to extract the piece, but in such a way as not to leave too obvious marks on the molded product, or to damage it.
Cooling plugs on mold structures are refrigerant inlet/outlet.

For each half-mold, a removable plate is provided to fit the central rectangular hole. The use of removable plate was chosen in order to be able to reuse the same mold even for future applications.
Inside each plate the cooling circuit has been obtained creating the cooling path by holes in different positions and with different lengths. A special undercut has been made in mobile and fixed plates to insert insulating panels, which are necessary in order to provide a thermal isolation between mold and cavity, as it was desired to maintain mold temperature as homogeneous and stable as possible, while cavity needs to be cooled down.

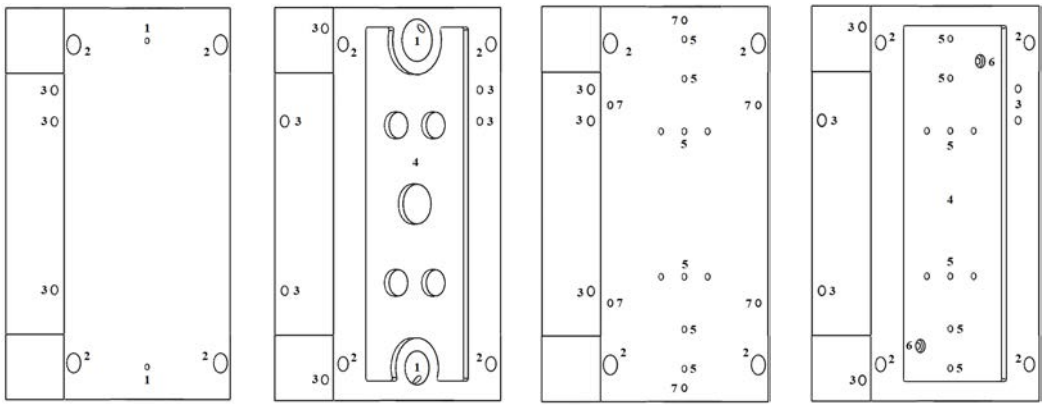

Fixed plate Mobile plate

Figure 87. Fixed and mobile plates

Besides holes created for the cooling channels design (3), the holes for the fixing screws (2), for the passage of the melted polymer from the nozzle to the cavity (1), to place insulating panels (4), to allow the operation of the ejector pins (5), to achieve the correct assembly (6) and to fix cavity insert (7) can be seen on plates faces. In Figure 87 plates are presented, flipping the first view by 180° to show both lateral surfaces.

3.3.2 Cavity design

A single dogbone specimen cavity has been created over a steel insert designed to be fixed to the mobile plate. Once again, it was chosen a removable insert to be able to reuse the mobile plate even for other cavity geometries.
Geometry of designed cavity is shown in Figure 88. Cavity has been placed in the middle of the insert.

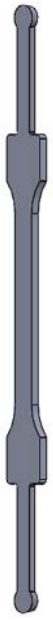

Figure 88. Double-nozzle configuration cavity geometry

As it can be seen, geometry to be realized comprises runners to let the polymer reach the final product-to-be-molded cavity and they will be eliminated after molding process to obtain the actual

specimen for tensile test. The resulting part is the actual dogbone specimen, whose geometric specifications are, according to ASTM D638-14 [51] nomenclature (Table 15):

Dogbone specimen principal dimensions [mm]	
Width of narrow section	10
Length of narrow section	82
Overall width	20
Overall length	150
Radius of fillet	22.1

Table 15. Dogbone specimen dimensions

Holes within dogbone figure are provided to let ejector pins remove the polymer product, while the six holes outside dogbone figure are designed for the fixing screws insertion, to keep insert and mobile plate together. A draft angle of 10° has been provided to easily extract molded parts from cavity. Insert design is shown in Figure 89.

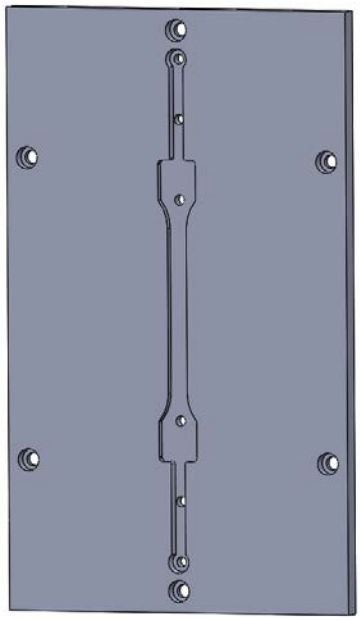

Figure 89. Insert geometry design

According to *BATTENFELD HM 110/525H/210S®* and *Dafnelen HP 1003S®* specifics, process parameters have to be set. Main process values to be considered are temperature and pressure for each phase and cooling time. In Table 16 are listed the parameters used in this study.

Filling					Packing			Cooling
Flow rate [cm^3/s^{-1}]	Vol. [cm^3]	Pressure [bar]	Mold temp. [°C]	Melt temp. [°C]	Velocity vs. pressure switch-over [% filling]	Pressure [bar]	Time [s]	Time [s]
33.6	24.05	1000	50	260	98	400	12	50

Table 16. Injection molding process parameters

In filling phase flow rate control is applied to then switch to pressure control when the cavity is nearly full filled.

3.3.3 Numerical process parameters simulation via Autodesk Moldflow Insight®

A numerical analysis has been implemented using *Autodesk Moldflow Insight*® software, also for this case. Below, the main stages implemented in this case to obtain a numerical response will be listed and described, as in paragraph 3.2.4.

The analysis to be used is called "Multiple barrel thermoplastics injection molding". Multiple barrel thermoplastics injection molding enables the user to simulate the injection of a single material using up to 15 sub barrels. This approach is used to fill the part faster and pack it more evenly than is possible using standard injection molding with a single barrel. It enables the user to simulate a single thermoplastic material in multiple barrels with different barrels properties, melt temperatures, delay times and different filling, packing and cooling controls.

First of all, the CAD file generated with *SolidWorks*® has been imported using a 3D importing option. As the part produced comprises sprues, they have to be added to evaluate the real process conditions. The final part is shown in Figure 90.

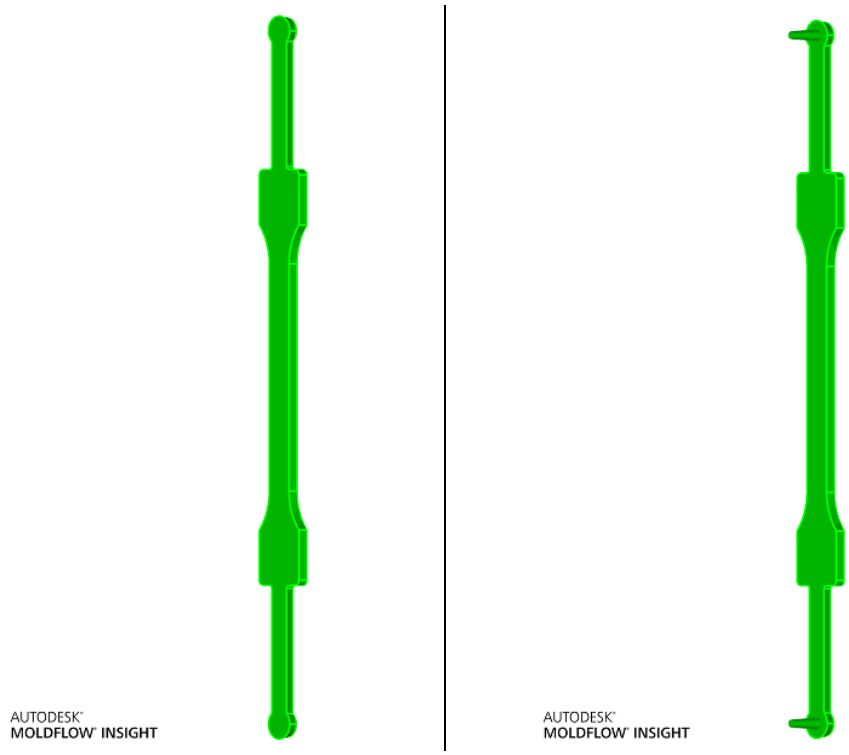

Figure 90. CAD geometry of specimens in Moldflow® with (right) and without (left) sprues

Secondly, the object has been meshed using tetrahedral elements, with a global edge length of 0.5 mm. As the mesh was completed, hot runner and cooling channel were added and meshed. Then, injection positions, cooling inlets and mold were set (Figure 91). Mold surface is needed in Cool (FEM) analysis.

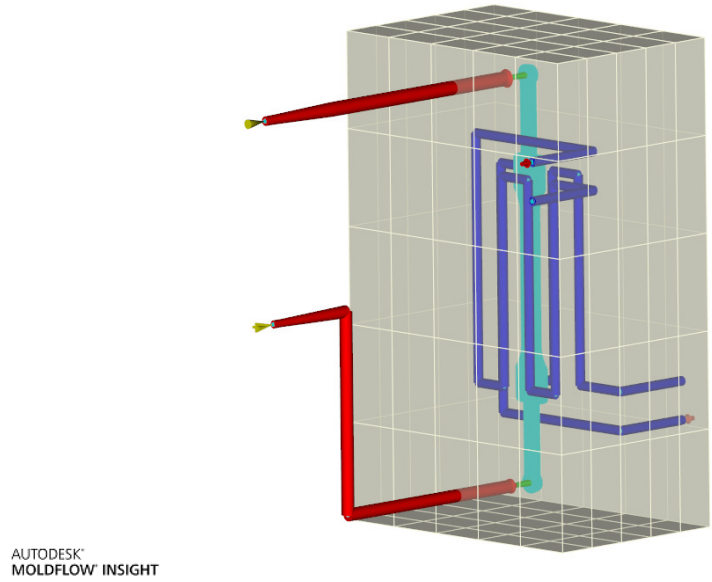

Figure 91. Hot runners, mold, cooling inlets and injection positions on meshed specimen

Now that geometry of cavity and mold features are defined, analysis sequence has to be chosen. For this process, it was performed a "Cool[FEM]+Fill+Pack" analysis.

Material parameters has to be specified, and the same material of the previous study has been selected (Figure 68).

Before running analysis, process parameter needs to be set both for injection locations and cooling inlets.

- Cooling inlets: in this study, "Rapid heating and cooling" property type was used. This function let the user set sequential mold heating and cooling. In Figure 92, the parameters used in this study are shown.

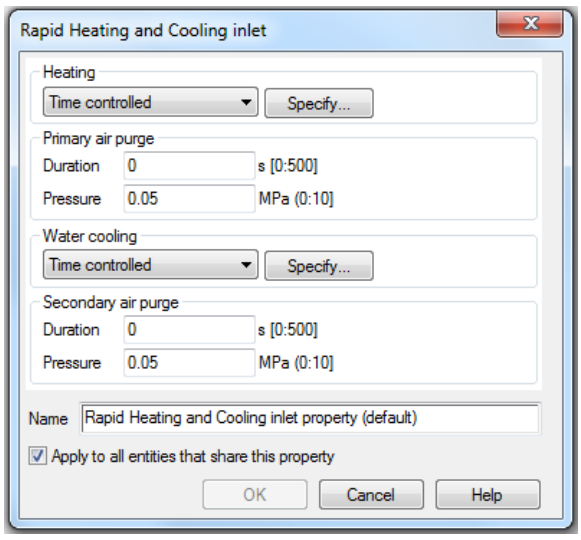

Figure 92. Rapid heating and cooling parameters setting

Heated water has been set with at a temperature of 170°C for 17s, while the coolant temperature is 25°C for 20s. A flow rate of 10 l/min has been used for both.

– Primary injection location: it was set from the Home tab, and its parameters are the one set via "Process settings" in Home tab (Figure 93). This barrel is the one that will be used also for packing phase, while the other will be active only during filling phase.

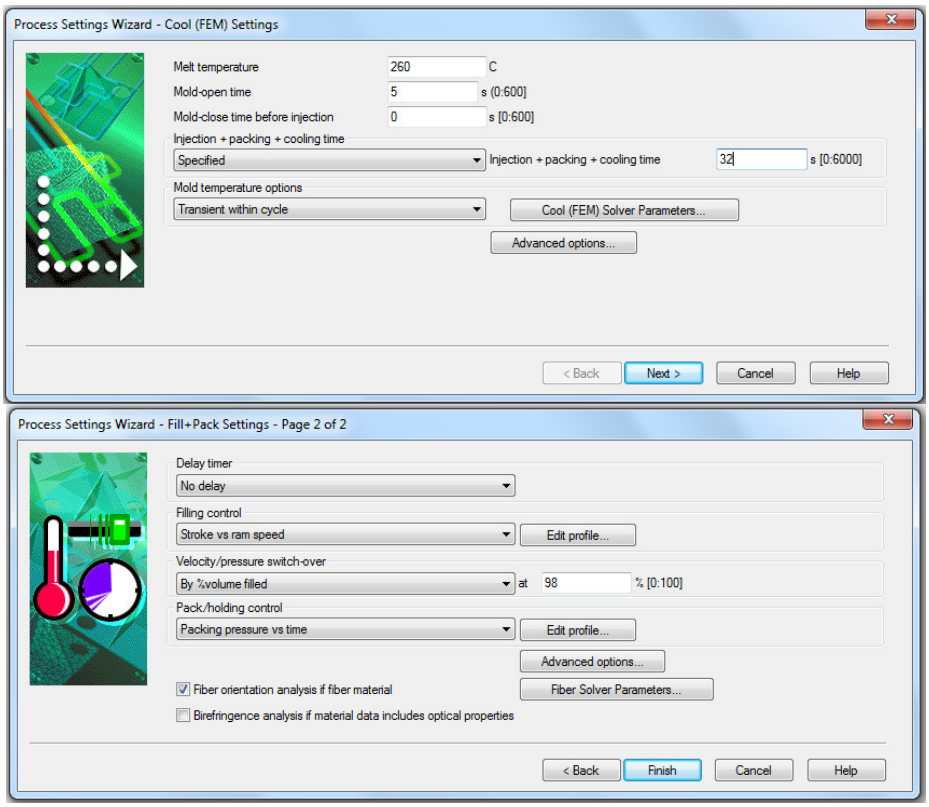

Figure 93. Primary injection location parameters setting

Sub-menus selections are shown in Figure 94-Figure 95 below. They represent the parameters to be set for filling and packing phase. For packing phase, two different set of parameters have been used, one for no-in-flow conditions and the other one to promote in-flow phenomena, but only for the other injector, while for the primary one, they still the same.

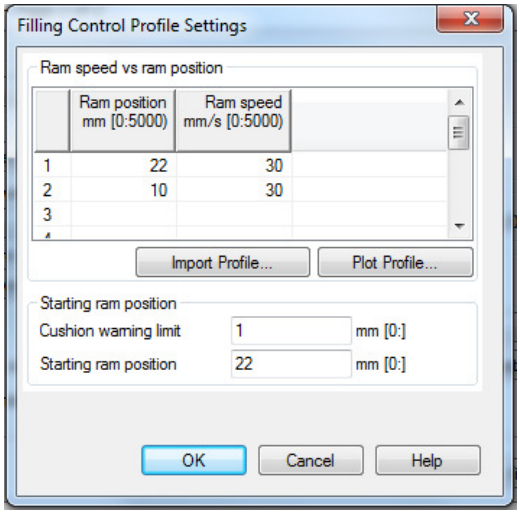

Figure 94. Stroke vs. ram speed

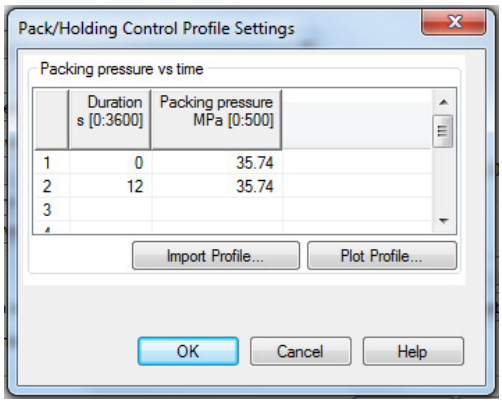

Figure 95. Packing pressure vs. time for no-in-flow conditions

– Secondary injection location: via "Boundary conditions → Multiple barrel → Set locations" can be assigned the secondary injection locations, that can be set with different parameters compared to the primary ones. They also appear with a different symbol, indeed, the primary injection location is represented by a cone, while the secondary injection locations are represented as a cross-based prism. In Figure 96 are shown the parameters set.

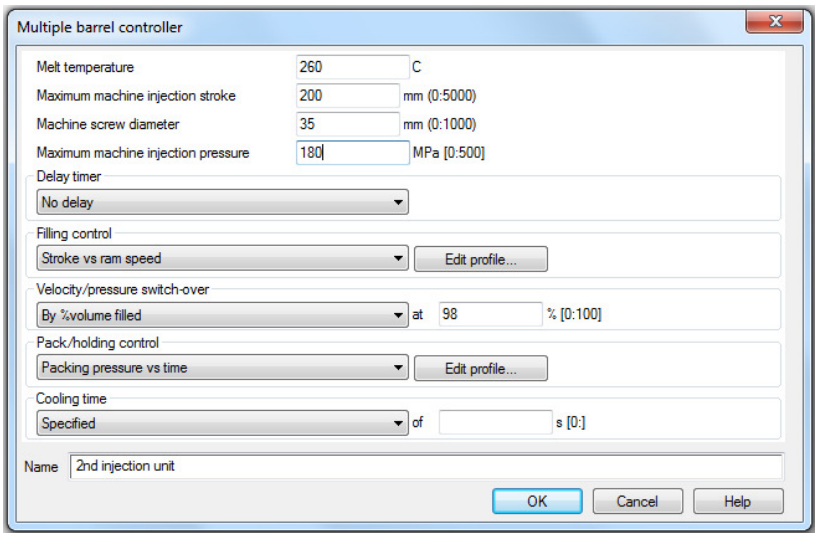

Figure 96. Secondary injection location parameters setting

In terms of stroke vs. ram speed filling parameters, the inputs to be set are the same shown in Figure 94, while for packing phase the parameters to be used are the ones in Figure 95 for no-in-flow specimens, while to promote in-flow, the pressure is set to zero (Figure 97).

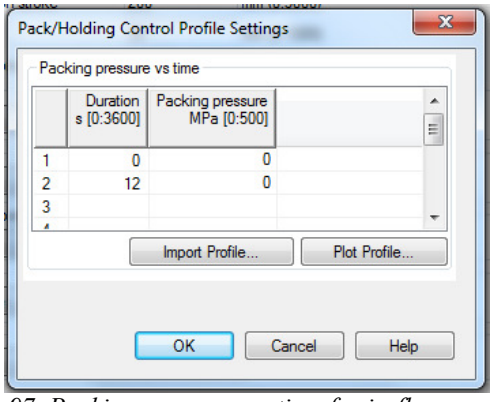

Figure 97. Packing pressure vs. time for in-flow conditions

Now that all is set, the analysis can be performed. In particular will be analyzed weld line area and fiber orientation tensor.

3.3.4 Uniaxial tensile test simulation via Ansys®

Since dogbone specimen dimensions are the same in the two configurations, the proceeding described to simulate a tensile test on sample in 3.2.5 are valid also in this case. The parameters used to set import CAD geometry, obtain a suitable mesh density, constrain the two edges and to run the analysis remain unchanged.

3.3.5 Autodesk Helius PFA® modelling

The same procedure described in paragraph 3.2.6 has been adopted to this configuration. *Moldflow*® and *Ansys*® results for this configuration, along with stress and strain curves at 0°, 45° and 90° derived in 3.2.6.1 are used to set the analysis. Weld line strength reduction factor of 0.9 has been maintained also for this case.

CHAPTER 4

Results and discussion

In this chapter, will be exposed the present study results, both for single and double nozzle configuration, and the comparison between no-in-flow and in-flow outcome.
Stress vs. strain experimental curves obtained by no-in-flow specimen's tensile tests will be displayed and mechanical properties will be derived. Subsequently, numerical modelling solutions are shown and the correlation with the experimental values for no-in-flow case is exposed. This section ended with no-in-flow and in-flow comparison in term of structural analysis, and relative consideration about the effectiveness of the technique proposed in this study.

4.1 Single nozzle configuration

4.1.1 Stress vs. strain experimental curves

Stress and strain curves for 8 samples have been obtained in no-in-flow specimens. When tensile test is performed, instead of stress vs. strain curves, the output consists in load vs. extension curves, and those are shown in Figure 98.

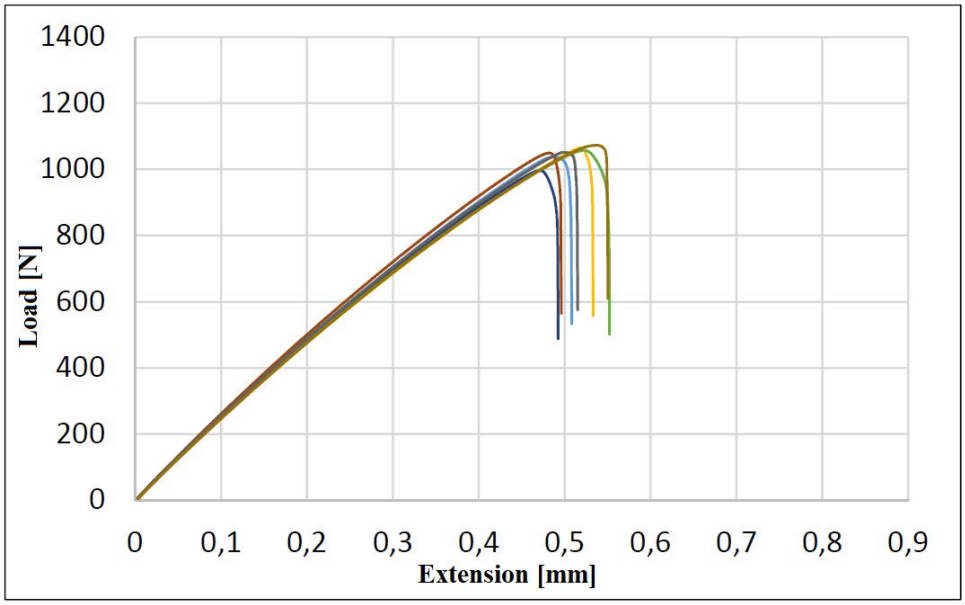

Figure 98. Load vs. extension curves for no-in-flow specimens

It is possible to notice a discrete repeatability of the different curves. The curves generated by the specimens of the same sample, in fact, are very close between them and sometimes overlap.
Maximum load at break never exceeds 1128.994 N, and al specimens break between 0.47 and 0.56 mm extension. Load at break and break extensions are individuated in the curves by the pick, right before the curves drop nearly vertically.

These load vs. extension curves can be converted into stress vs. strain curves, using Eqns. *(35)*, *(36)*. As already mentioned, they maintain the same trends, but with different quantities value. Stress vs. strain curves are shown in Figure 99.

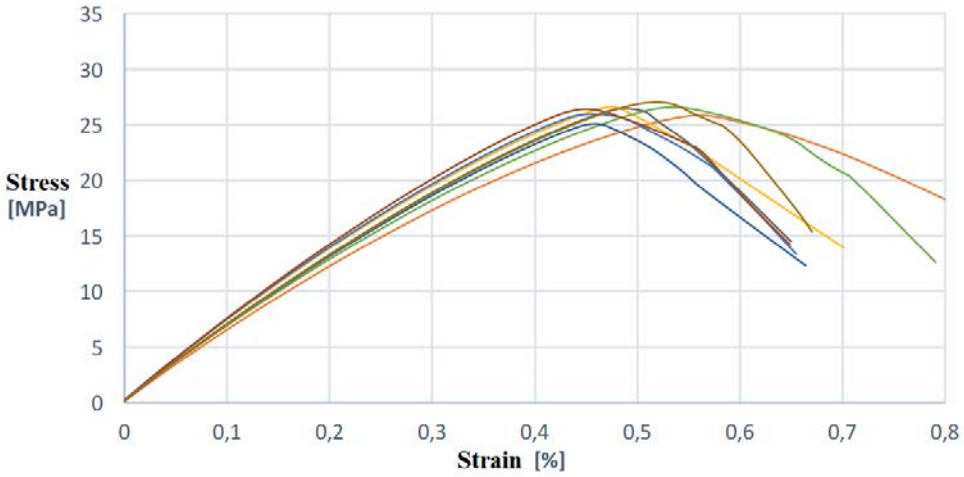

Figure 99. Stress vs. strain curves for no-in-flow specimens

Ultimate tensile strength is measured by the maximum stress that a material can withstand while being stretched or pulled before breaking, and the values obtained for the 8 tested samples are summarized in Table 17. In terms of load applied, the average load at break is 1048.94 N.

NO-IN-FLOW SPECIMENS										
Sample	1	2	3	4	5	6	7	8	Avg	STD
UTS[MPa]	25.87	26.62	25.93	26.60	25.08	26.40	26.45	27.00	26.24	0.59

Table 17. UTS values for no-in-flow specimens

From stress vs. strain curves, by measuring the slope in the elastic deformation region of the curves themselves, it is possible to determine the value of the elastic modulus. Values are shown in Table 18.

NO-IN-FLOW SPECIMENS										
Sample	1	2	3	4	5	6	7	8	Avg	STD
Elastic modulus [MPa]	6292.66	7075.34	7062.79	6514.43	6656.17	7224.35	6731.56	6741.55	6787.00	314.00

Table 18. Modulus of elasticity for no-in-flow-specimens

Since the components are highly anisotropic, it is preferred to evaluate part stiffness instead of modulus of elasticity, as in tensile test, not only material properties is evaluated, due to its nature, but the overall part response. Values are listed in (Table 19).

NO-IN-FLOW SPECIMENS										
Sample	1	2	3	4	5	6	7	8	Avg	STD
Stiffness [N/mm]	2463.861	2527.758	2485.5	2516.7	2579.3	2509.8	2450.9	2504.8	2504.831	39.99576

Table 19. Stiffness for no-in-flow specimens

4.1.2 Autodesk Moldflow Insight® output

4.1.2.1 Weld line

Among *Autodesk Moldflow Insight*® results, it is possible to visualize weld line formation region. In particular, it can be seen a line, which indicates weld line position, as in Figure 100.

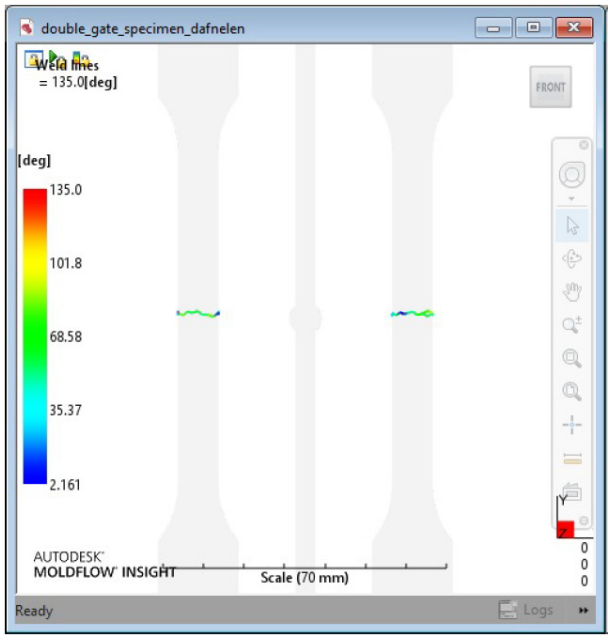

Figure 100. Weld line position in single nozzle no-in-flow specimen

Figure 100 shows how weld line forms half way between gate locations, which correspond to the middle of molded samples. Worth mention to notice that in no-in-flow specimens, weld lines are nearly straight and perpendicularly oriented to flow direction.

As the flow is balanced due to single injection point and balanced runners, this result was expected and confirmed by simulation. Samples molded also agreed with simulation output, as it will be described in 4.1.3.

4.1.2.2 Fiber orientation

Fiber orientation is one of the main factors influencing reinforced polymer parts production, thus is fundamental to find a reliable algorithm to predict this property. In the past century, methods to model fiber orientation have been implemented and improved, but they are always based on two rules of thumb:

- shearing flows tend to align fibers in the direction of flow;
- stretching flows tend to align fibers in the direction of stretching.

Fiber orientation tensor comprises information about the probability of fiber alignment in the three cardinal direction, in a matrix where 1 is the first principal direction, i.e. the direction of the highest probability that the fiber align, that may not coincide with the flow direction. Second and third principal directions are based on, and are at the right angles to, the first principal direction. As values approaches 1, the fibers are mostly aligned in this direction.
Using *Autodesk Moldflow Insight*® result options to visualize fiber orientation tensor, we can obtain two different graphic outputs.

"Fiber orientation tensor" is a quick plot option, which shows fiber orientation tensor values using a colour-scale graph. To obtain this graph, the thickness is normalized in a scale from -1 to 1, a specified numbers of steps in the interval are chosen and the thickness is divided in a number of layers that correspond to the number of steps. The results shown are referred the single layer selected. This result can be seen in Figure 101.

"Probe XYPlot" let the user select a specific point (node) and the results that will be shown will be the fiber orientation tensor through thickness. It is not a quick plot option and it must be added by the user as plot to be shown in results list. This result can be seen in Figure 102.

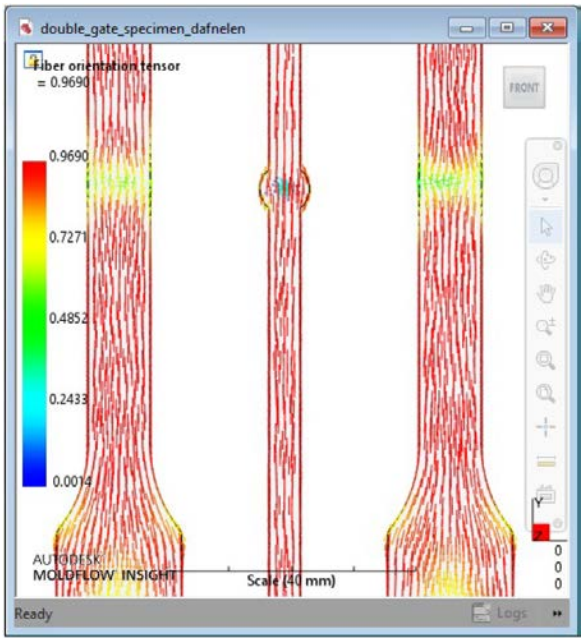

Figure 101. Fiber orientation tensor at 0-thickness

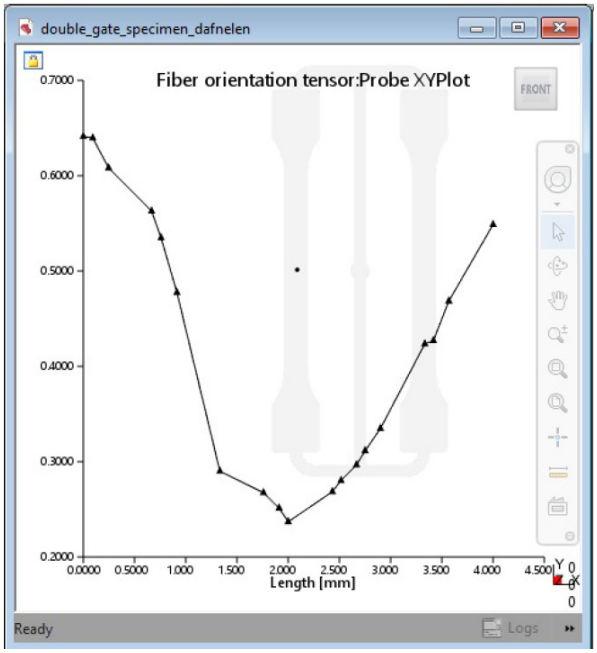

Figure 102. Fiber orientation tensor Probe XYPlot at weld line

As it can be seen, in the weld line region, fibers are poorly oriented, and the core is even more disoriented than the skin layer region. As previously mentioned, this condition reduces component strength and the part tends to break in correspondence of this weaker region.
The fiber orientation trends are typical of weld line in no-in-flow samples, and the expected result trends have been confirmed.

4.1.3 Results of comparison between numerical and experimental output

Comparing load vs. extension curves obtained experimentally and the one given from numerical analysis, it can be seen how numerical model overestimates the value of force at break and the slope of the linear section. The extension at break, on the other hand, approaches the experimental values more accurately and respecting the same values interval. (Figure 103).

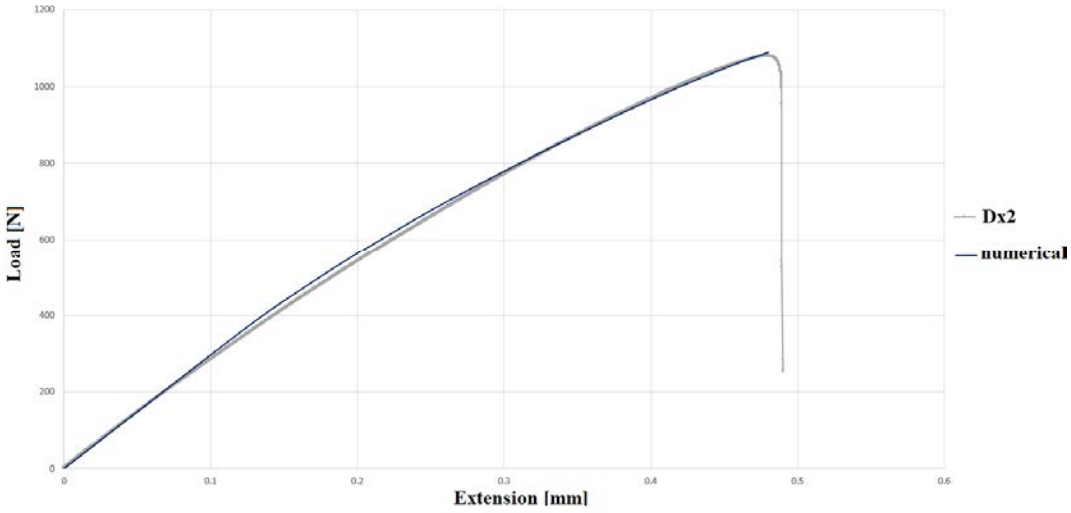

Figure 103. Load vs. extension numerical (blue) and experimental (grey) curves

In terms of load at break, numerical model computes a load at break of 1050 N instead of 1048.94 N obtained experimentally, committing a 0.1 % error. In terms of stiffness, numerical model predicts a 2776.875 N/mm value, instead of 2504.831 N/mm measured during tests, so with a 10.86 % error. These errors could probably be an effect of an inaccurate numerical representation of the real specimens' fiber orientation; however, since the trends are respected it can be used as a good starting point for simulations. Better response accuracy can be achieved refining mesh or providing smaller sub-steps during tensile tests, in order to collect more data and obtain a more accurate curve.

In terms of weld line morphology and structure, SEM analysis has been performed on tensile tested specimens, after a thin film of gold was applied on fracture surfaces. First of all samples actually broke across weld line surfaces, confirming this is the weaker section in molded specimens (Figure 104), and molded samples show how numerical model well predicts weld line morphology.

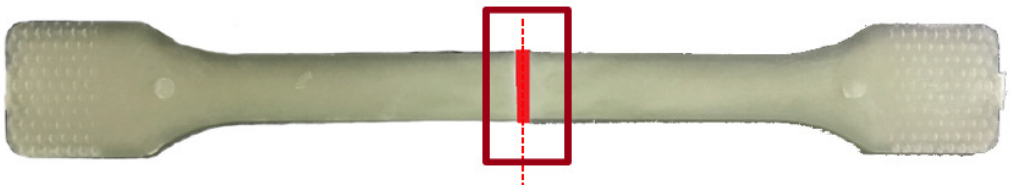

Figure 104. Fracture surface corresponding to weld line position

SEM image shows how fibers at the weld line region are oriented parallel to fracture surface, according to fountain flow phenomena during filling, verifying the good fiber orientation prediction from numerical simulation (Figure 105).

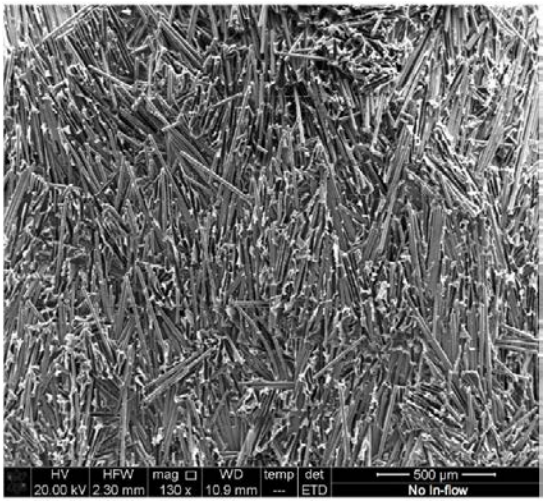

Figure 105. Fracture surface SEM image for no-in-flow specimen

4.2 Double nozzle configuration

4.2.1 Comparison of Moldflow® results between no-in-flow and in-flow cases

4.2.1.1 Weld line

The aim of the double nozzle configuration has been the under-skin-layer flow control to induce in-flow in the cavity after filling. As can be seen in Figure 106, the fill time of 0.227 s is equal for both no-in-flow and in-flow cases, as the filling parameters are the same for both injectors in both cases.

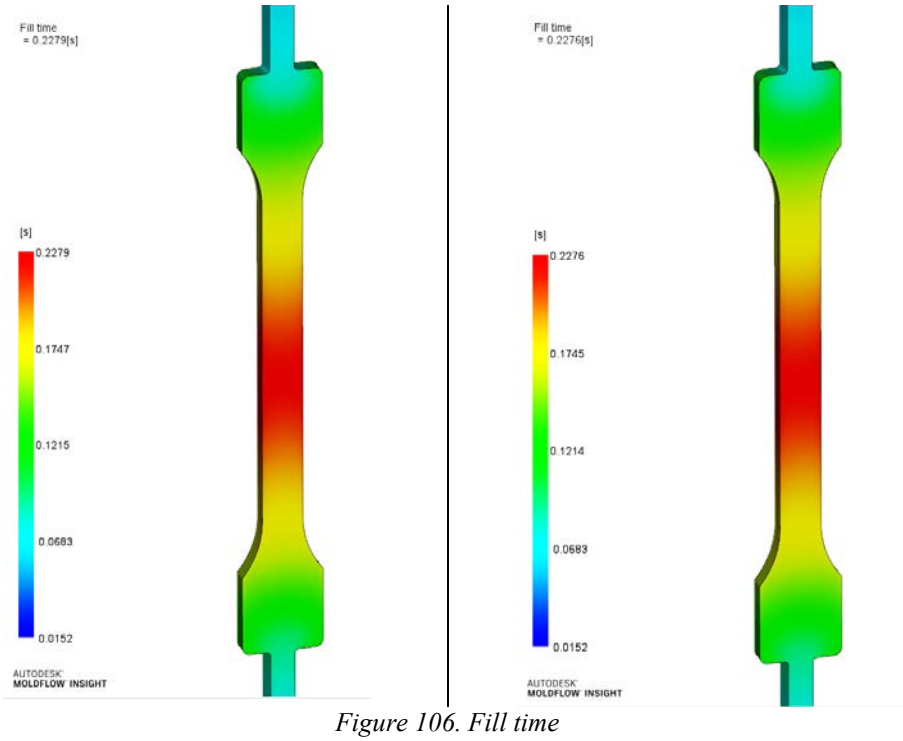

Figure 106. Fill time

As previously mentioned, the in-flow phenomenon has been induced creating a pressure gradient between the two injector locations. The parameters set in 3.3.3 led to the pressure gap between injectors that promotes this phenomenon. Weld line surface is expected to be re-positioned thanks to in-flow effects.
Weld line position displayed in *Moldflow*®, is the section in which the weld line first forms. The figure below (Figure 107) shows how weld line first forms in the same section for both cases. This fact is a direct consequence of filling phase, as the weld line first position is where the two flow fronts first met, that coincides with the latest section to be filled during process, and since the two filling phases were identical, the weld line position was expected to be the same.

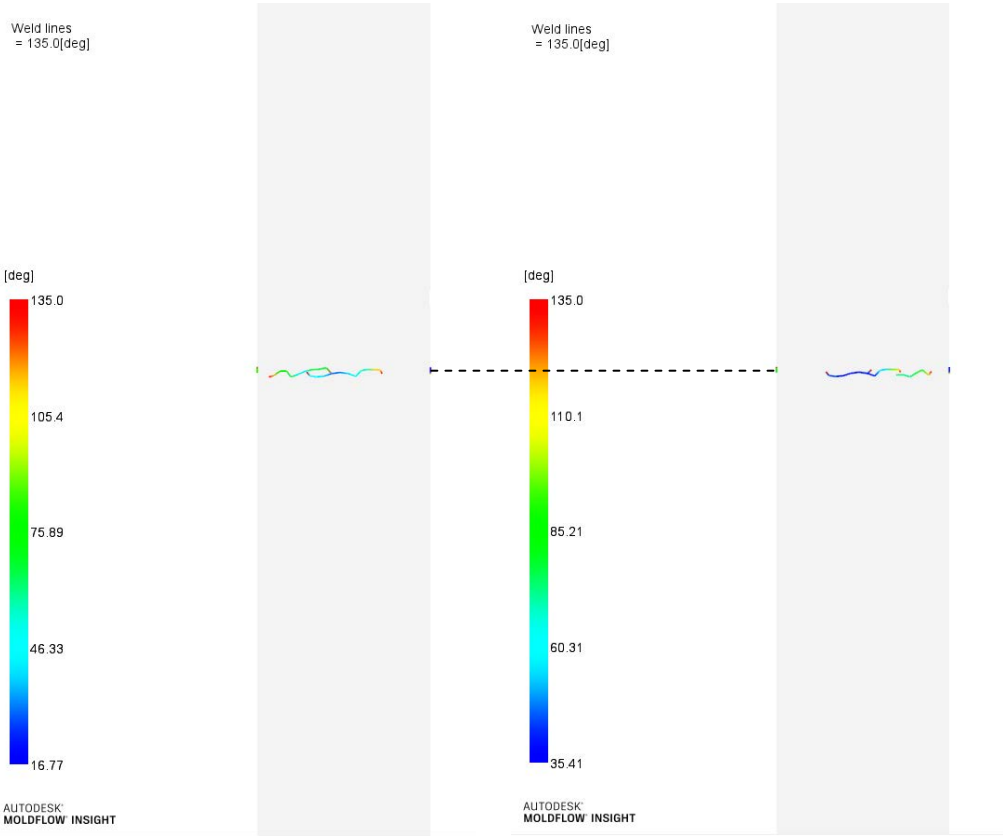

Figure 107. Weld line position

Moldflow® let the user visualize the calculated weld line movement during process, in a 3D representation. In "Result" tab, a back-play-forward set of icons can be used to highlight different results moving between substeps (that in this case are time intervals), to evaluate the evolution of weld line position in time. In Figure 108 some frames are reported to display how in-flow phenomenon has been effective in weld line surface transformation, compared with no-in-flow case.

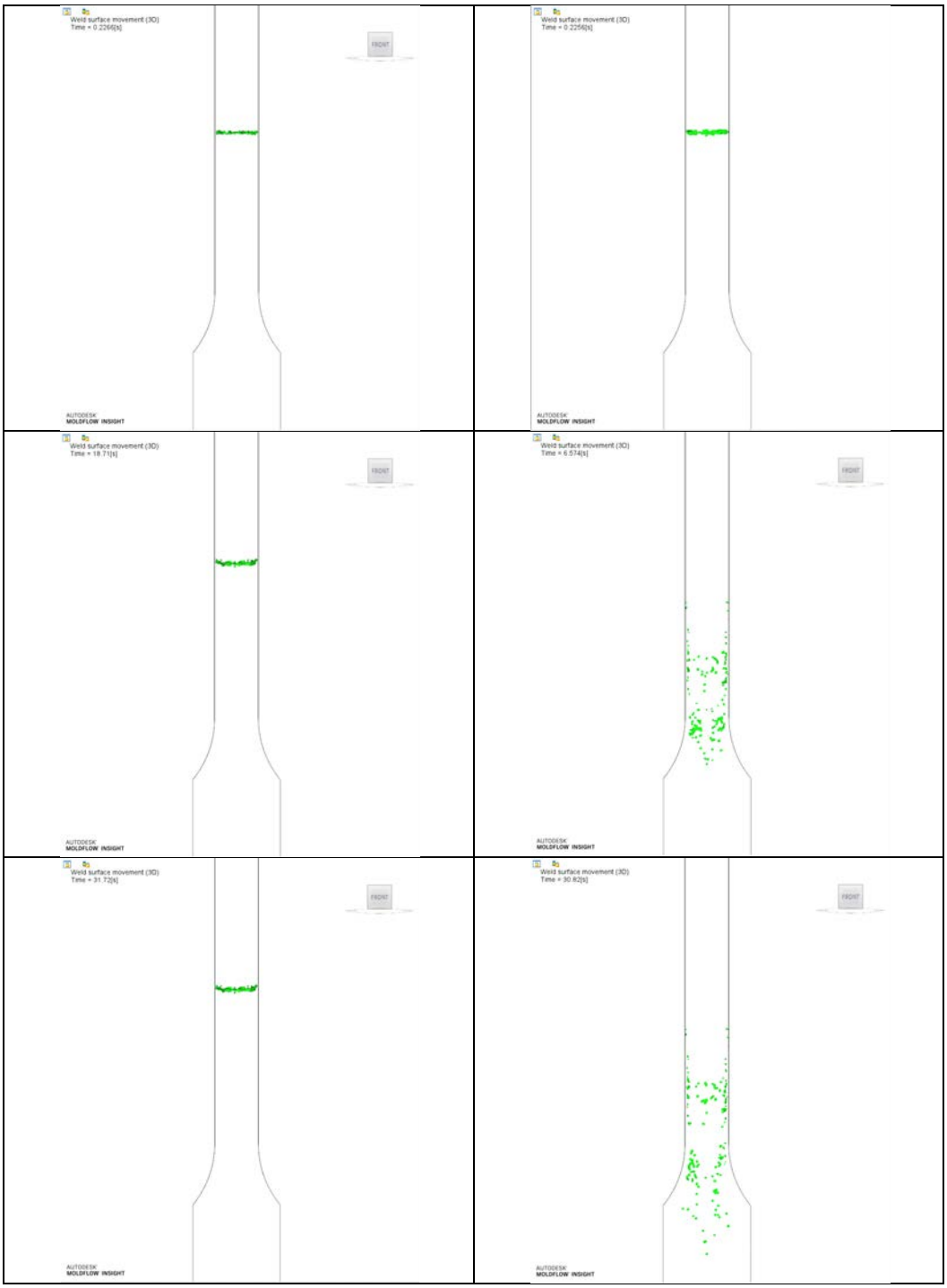

Figure 108. Weld line movement during process, no-inflow (left) and in-flow (right) cases

The fact weld line surface has been stretched and deformed as can be seen in Figure 108, involves that also fiber orientation has been influenced by in-flow, in particular, the expected outcome is that fibers at weld line are now bonded and better oriented in cavity than no-in-flow case, leading to better local mechanical properties. The overall weld line surface movement measured in *Moldflow*® along flow direction is nearly 59 mm, as shown in Figure 109.

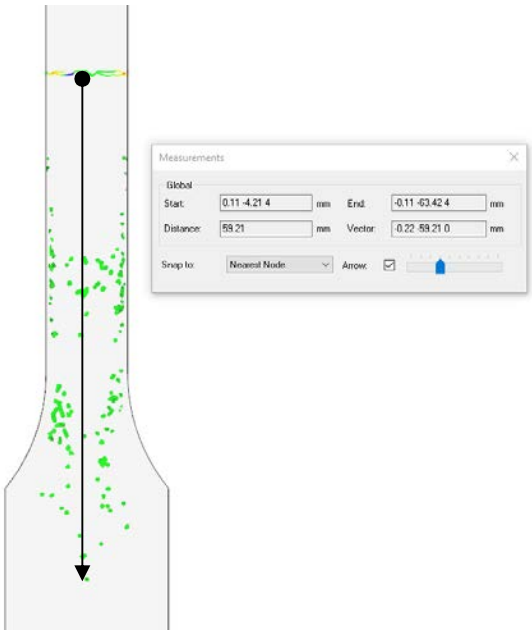

Figure 109. Weld line movement along flow direction due to in-flow

Worth noticing that using VARIOTHERM, mold temperature can be kept as high as 152°C during process, as highlighted in Figure 110.

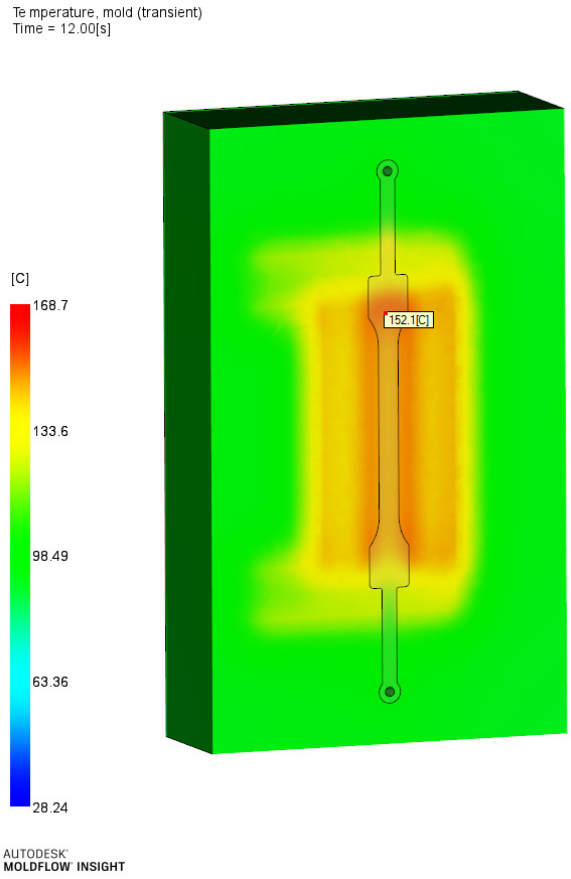

Figure 110. Mold temperature at cavity at 12 s

The fact that mold temperature is higher than without using VARIOTHERM means that a smaller skin layer will form due to a lower temperature gradient between mold surface and melt. In-flow involves polymer that still melt under the frozen skin layer, thus the greater the

melted polymer layer available, the greater the amount of material subject to the in-flow phenomenon.

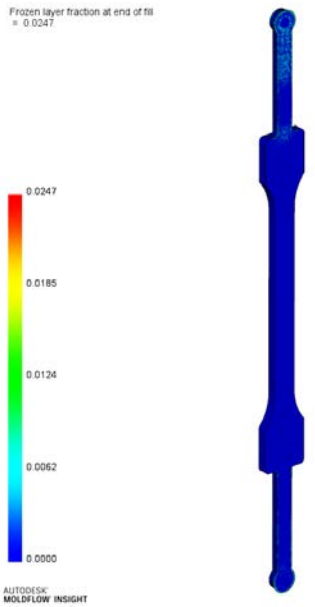

Figure 111. Frozen layer fraction at the end of fill

Rapid heat and cooling has been proven capable of eliminating weld line skin marks and the result shown in Figure 111, where it can be seen how the frozen skin layer has been reduced to a very small thickness, seems promising in obtaining the same effect, also with this experimental setup.

4.2.1.2 Fiber orientation

As previously mentioned in 4.1.2.2, fiber orientation is one of the main factors influencing reinforced polymer parts production, and the same plot shown in the cited paragraph are shown below, highlighting the differences between no-in-flow and in-flow cases.

In Figure 112, the "Fiber orientation tensor" quick plot is displayed. The colour-scaled graph is useful to have an immediate feedback on how fibers are aligned respect to flow direction, in a scale where blue is normal to flow direction (worst case) and red is along flow direction (best case).It can be seen how in-flow enhanced fiber orientation.

The weld line region in blue-green for no-in-flow case disappears when in-flow is present; in fact, the same region becomes red after in-flow phenomenon occurs. The effects of weld line surface repositioning with this techniques can also be seen in the lower part of the specimen, even overshooting the final weld line position, probably due to flow inertia. Indeed, the lower rectangular portion of the dogbone specimen and the runner are now more oriented, and it can be stated noticing that where first there was a green-yellow region, with in-flow it has been replaced with a yellow-red one.

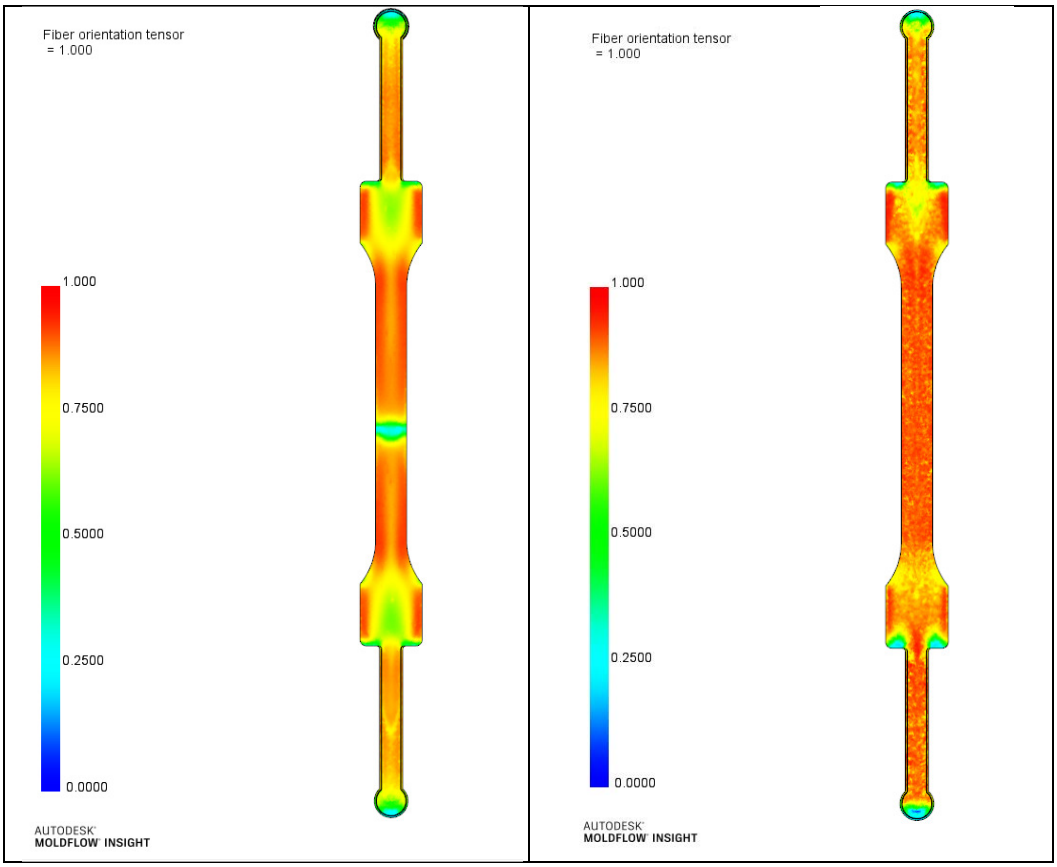

Figure 112. Fiber orientation tensor for no-in-flow (left) and in-flow (right) cases

Even if this graph let the user immediately understand if fibers are oriented or not, thus, if mechanical properties of the part are good or not, the "Fiber orientation tensor" XYPlot shows fiber tensor a11 entrance for a single node through thickness. A node in the middle of weld line first position has been chosen, to display how in-flow improves fiber orientation, and the relative results are shown in Figure 113.

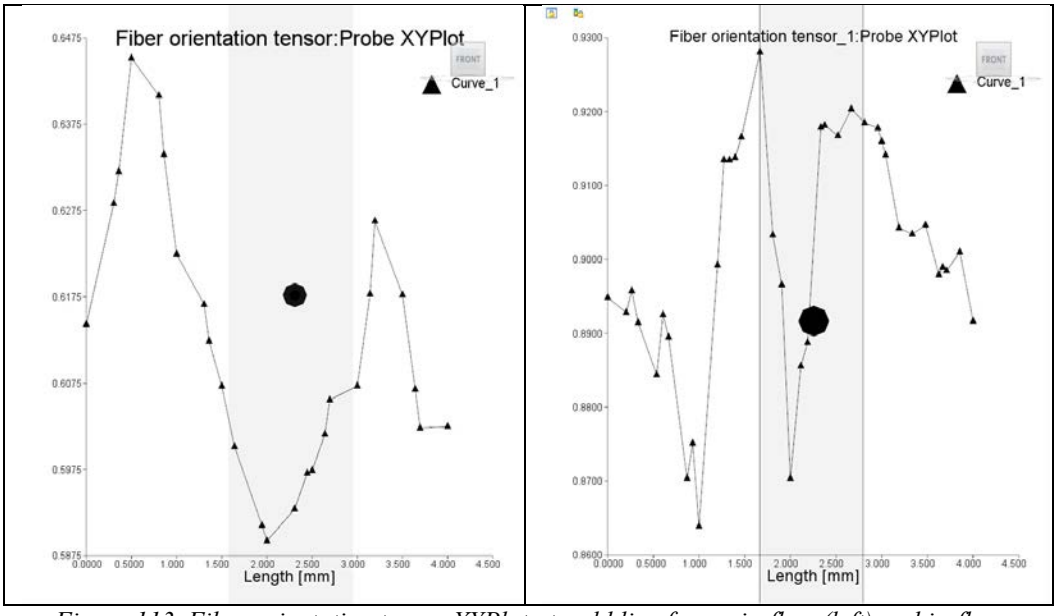

Figure 113. Fiber orientation tensor XYPlot at weld line for no-in-flow (left) and in-flow (right) cases

As can be seen, fiber orientation tensor a11 had value from a minimum of 0.5875, to a maximum of 0.6475, through thickness. Thanks to in-flow, values are shifted from a minimum

of 0.86, to a maximum of 0.96. This excellent result is believed to lead to better mechanical properties, since they are linked to how fibers are oriented in respect to load direction, which in case of tensile test corresponds to flow direction.

4.3 Comparison between no-in-flow and in-flow structural analysis

The previous illustrated results are used to set the structural analysis. First, the specimen geometry has been acquired in *Ansys*®, to generate the input file. This input file contains mesh information, constraints and the number of substeps for the analysis. Thanks to *Helius PFA*®, *Moldflow*® results are mapped on the specimen model prepared with *Ansys*® and a weld line strength reduction factor of 0.65 has been set. Once the structural model has been exported, the analysis has been run.

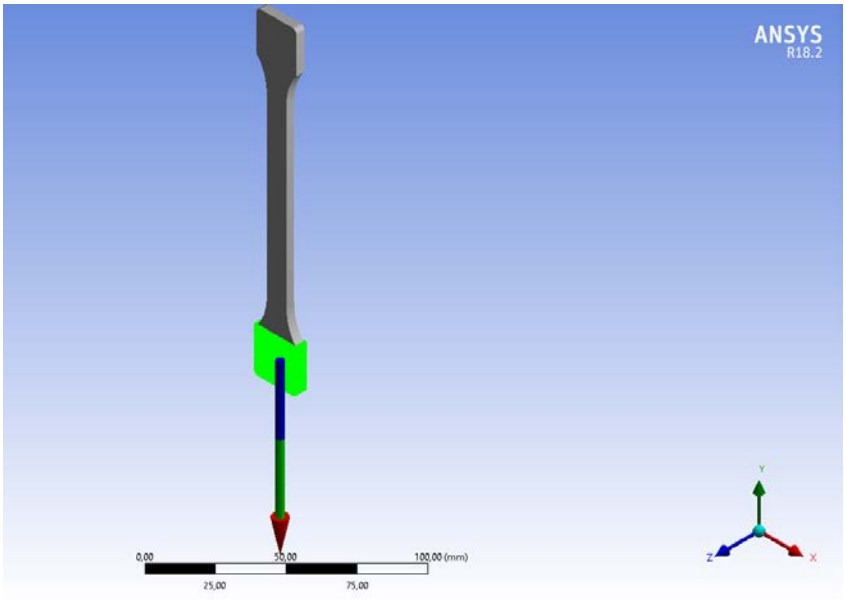

Figure 114. "Force reaction" result display

Thanks to this analysis it has been possible to simulate a tensile test on specimen, and results obtained, like the one shown in Figure 114, have both a graphical and a tabular result output. It has been possible to plot the load vs. extension curve for in-flow specimen, to be hen compared to the numerical curve obtained for the no-in-flow case. The comparison between the curves is displayed in Figure 115.

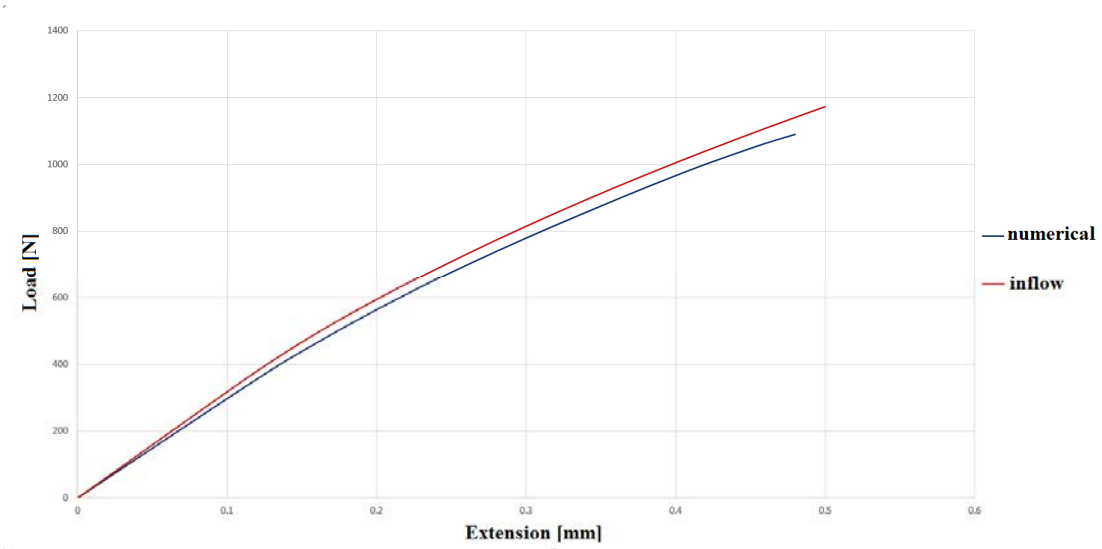

Figure 115. Comparison between no-in-flow numerical model and in-flow simulation

As it can be noticed, both curve slope and load at break has been incremented. The load at break value from inflow simulation is 1173.3 N, which correspond to an 11% increment respect to no-in-flow specimen tested value and to a 7.68% increment respect to the numerical simulated no-in-flow case.
From the curve slope, it is possible to evaluate stiffness, that for no-in-flow tested specimen was 2504.83 N/mm and for the no-in-flow numerical model resulted in 2776.875 N/mm. In-flow case shows a value of 2920.31 N/mm, which correspond to an increment of 14.23 % and 4.9% respectively.

CHAPTER 5

Conclusions

In this thesis work the effects of in-flow on the mechanical resistance of the weld line surface in injection molded specimens has been tested. In-flow is defined as the flow inside the mold cavity, below the frozen skin layer, which continues after the cavity filling has been achieved. The aim of the present DOE is the generation of a pressure gradient in cavity during the packing phase which causes a subsequent migration of material, in order to change the position and morphology of the weld line surface and locally reorient the fibers, thus improving the mechanical properties in this area. Numerical and experimental approach has been applied to single nozzle configuration to validate numerical model results, which has then been use to simulate the double nozzle configuration outcome and to compare results.

Single-nozzle configuration

Numerical simulations showed a good agreement with experimental results. Even if numerical model overestimates load at break and curve slope, trends are maintained, giving a good starting point for analysis. The latter constitutes the base to assume this model could provide a reliable load at break and stiffness increase prediction for in-flow specimens.

SEM analysis demonstrates that numerical model well predicts weld line morphology and position.

Double-nozzle configuration

Double-nozzle configuration was used to operate flow control during process. Results show how this design can be effective in repositioning weld line surface, promoting interfacial bonding, thus increasing local mechanical properties. Thanks to Moldflow®, Ansys® and Helius PFA® softwares it has been possible to simulate both injection molding process and tensile test.

In terms of process outcome, the simulation shows how weld line surface can be moved from its original position applying a pressure gradient between injectors, and for the parameters used in this study a 59 mm displacement has been achieved. The fact that weld line surface is stretched and moved means that also fibers have been reoriented during process leading to better mechanical properties of samples, since the fiber orientation tensor is higher than in no-in-flow case. According to results, fiber orientation tensor a11 can be strongly enhanced, thanks to in-flow phenomenon.

In terms of mechanical properties, tensile test simulation of in-flow specimens let to 11% and 7.68% increments of load at break respect to experimental and numerical no-in-flow cases, respectively. Stiffness has been increased by 14.23% and 4.9% respects to same cases.

Moreover, VARIOTHERM technique has been applied letting mold temperature to be kept as high as 152°C. The combination of higher mold temperature and in-flow phenomenon generated specimens with nearly absent frozen skin layer at the end of fill, and the subsequent flow is believed to be capable of weld line surface marks elimination.

Future researches

By virtue of the interesting numerical results obtained, present study could be further investigated and completed. First of all, in-flow specimens could be actually molded and tested, as for the single-nozzle ones. Weld line properties could be evaluated and compared with no-inflow ones. Numerical model could be then improved so that future results could better suits experimental outcome.

Secondly, also a fatigue characterization could be performed, to effectively evaluate component behaviour once molded, not only in terms of tensile strength, so that numerical model could be improved and refined to match actual experimental outcomes. At the end of this phase, the numerical model could then be useful to simulate injection molding processes for real components using this material, with a reduction in costs and time of the final part production.

REFERENCES

[1] C.-Y. L. Ming-Shyan Huang, "A novel clamping force searching method based on sensing tie-bar elongation for injection molding," *International Journal of Heat and Mass Transfer,* 2017.

[2] IUPAC Polymer Division, Subcommittee on Polymer Terminology, "A brief guide to polymer nomenclature," 2012.

[3] L. H. Chunze Yan, "Investigation into the Differences in the Selective Laser Sintering between Amorphous and Semi-crystalline Polymers," *International Polymer Processing Journal of the Polymer Processing Society,* 2011.

[4] S. Savage, "Fiberglass," redorbit.com, 2010.

[5] "What is carbon fiber?," innovativecomposite.com, 2015.

[6] B. Y. H. N. a. M. N. Ammar O, "Talc as Reinforcing Filler in Polypropylene Compounds: Effect on Morphology and Mechanical Properties," *Polymer sciences iMedPub,* 2017.

[7] D. M. Flanagan, "Wollastonite," *U.S. Geological Survey, Mineral Commodity Summaries,* 2017.

[8] M.-C. J. Hsien-Chang Kuo, "Effects of part geometry and injection molding conditions on the tensile," *Materials and Design,* 2010.

[9] A. A.-K. Shaoyun Guo, "A Study on Weld Line Morphology and Mechanical Strength of Injection Molded Polystyrene/Poly(methyl methacrylate) Blends," *Journal of Applied Polymer Science,* 2002.

[10] T. Nguyen-Chung, "Flow analysis of the weld line formation," *Rheologica Acta,* 2004.

[11] Y. C. L. C. K. A. M. Zhai, "Runner sizing and weld line positioning for plastics injection," *Engineering with Computers,* 2006.

[12] S. Hashemi, "Temperature, strain rate and weldine effects on strength and micromechanical parameters of short glass fibre reinforced polybutylene terephthalate (PBT)," *Polymer Testing,* 2011.

[13] G. Z. Lei Xie, "Effect of gate dimension on micro injection molded weld line strength with polypropylene (PP) and high-density polyethylene (HDPE)," *International Journal of Advanced Manufacturing Technology,* 2010.

[14] N. T. Yusuf Caglar Kagitci, "The effect of weld line on tensile strength in a polymer composite part," *International Journal of Advanced Manifacturing Technology,* 2016.

[15] C. S. W. Wenig, "The influence of molecular weight and mould temperature on the skin-core morphology in injection-moulded polypropylene parts containing weld lines," *JOURNAL OF MATERIALS SCIENCE,* 1996.

[16] A. O. E. D. Babur Ozcelik, "Influence of injection parameters and mold materials on mechanical properties of ABS in plastic injection molding," *International Communications in Heat and Mass Transfer,* 2010.

[17] "Sreedharan J, A.K Jeevanantham," *International Conference on Materials Manufacturing and Modelling,* 2017.

[18] G. Z. Lei Xie, "Mechanical properties of the weld line defect in micro injection molding for various nano filled polypropylene composites," *Journal of Alloys and Compounds,* 2011.

[19] M. A. Azieatul Azrin Dzulkipli, "Study of the Effects of Injection Molding Parameter on Weld Line Formation," *Procedia Engineering (Advances in Material & Processing Technologies Conference) ,* 2017.

[20] Z. M. A. A. M. K. Tan Yizong, "Influence of Processing Parameters on Injection Molded Polystyrene using Taguchi Method as Design of Experiment," *Procedia Engineering,* 2017.

[21] B. Ozcelik, "Optimization of injection parameters for mechanical properties of specimens with weld line of polypropylene using Taguchi method," *International Communications in Heat and Mass Transfer,* 2011.

[22] F. J. B. C. S. F. I. K. G. M. M. BOYANOVA, "Influence of Processing Conditions on the Weld Line in Doubly Injection-Molded Glassy Polycarbonate and Polystyrene: Microindentation Hardness Study," *Advances in Polymer Technology,* 2005.

[23] E. K. M. M. T. Babur Ozcelik, "Investigation the effects of obstacle geometries and injection molding parameters on weld line strength using experimental and finite element methods in plastic injection molding," *International Communications in Heat and Mass Transfer,* 2012.

[24] J. A. d. S. A. S. P. Carolina L. Morelli, "Assessment of Weld Line Performance of PP/Talc Moldings Produced in Hot Runner Injection Molds," *JOURNAL OF VINYL & ADDITIVE TECHNOLOGY,* 2007.

[25] B. S. A. K. T. L. C. H. Marian Janko, "Weld line improvement of short fiber reinforced thermoplastics with a movable flow obstacle," *Journal of Applied Polymer Science,* 2015.

[26] D.-H. S. a. K.-H. C. Keun Park, "Eliminating weldlines of an injection-molded part with the aid of high-frequency induction heating," *Journal of Mechanical Science and Technology,* 2010.

[27] W.-R. J. J.-A. C. Shia-Chung Chen, "Dynamic Mold Surface Temperature Control Using Induction Heating and Its Effects on the Surface Appearance of Weld Line," *Journal of Applied Polymer Science,* 2006.

[28] G. Z. X. W. Guilong Wang, "Effects of cavity surface temperature on mechanical properties of specimens with and without a weld line in rapid heat cycle molding," *Materials and Design,* 2013.

[29] G. Z. Y. G. Guilong Wang, "Thermal Response of an Electric Heating Rapid Heat Cycle Molding Mold and Its Effect on Surface Appearance and Tensile Strength of the Molded Part," *Journal of Applied Polymer Science,* 2013.

[30] D. M. G. L. L. O. M. Sorgato, "Effect of different laser-induced periodic surface structures on polymer slip in PET injection moulding," *CIRP Annals Manufacturing Technology,* 2018.

[31] M. S. A. B. S. D. G. L. D. Masato, "Effect of laser-induced periodic surface structures on wall slip of polypropylene in thin-wall injection molding," *WCMNM 2018,* 2018.

[32] Y. C. Y.-P. C. Y.-C. C. C.-Y. T. Shia-Chung Chen, "Effect of cavity surface coating on mold temperature variation and the quality of injection molded parts," *International Communications in Heat and Mass Transfer,* 2009.

[33] H. Y. Y. Z. W. Y. L. C. W. Y. H. Y. J. T. Pengcheng Xie, "Carbide-bonded graphene coating of mold insert for rapid thermal cycling in injection molding," *Applied Thermal Engineering,* 2017.

[34] M. S. M. B. B. W. G. L. Davide Masato, "Thin-wall injection molding of polystyrene parts with coated and uncoated cavities," *Materials and Design,* 2018.

[35] X. Y. S. G. CHANG LU, "The Mechanism of Ultrasonic Improvement of Weld Line Strength of Injection Molded Polystyrene and Polystyrene/Polyethylene Blend Parts," *Journal of Polymer Science: Part B: Polymer Physics,* 2006.

[36] G. Z. B. J. Lei Xie, "Reinforcement of micro injection molded weld line strength with ultrasonic oscillation," *Microsystem Technologies,* 2009.

[37] G. Z. a. J. W. Shuai Li, "A method to improve dimensional accuracy and mechanical properties of injection molded polypropylene parts," *Journal of Polymer Engineering,* 2017.

[38] J. P. C. R. R. G. A. Kikuchi, "Assessing the Effect of Processing Variables on the Mechanical Response of Polysytrene Molded Using Vibration-Assisted Injection Molding Process," *Journal of Applied Polymer Science,* 2006.

[39] C. H. T. A. S. A. b. o. N. Bangshu Cao, “INJECTION SPIN MOLDING PROCESS AND ARTICLES MADE THEREWITH”. U.S.A. Patent 5571583, 5 November 1996.

[40] P. S. A. a. M. J. B. KEITH W. RAWSON, “Controlled Orientation of Reflective Pigment and Optical Property Characterization of Injection-Molded Polypropylene,” *POLYMER ENGINEERING AND SCIENCE,* 1999.

[41] A. K. J. C. K. Waschitschek, “Influence of push-pull injection moulding on fibres and matrix of fibre reinforced polypropylene,” *Composites: Part A applied science and manufacturing,* 2002.

[42] R. Kazmer, “Exploiting melt compressibility to achieve improved weld line strengths,” *PLASTICS RUBBER AND COMPOSITES PROCESSING AND APPLICATIONS,* 1998.

[43] R. Kazmer, “ INCREASING WELD-LINE STRENGTH THROUGH DYNAMIC CONTROL OF VOLUMETRIC SHRINKAGE,” *ANTEC 94 - PLASTICS: GATE WAY TO THE FUTURE, VOLS 1-3,* 1994.

[44] C. F. D. K. C. S. S. T. Adam DiTocco, “Design for In-Flow to Strengthen Weld Lines in Injection Molded Polypropylene Parts,” *SPE ANTEC® Anaheim 2017,* 2017.

[45] M. S. L. G. e. G. L. A. Scantamburlo, “Investigation of the In-Flow Effect on Weld Line Strength and Local Morphology in Injection Molding of Fiber-Reinforced Polypropylene,” *XIV Convegno dell’ Associazione Italiana Tecnologie Manifatturiere, AITEM,* 2019.

[46] N. Z. M. D. G. Quanliang Su, “The use of variotherm systems for micro injection molding,” *Journal of Applied Polymer Science,* 2016.

[47] H. T. a. H. H. KIYOTAKA TOMARI, “Improvement of Weldline Strength of Fiber Reinforced Polycarbonate Injection Molded Articles Using Simultaneous Composite Injection Molding,” *Advances in Polymer Technology,* 1995.

[48] D3835, “Standard Test Method for Determination of Properties of Polymeric Materials by Means of a Capillary Rheometer,” *ASTM International,* 2016.

[49] D3418, “Standard Test Method for Transition Temperatures and Enthalpies of Fusion and Crystallization of Polymers by Differential Scanning Calorimetry,” *ASTM International,* 2015.

[50] E1269, “Standard Test Method for Determining Specific Heat Capacity by Differential Scanning Calorimetry,” *ASTM International,* 2018.

[51] D638, “Standard Test Method for Tensile Properties of Plastics,” *ASTM International,* 2014.

[52] KUGLER, “www.kugler-precision.com,” [Online].